ASSESSMENT OF THE PERFORMANCE OF A PHOTOVOLTAIC (PV) SYSTEM FOR POWERING ELECTROLYSERS IN THE GREEN HYDROGEN PROJECT AT TSAU//KHAEBS NATIONAL PARK USING MODELLING AND SIMULATION APPROACH

A THESIS SUBMITTED IN PARTIAL FULFILMENT OF THE REQUIREMENTS OF THE

DEGREE OF

MASTER OF SCIENCE IN RENEWABLE ENERGY

OF

THE UNIVERSITY OF NAMIBIA

BY

JEREMIA TANGI PETRUS

201310573

APRIL 2025

SUPERVISOR: Dr. PETJA DOBREVA (UNIVERSITY OF NAMIBIA)

CO- SUPERVISOR: Dr.-Ing. MATTHEW BERWIND (FRAUNHOFER INSTITUTE FOR SOLAR ENERGY SYSTEM)

Abstract

The Namibian government, through the Southern Corridor Development Initiative (SCDI), aims to produce 300,000 tons of hydrogen annually at Tsau //Khaeb National Park using wind and solar energy. This thesis focuses on the PV system required to power the electrolyser, involving site analysis, component selection, and system optimisation using PVsyst and Fraunhofer Zenit. Economic evaluation was conducted via Levelized Cost of Energy (LCOE) calculations. A site investigation using QGIS, Google Earth, and SolarGIS determined the coordinates, area, topography, and solar resources. System sizing and optimisation indicated that 4,586,736 monofacial modules (610 W) are needed for the fixed-tilt system and 4,181,184 modules for the tracked system. The fixed system requires 803 inverters, while the tracked system needs 732. The land area required is 21.7 km² for the fixed system and 32.2 km² for the tracked system across both Springbok and Dolphin sites, respectively. Simulation results showed differences in performance ratio (PR). At Springbok, PVsyst reported 83.55% for the fixed system and 82.42% for the tracked system. At Dolphin, PR was 83.99% (fixed) and 82.75% (tracked). In Zenit, Springbok's PR was 76% (fixed) and 81.4% (tracked), while Dolphin's PR was 76.1% (fixed) and 81.6% (tracked). Zenit's results were deemed more realistic due to its comprehensive modelling. The purpose of this study is to address the lack of independent research on the proposed SCDI Namibian Green Hydrogen project. The tracked system is recommended due to its superior performance, though further cost evaluations are necessary to address uncertainties.

Keywords: Green Hydrogen, Photovoltaics, PVsyst, SCDI.

CONTENTS

CHAPTER 1 INTRODUCTION 1

1.1 BACKGROUND OF THE STUDY 1
1.2 STATEMENT OF THE PROBLEM 4
1.3 OBJECTIVES OF THE STUDY 4

CHAPTER 2 THEORETICAL_BACKGROUND 6

2.1 HYDROGEN PRODUCTION 6
2.1.1 Comparison of AWE and PEM Electrolysers 7
2.2 PHOTOVOLTAICS SYSTEMS 9
2.2.1 Types of Photovoltaics Systems 9
2.2.2 Solar Resource Assessment and Site Analysis 12
2.2.3 Photovoltaic Plant System Components 21
2.2.4 Photovoltaic Plant Performance Parameters 34
2.2.5 Photovoltaic System Simulation Tools 45

CHAPTER 3 PV_SYSTEM_DESIGN_AND_SIMULATION 49

3.1 SIMULATION SOFTWARE SELECTION 49
3.2 SITE AND HORIZON 51
3.3 SOLAR RESOURCE ANALYSIS 54
3.4 SELECTION OF ELECTROLYSER 57
3.5 PROJECT CAPACITY REQUIREMENT 58
3.6 COMPONENTS SELECTION: 60
3.6.1 PV Module 60
3.6.2 Inverter 62
3.6.3 Trackers 62
3.6.4 Battery 64
3.7 PLANT SIZING 65
3.7.1 Determining and Configuring String Sizes 65
3.7.2 Configuration of PV Modules 69
3.7.3 Determining and Configuring Battery Storage System Sizes 71
3.7.4 PV System Losses 73
3.7.5 PV System Lifetime 75
3.8 OPTIMISED PV SYSTEM, ELECTROLYSER, AND BATTERY SIZING: SIMULATION INPUTS 75
3.8.1 Optimisation Based on Row Distance and Tilt Angle for Fixed and Tracked Systems 75
3.8.2 Electrolyser selection Results 77
3.8.3 Project System Sizing Results 77

CHAPTER 4 TECHNO-ECONOMIC EVALUATION....81
4.1 ENERGY OUTPUT AND SYSTEM PERFORMANCE ASSESSMENT....81
4.1.1 Springbok Site Simulation Performance Analysis....81
4.1.2 Dolphin Site Simulation Performance Analysis....83
4.1.3 Subsection Summary....85
4.2 SIMULATION RESULT FOR A SUBSYSTEM WITH STORAGE WITH SELF-CONSUMPTION STORAGE STRATEGY (PVSYST)....86
4.2.1 Monthly Interaction Between PV System, Storage, and Grid Results....88
4.2.2 Daily Interaction Between PV System, Storage, and Grid Results....90
4.2.3 Subsection Summary....93
4.3 ECONOMIC EVALUATION OF PV SYSTEMS....94
4.3.1 Economic Analyses for Both Sites....95
CHAPTER 5 CONCLUSION AND RECOMMENDATIONS....99
5.1 INTRODUCTION....99
5.2 SUMMARY OF THE STUDY....99
5.3 ANALYSIS OF KEY FINDINGS....100
5.4 RECOMMENDATIONS....102
5.4.1 Optimising System Design for Space Efficiency....102
5.4.2 Leveraging Grid Interaction for Energy Management....103
5.4.3 Adopting the Tracked System as the Preferred Configuration....103
5.4.4 Utilisation of Tier One Equipment....103
5.5 LIMITATIONS....104
5.6 AREAS OF FURTHER RESEARCH....104
REFERENCES....106
APPENDICES....115

List of Tables

Table 2.1: Summary of Environmental Ratings for Different Types of Hydrogen [10]....7
Table 2.2: Advantages and Disadvantages of AWE and PEM electrolysers technologies8
Table 2.3: Common Decomposition models....18
Table 2.4: Common Transposition models....19
Table 2.5: Several solar radiation data sources [44][45]....21
Table 2.6: Advantages and Disadvantages of MPPT and PWM charge controllers....33
Table 2.7: Factors influencing LCOE in PV system....40
Table 2.8: Key Features in Solar PV Software Packages [92]....46
Table 2.9: Steps for Modelling and Forecasting Energy Yield in PV Systems....47
Table 2.10: Solar PV Simulation Software Packages....48

Table 3. 1: Difference Between PVsyst and Zenith....50
Table 3. 2: Investigation outcome....53
Table 3. 3: Coefficient of Variation for various Sources of Solar Radiation Data for PV Site....56
Table 3. 4: Selected Electrolyser Specifications....58
Table 3. 5: Selected Module Specifications....61
Table 3. 6: Selected Inverter Specifications....62
Table 3. 7: Specifications of the Selected Tracker for the Study....63
Table 3. 8: Selected Battery Specifications....65
Table 3. 9: Module Output Voltage and Number of Modules per String....67
Table 3. 10: Chosen Subsystem Configuration and Performance Parameters....68
Table 3. 11: System Configuration Parameters for Fixed and Tracked PV Systems....70
Table 3. 12: Assumed Input Loss Parameters in the Study....74
Table 3. 13: Technical Specifications of the PV Plant at Springbok Site....78
Table 3. 14: Technical Specifications of the PV Plant at Dolphin Site....78
Table 3. 15: Needed Battery Capacity and Unit Parameters....79
Table 3. 16: Needed Battery Capacity and Unit Parameters for one Sub System....79

Table 4. 1: SY Comparison for Fixed and Tracked Systems at Springbok Site 82
Table 4. 2: PVsyst and Zenit Simulation Results for Springbok Site. 83
Table 4. 3 SY Comparison for Fixed and Tracked Systems at Dolphin Site.....84
Table 4. 4: PVsyst and Zenit Simulation Results for Dolphin Site.....85
Table 4. 5: PVsyst Simulation Results for Springbok and Dolphin Site Subsystem with Storage.....88
Table 4. 6: Monthly Interaction Between PV System, Storage, and Grid Results 90
Table 4. 7 Legend for Subsection figures 91
Table 4. 8: Assumed economic parameters.....95
Table 4. 9: Economic Evaluation for the Springbok Site 96
Table 4. 10: Economic Evaluation for the Dolphin Site.....96

List of Figures

Figure 1. 1: Proposed solar plant sites in Tsau //Khaeb National Park. Adapted from [3] 2

Figure 1. 2: Components of the Proposed Green Hydrogen Export Project. Adapted from [3] 2

Figure 2. 1: Schematic of AWE and PEM Electrolysers [6].....8

Figure 2. 2: Stand-alone PV Systems.....10

Figure 2. 3: Grid-tied PV Systems 11

Figure 2. 4: Hybrid PV Systems 12

Figure 2. 5: Earth's Orbital Positions During Equinoxes and Solstices June and December 13

Figure 2. 6: Annual Variation of Solar Declination.....14

Figure 2. 7: The solar angle of altitude [23].....15

Figure 2. 8: Solar angle of azimuth[24] 15

Figure 2. 9: Solar Hour angle [25] 16

Figure 2. 10: Components of solar irradiance [25] 19

Figure 2. 11: Structure of crystalline silicon solar cell [48].....22

Figure 2. 12: Equivalent circuit diagram of a PV cell, illustrating series and shunt resistances with a single-diode model.....23

Figure 2. 13: (a). Module I-V Curve under STC (b). versus Real-World Losses [52]. ...24

Figure 2. 14: IV and Power Curves for varying irradiance and temperature [53]. 25

Figure 2. 15: Different Types of Solar Panels.....26

Figure 2. 16: Module Technology Efficiencies and their improvement over the years [57] 27

Figure 2. 17 PV Production by Technology and Year [57] 26

Figure 2. 18: Circuit configuration in (a). Traditional panel VS (b). Half-Cut cell panel[61]. 29

Figure 2. 19: Common Mounting Methods 30

Figure 2. 20: Comparison of output power generated with a dual-axis tracking system and without any tracking system.....31

Figure 2. 21: Global Weighted Average LCOE for Large PV Systems [78].....38

Figure 2. 22: LCOE Forecast [77].....39

Figure 2. 23: Illustration of Key Variables in Inter-Row Spacing Optimisation for PV Arrays 42

Figure 3. 1: Georeferencing and Scale Adjustment of the Provided Map Using QGIS ..52
Figure 3. 2: Location of PV System Sites and Electrolyser Site 53
Figure 3. 3: Sun Path Diagram with Horizon Line Overlay for Springbok 54
Figure 3. 4: Different Sources of Solar Radiation Data for Springbok Site 55
Figure 3. 5: DNI, GHI, and DHI Data for PV Sites 56
Figure 3. 6 Monthly Albedo Values 57
Figure 3. 7: The DQ1000 Alkaline Electrolyser 57
Figure 3. 8: Ideematec Horizon L: TEC 1P tracker, sourced from [103] 63
Figure 3. 9: Module mounting configuration for fixed system. 69
Figure 3. 10: Module mounting configuration for 1P single-axis tracked system. 70
Figure 3. 11: Energy Output and Tilt Angle Optimisation for Fixed Solar System 76
Figure 3. 12: Land Usage and Energy Gain Optimisation for Tracked Solar System 76

Figure 4. 1: PR comparative software simulation results for the Springbok site 82
Figure 4. 2: SY comparative software simulation results for the Springbok site 83
Figure 4. 3: PR comparative software simulation results for the Dolphin site 84
Figure 4. 4: PR comparative software simulation results for the Dolphin site 85
Figure 4. 5: Springbok and Dolphin site comparative simulation results, of performance ratio (PR), With Storage 87
Figure 4. 6: Springbok and Dolphin site comparative simulation results for SP With Storage 87
Figure 4. 7: Energy Storage Comparison for Fixed Systems at Springbok and Dolphin 89
Figure 4. 8: Energy Storage Comparison for Tracked Systems at Springbok and Dolphin 90
Figure 4. 9: Springbok Fixed Configuration with Storage Results 91
Figure 4. 10: Springbok Tracked Configuration with Storage Results 92
Figure 4. 11: Dolphin Fixed Configuration with Storage Results 93
Figure 4. 12: Dolphin Tracked Configuration with Storage Results 93
Figure 4. 13: Comparison of OPEX and Energy Output over the 30 years 97

List of Abbreviations and Accronyms

AC: Alternating Current

AWE: Alkaline Water Electrolysis

BESS: battery energy storage system

CAPEX: Capital Expenditure

C_{opt}**:** Optimal battery capacity

CV: Coefficient of Variation

DC: Direct Current

DHI: Diffuse Horizontal Irradiance

DNI: Direct Normal Irradiance

DoD: Depth of Discharge

GHI: Global Horizontal Irradiance

GH_2**:** Green hydrogen

ILR: Inverter Loading Ratio

LCOE: Levelised Cost of Energy

LiFePO4: Lithium Iron Phosphate

MPPT: Maximum Power Point Tracking

OPEX: Operational Expenditure

PEM: Proton Exchange Membrane

PR: Performance Ratio

PWM: Pulse Width Modulation

PVsyst: Photovoltaic System Simulation Software

SCDI: Southern Corridor Development Initiative

SY: Specific Yield

STC: Standard Test Conditions

TMY: Typical Meteorological Year

WACC: Weighted Average Cost of Capital

Acknowledgements

Firstly, I would like to express my deepest gratitude to my supervisor, Dr. Petja Dobreva from the Department of Physics, Chemistry & Material Science at the University of Namibia, for her unwavering support and insightful guidance throughout this journey. Her consistent and detailed feedback helped me understand concepts I initially found challenging. It also encouraged me to think more creatively in addressing the problems I encountered. I am truly grateful to her for this support.

I would also like to express my sincere gratitude to my co-supervisor, Dr.-Ing. Matthew Berwind, from the Fraunhofer Institute for Solar Energy Systems ISE, Department of Analysis, Modules, and Power Plant. I am grateful for the opportunity he granted me to conduct my research at one of the best research institutes in Europe. His confidence in my abilities empowered me to tackle problems independently, which enhanced my learning experience.

A heartfelt thank you to Mr. Alfons Armbruster, my mentor in simulation. His insights and guidance in using the simulation tools and being available to answer all my questions were crucial in advancing my research. I am grateful for his generous support and advice relating to German matters. Vielen Dank.

I am immensely thankful to the great humans I met at the Fraunhofer Institute ISE for providing a stimulating research environment that fostered my learning and professional growth. Lastly, I would like to acknowledge the University of Namibia and its academic community for their continuous support throughout this process.

Dedications

I dedicate this thesis to my family, whose unwavering support and constant encouragement help keep my mind positive through the hard times. To my parents who instilled in me the values of hard work, perseverance, and self-accountability, and to everyone who had a positive impact on my life.

I would also like to dedicate this work to the future of renewable energy and sustainable energy, particularly in Namibia, and to all of those who are committed to building a greener future. May this research contribute to the growing body of knowledge that will help save our planet.

Lastly, I dedicate this thesis to myself for my perseverance and unwavering commitment to trying my best every day**.**

Declarations

I, Jeremia Tangi Petrus, hereby declare that this study is a true representation of my original research and that no part of this work has been submitted for a degree at any other higher education institution.

No section of this thesis may be copied, stored in a retrieval system, or transmitted in any form or by any means (including electronic, mechanical, photocopying, recording, or other methods) without the prior consent of the author or the University of Namibia.

I, Jeremia Tangi Petrus, grant the University of Namibia the right to reproduce this thesis, either in full or in part, in any manner or format deemed appropriate by the University, for use by any individual or institution for research and study purposes. However, this right shall be waived by the University of Namibia if the entire thesis has been or is being published in a manner that meets the University's approval.

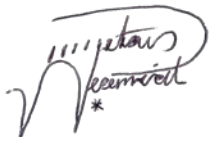

……. Date:…….……

April 2025

Jeremia Tangi Petrus

Chapter 1

Introduction

1.1 Background of the Study

With its abundant solar and wind resources, Namibia is poised to play a significant role in the global transition to sustainable energy solution producers [1].The Namibian government through the Southern Corridor Development Initiative (SCDI) Namibian Green Hydrogen Project aims to generate 300,000 tons of hydrogen annually at Tsau //Khaeb National Park using combined wind and solar energy [2]. The solar plants will be developed in two phases: the first will be located at the Springbok site, and the second will be located at the Dolphin site, as illustrated in Figure 1.1 [3]. The Tsua //Khaeb area located in the south of Namibia has the potential to produce about 5 Mt/a of green hydrogen equivalent by 2050[3]. The proposed project intends to employ a hybrid photovoltaic (PV)-wind system, complemented by a battery energy storage system (BESS) to power a 1.5 GW electrolyser as illustrated in Figure 1.2 [4]. Hyphen, the contracting company is considering the possibility of connecting the PV system to the national grid [2], [4]. It is envisaged that the PV system will provide 40% of the electrolysers energy needs, the rest from wind [4].

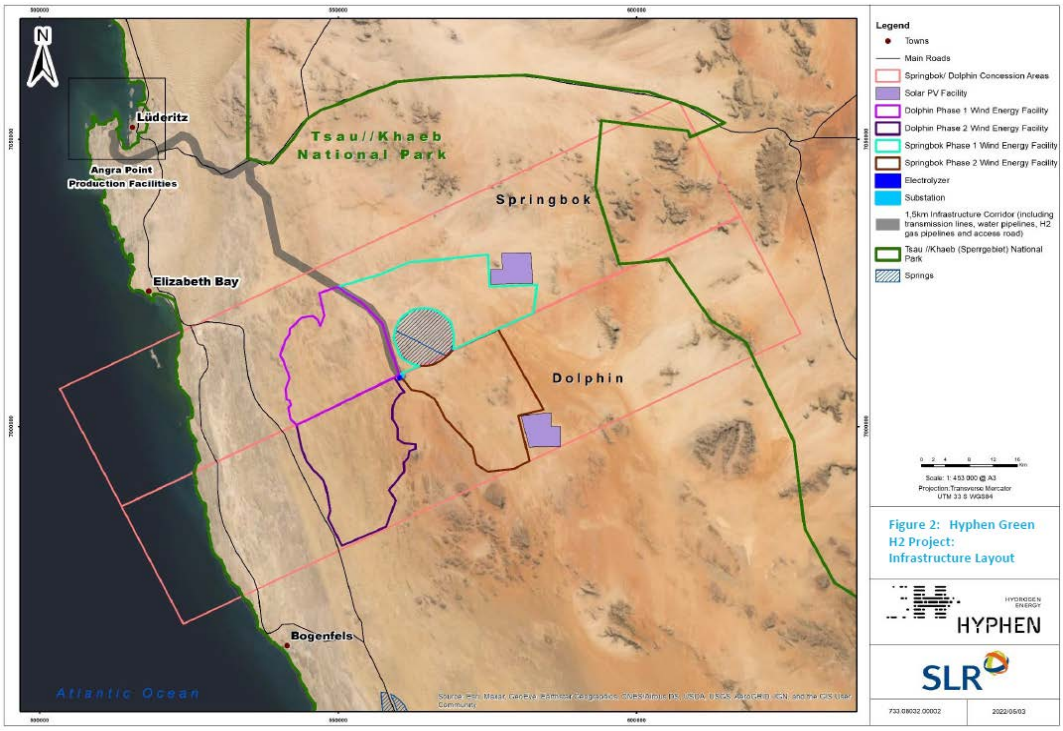

Figure 1. 1: Proposed solar plant sites in Tsau //Khaeb National Park. figure data adapted from[3]

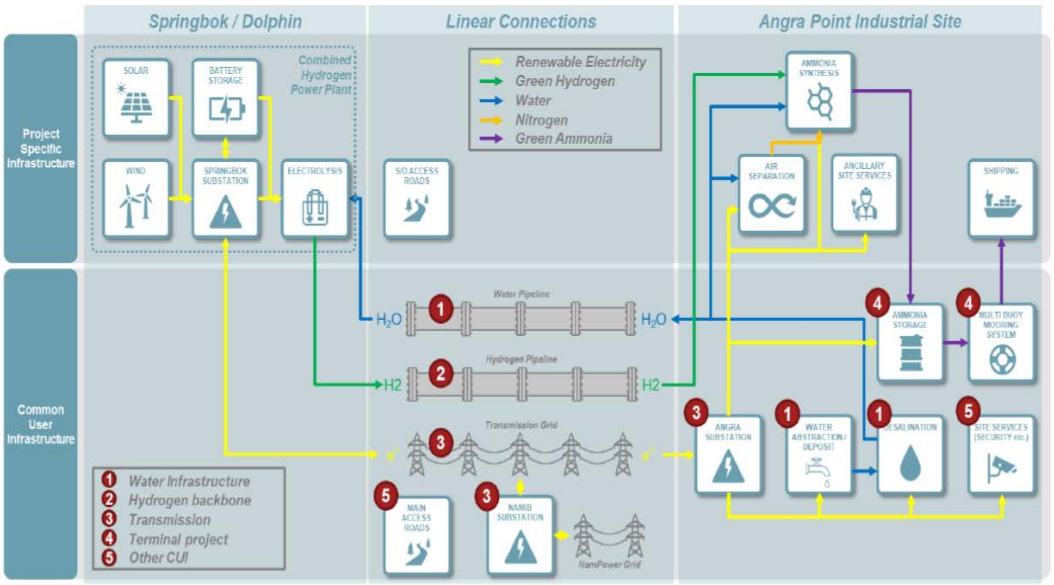

Figure 1. 2: Components of the Proposed Green Hydrogen Export Project. figure data adapted from[3]

This project aims to contribute to reducing CO_2 emissions, aligning with the Paris Agreement's 2015 climate goal of limiting global warming to 1.5°C. Achieving this goal requires greenhouse gas emissions to reach net zero by 2050 [5].

Green hydrogen (GH_2) will be produced in Namibia by splitting water into hydrogen and oxygen via electrolysis [7]. Electrolysers are apparatus that facilitate the electrolysis process, in which two main types of electrolysers are commonly utilised: proton exchange membranes (PEM) and alkaline [8]. Alkaline electrolysers are suited for large scale applications, like those in the HYPHEN Green Hydrogen project. Alkaline electrolysers are a matured technology which has been in use for many decades and are cheaper than PEM, but their efficient operation is dependent on continuous running rather than frequent up and down ramping [7]. The electrolysers in the SCDI Namibian Green Hydrogen Project are expected to have uninterrupted operation. Therefore, they need a battery energy storage system to provide storage and backup power to supply the load during night time operation and during cloudy or windless periods [4]. The SCDI Namibian Green Hydrogen Project includes seawater desalination, water electrolysis for H_2 production, conversion of hydrogen to ammonia, and a deep-water port in Lüderitz [1]. The project requires a capital expenditure (CAPEX) of US$10 billion (equivalent to N$190.75 billion as of March 4, 2024), with the Namibian government (GRN) entitled to co-invest by taking up to a 24% equity interest at cost [2].

1.2 Statement of the problem

The Tsau //Khaeb Green Hydrogen project is estimated to cost USD 10 billion, with the Namibian government holding a 24% stake, amounting to USD 2.4 billion. However, no independent techno-economic assessment has been conducted to evaluate the feasibility of producing the targeted 300,000 tons of hydrogen at the Tsau //Khaeb site. This hydrogen is intended to be produced via water electrolysis powered by renewable sources such as solar photovoltaics and wind, as part of the SCDI Namibian Green Hydrogen Project. The projected renewable energy capacities and the techno-economic performance of the project have not been independently verified, raising concerns about the credibility and accuracy of the project's expected outcomes.

1.3 Objectives of the Study

This study aims to conduct an independent design and a techno-economic evaluation of a photovoltaic plant expected to meet 40% of the energy demand for electrolysers in the Green Hydrogen Project at the Tsau//Khaeb National Park.

To achieve the aims of this project, it is necessary to:

- Conduct a comprehensive site analysis of the proposed location to evaluate the solar potential, land area size, and investigate the far shading effects at the proposed site.
- Select components for the PV plant based on the following criteria:

  technical performance, cost-effectiveness, technology maturity, reliability, and compatibility with the existing infrastructure.

- Design and simulate a detailed PV Plant system to energise the electrolyser in the Tsau //Khaeb National Park green hydrogen project.
- Perform a techno economic Levelised Cost of Energy (LCOE) assessment of a simulated PV plant.

Chapter 2

Theoretical background

The SCDI Green Hydrogen project involves hydrogen production via renewable energy technologies. This study focuses specifically on a PV system to be used in the SCDI project. It is essential to have a comprehensive theoretical understanding of the project components, from the power supply system (photovoltaic system) to the load (electrolyser). This chapter focuses on a theoretical review of hydrogen production, the operation, characteristics, and simulation of PV plant systems, and the Levelised Cost of Energy (LCOE) for PV plant systems.

2.1 Hydrogen Production

Molecular hydrogen is the most abundant chemical substance in nature. The process of electrolytically decomposing water was initially conducted by William Nicholson and Anthony Carlisle in the year 1800, shortly following the invention of the voltaic pile by Alessandro Volta [8]. Hydrogen, in its unbound state, is absent from the planet. Thus, it is excluded as a primary energy reservoir. White or naturally occurring hydrogen exists only in limited quantities within underground reservoirs, which are not economically exploitable. Hence, alternative methodologies have been employed to synthesise hydrogen. This gave rise to the practice of assigning colours to hydrogen, denoting the origin of the energy source or manufacturing process [9]. Despite ongoing advancements, the current cost of hydrogen production remains high, ranging between €50-55/kg H_2 via

the electrolysis process [8]. The types of hydrogen production by the colour classification and their environmental impacts are summarised in Table 2.1:

Table 2.1: **Summary of Environmental Ratings for Different Types of Hydrogen** [10]

TYPE OF HYDROGEN	METHOD	ENVIRONMENTAL RATING
Grey Hydrogen	Steam Reformation	Dirty
Blue Hydrogen	Steam Reformation	Moderately clean
Turquoise Hydrogen	Methane Pyrolysis	Moderately clean
Green Hydrogen	Renewable Energy Sources Electrolysis	Clean
Black and Brown Hydrogen	Coal Gasification	Not climate-friendly
White Hydrogen or gold hydrogen	Naturally Occurring	clean
Purple hydrogen	Nuclear-powered and Heat	Moderately clean
Red hydrogen	Thermal nuclear power	Moderately clean
Pink Hydrogen	Nuclear power	Moderately clean

Although numerous hydrogen production methods exist, only a few have garnered significant research attention and are widely used today. The three primary methods are steam reforming of natural gas, biomass thermochemical conversion, and electrolysis. These approaches represent the key technologies in modern hydrogen production, with electrolysis being the primary focus of the proposed project. This process relies on electrolysers, with Alkaline Water Electrolysis (AWE) and Proton Exchange Membrane (PEM) being the two most commonly used technologies for producing green hydrogen, typically powered by solar and wind energy.

2.1.1 Comparison of AWE and PEM Electrolysers

AWEs are more established and have a lower capital cost than PEM electrolysers. AWE operates well at large scales, offering robustness and durability, but it struggles with dynamic load changes. PEM, on the other hand, provides better flexibility with faster response times and can operate efficiently at a wide range of loads, but it is more

expensive and less suited for large-scale industrial applications due to its reliance on scarce and costly materials [7].

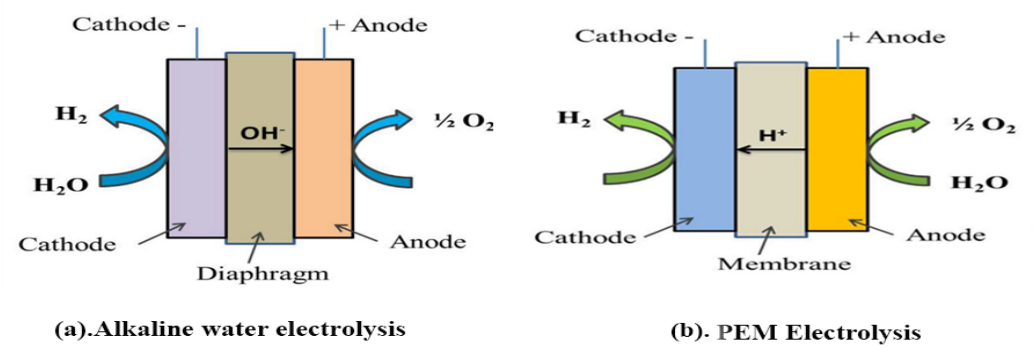

Figure 2. 1: Schematic of AWE and PEM Electrolysers[6]**.**

2.1.1.1 Advantages and Disadvantages for AWE and PEM are shown in Table 2.2 below electrolysers [7] [6], [8], [11]**.**

Table 2.2: Advantages and Disadvantages of AWE and PEM electrolysers technologies

Aspect	AWE	PEM
Cost	Lower CAPEX, due to the use of common materials, Large economies of scale and technology maturity	Higher CAPEX due to noble materials
Scalability	Excellent for large-scale projects	Better suited for small to medium-scale applications
Operating Range	Limited part-load range, operates best near full load	Wider dynamic range (0-100%), suitable for variable loads
Durability	Established and durable technology	Newer technology with less long-term data on degradation
Response Time	Slower ramp-up, not ideal for fluctuating loads	Fast ramp-up, ideal for fluctuating renewable energy
Maintenance	Low-maintenance and mature technology	Requires more maintenance due to sensitive components
Hydrogen Purity	High (99.9%)	Higher purity (99.999%)

Based on H_2 purity, PEM electrolysers are ideal for producing hydrogen for fuel cells, which require high-purity hydrogen. However, hydrogen used for applications such as ammonia production and other industrial processes does not require such high purity. If Namibia's objective is to produce hydrogen primarily for ammonia or similar industrial uses, then there is even more reason to opt for AWE.

2.2 Photovoltaic (PV) Systems

2.2.1 Types of Photovoltaic Systems

PV systems, which directly convert solar energy into electricity, comprise of solar modules and balance-of-system components [6]. Grid-connected, stand-alone, and hybrid systems are classified as the most common types of PV systems [13]. This subsection provides a brief overview of these three types of PV systems.

2.2.1.1 Stand-alone Photovoltaics Systems (off-grid)

These systems function independently from the utility grid. They typically rely on battery storage to provide power when solar production is low. The system usually comprises a solar panel, charge controller, battery storage, and a DC to AC inverter. Stand-alone systems can either use battery storage or can directly be connected to an electrical load without battery storage [14].

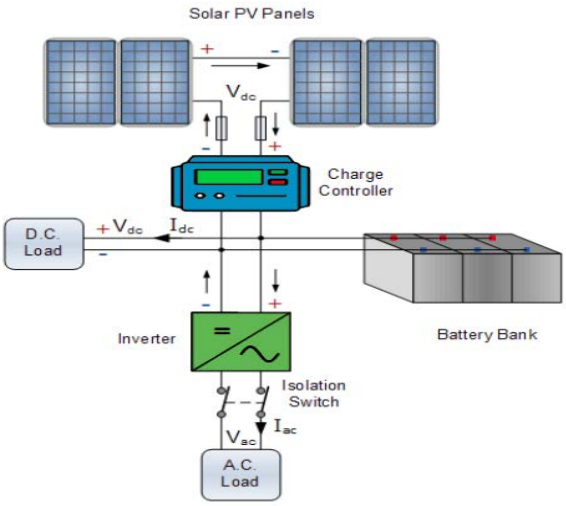

Figure 2. 2: Stand-alone PV System

2.2.1.2 Grid-tied Photovoltaics Systems (grid-connected)

Grid tied PV systems are directly integrated with the electrical utility grid and utilise the grid for energy storage, through a process known as net metering. In grid-tied PV systems, the DC-AC inverter plays a crucial role by converting the direct current generated from the PV panels into alternating current that meets the power quality, voltage and frequency standards required by the utility grid. These operational standards are defined by each country's grid code, which sets the technical specifications necessary for the safe and secure integration of renewable energy into the national grid. In Namibia, this is referred to as the Namibian Grid Code [15][16][17].

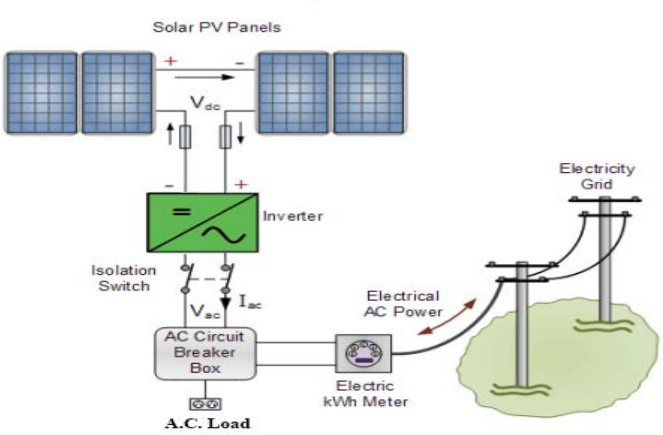

Figure 2. 3: Grid-tied PV Systems

2.2.1.3 Hybrid Photovoltaics Systems

Hybrid systems which are proposed to be used in the SCDI project combine both features of stand-alone and grid-connected systems by integrating battery storage alongside grid connection. This configuration enables energy self-consumption, with surplus energy exported to the grid, thereby minimising energy wastage. The advantages of such systems include enhanced reliability, as they can provide backup power during grid outages, and potential cost savings depending on grid tariffs. Additionally, they reduce grid dependence by allowing the use of stored energy during periods of high demand or grid unavailability [18].

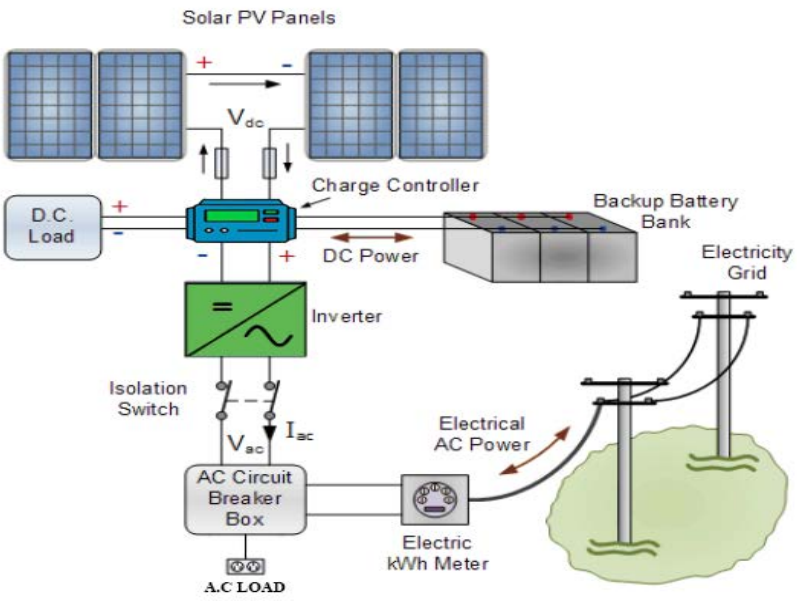

Figure 2. 4: Hybrid PV Systems

2.2.2 Solar Resource Assessment and Site Analysis

This section examines solar resources and site selection, both crucial for determining the feasibility and performance of a PV system. Solar irradiance, insolation, and meteorological factors including temperature and wind speed significantly impact energy yield and system design. Accurate long-term solar and weather data, ideally collected on-site over at least ten years, are essential for reliable performance modelling and energy output predictions. While solar resources are variable, the sun’s position is predictable through established equations and algorithms, aiding in precise site assessments [19][20]. To better understand these factors, the following subsections will examine the Sun's relative position to the Earth, key parameters of solar radiation, and sources of solar radiation data essential for accurate PV system design.

2.2.2.1 The Relative Position of the Sun to Earth

Two primary angles characterise the Sun's position: the azimuth angle, φ_s, and the altitude angle, α. Equations 2 and 3 enable the calculation of these angles based on the latitude (λ), the time of day (hour angle, ω) and the day of the year (declination angle, δ). Connections between these angles are outlined as follows [21]:

Solar Declination (δ) is the angle formed between the Earth's equatorial plane and the line that joins the Earth's and Sun's geometric centres. The angle varies over the year due to the Earth's orbit and the perceived movement of the Sun, illustrated in Figure 2.5. The Earth's axis is tilted at 23.45° relative to the ecliptic plane, causing the Sun to shift between the Northern and Southern hemispheres annually (Figure 2.6). Solar declination, δ, is calculated for any day of the year using Equation 1 [22].

$$\delta = 23.45° \, sin\left(\frac{360(284+n)}{365}\right) \quad \text{(eq. 1)}$$

In this equation, n represents the day of the year, with n =1 corresponding to January 1st.

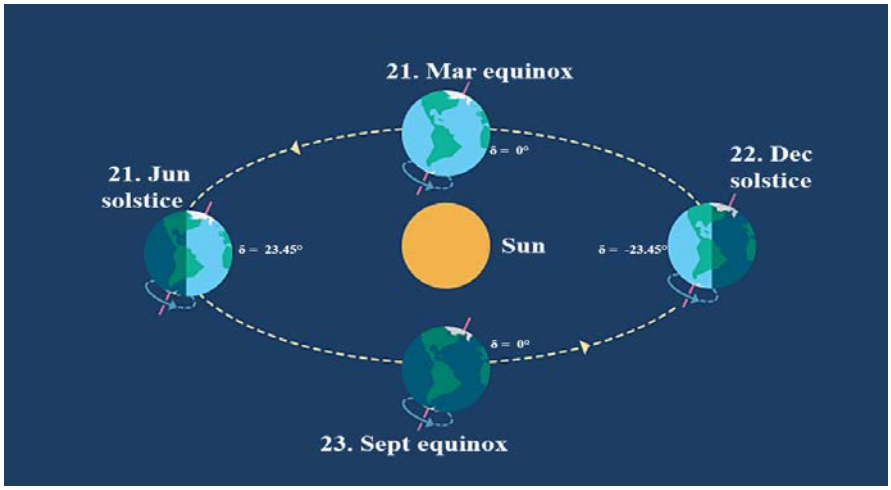

Figure 2. 5: Earth's Orbital Positions During Equinoxes and Solstices June and December

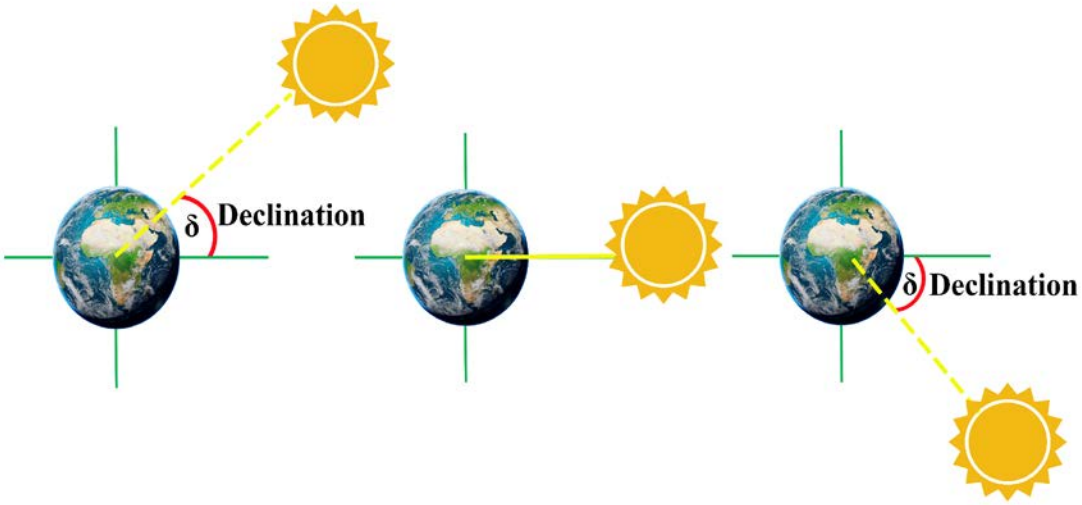

Figure 2. 6: Annual Variation of Solar Declination

The solar altitude (α) is the angle between the horizontal plane of a location on the Earth's surface and the line connecting that location to the sun, as illustrated in Figure 2.7. The complementary to the alpha angle is the zenith angle (z). The solar altitude angle can be determined by using Equation 3 and is obtainable for any time between sunrise and sunset for the northern hemisphere through Equation 2 [23], For the southern hemisphere, whenever the Sun is north of a location, the angle is given by ($\alpha = 90° + (\lambda - \delta)\ where\ \lambda < 0$) instead of (eq.2).

$$\alpha = 90° - z = 90° - (\lambda - \delta) \quad \text{(eq. 2)}$$

$$\alpha = sin^{-1}([cos\lambda \cdot cos\omega \cdot cos\delta] + [sin\lambda \cdot sin\delta]) \quad \text{(eq. 3)}$$

where α is the solar altitude angle (°), λ is the local latitude (°), δ the solar declination angle (°), ω the hour angle (°) and z is the zenith angle (°).

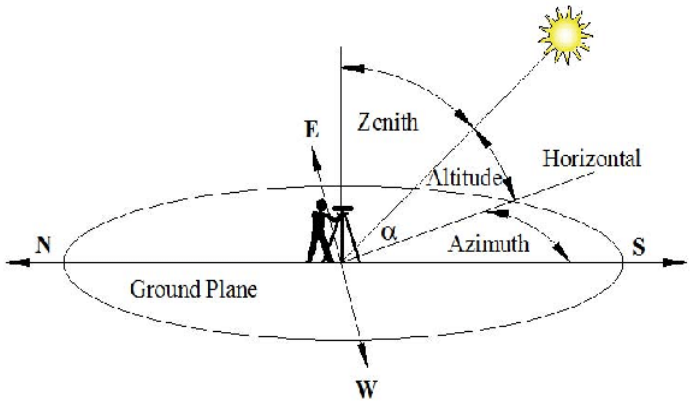

Figure 2. 7: The solar altitude angle [23]**.**

Solar Azimuth φ_s is the angle between the north-south direction and the projection of the sun's position in the horizontal plane . At solar noon, the sun is positioned directly south in the northern hemisphere and north in the southern hemisphere. This angle changes throughout the day. At the equinoxes, the sun's path across the sky is directly east-west, leading to sunrise azimuths of 90 degrees and sunset azimuths of 270 degrees. Typically, the azimuth angle varies by latitude and time of year and can be calculated for any date and time using Equation 4 [23].

$$\varphi_s = arccos\left(\frac{sin\alpha \cdot sin\lambda - sin\delta}{cos\alpha \cdot cos\lambda}\right) \quad \text{(eq.4)}$$

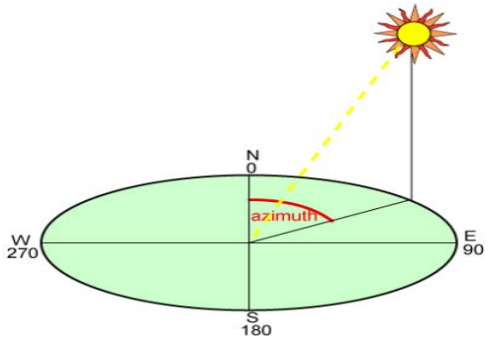

Figure 2. 8: Solar azimuth angle [24]

Hour angle (ω) is defined as the angle between the observer's meridian and the meridian where the sun is directly overhead. It represents the Earth's rotation since the last solar noon, being zero at solar noon and increasing by 15° per hour (negative before noon, positive after). To account for variations in solar meridian crossing, the hour angle must be adjusted with the equation of time (eq. 5) and adjusted for the observer's longitude. Sunrise and sunset occur when the zenith angle (z) is 90°, and daylight hours can be calculated using Equation 6 [25].

$$\omega = 15°(t_{solar} - 12h + \omega_{eq}) \text{ (eq.5)}$$

$$\omega = \frac{2\omega_{sr}}{15°} \text{ (eq.6)}$$

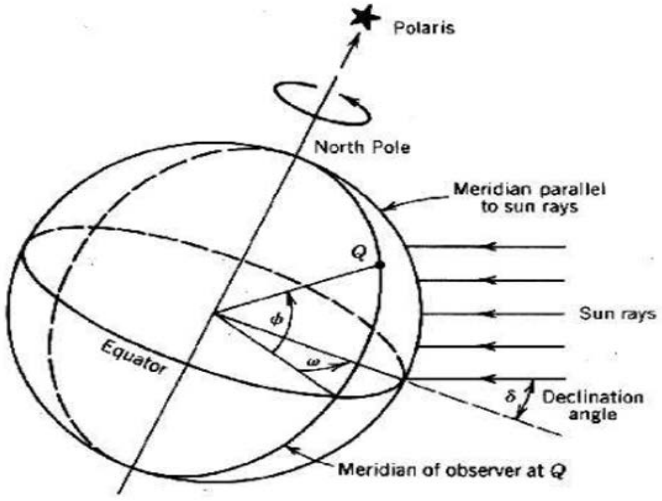

Figure 2. 9: Solar Hour angle [25]

2.2.2.2 Parameters of solar radiation

Three primary ground-level solar radiation parameters measured in the Earth's atmosphere define a specific location's solar resource. These parameters include:

2.2.2.2.1 Diffuse Horizontal Irradiance (DHI)

This measures the solar radiation received by a horizontal surface from sunlight scattered by atmospheric particles, such as dust and clouds. DHI is measured using a pyranometer that is shielded from direct sunlight [26].

2.2.2.2.2 Direct Normal Irradiance (DNI)

This is the amount of solar radiation received per unit area by a surface held perpendicular to the sun's rays, often called the beam component of solar radiation. A pyrheliometer, attached to a solar tracker, is typically used to measure DNI. If DHI and Global Horizontal Irradiance (GHI) values have been measured, equation 7 can be used to estimate DNI mathematically [26].

$$GHI = DHI + DNIcos(\theta z) \quad \text{(eq. 7)}$$

where (θz) is the zenith angle.

Decomposition models, which are fitted to data, can also be used to estimate DNI values for a specific location by examining the correlation between the diffuse fraction (k_d) and the clearness index (k_t) [27]. The clearness index, k_t, is specified by the ratio of GHI to extra-terrestrial irradiance GHI_{extra} :

$$k_t = \frac{GHI}{GHI_{extra}} \quad \text{(eq. 8)}$$

The ratio of DHI to GHI makes up the diffuse fraction:

$$k_d = \frac{DHI}{GHI} \quad \text{(eq. 9)}$$

Decomposition models estimate the relationship between k_t and k_d, often incorporating factors like solar altitude angle(α), clearness index variability (Δk_t) and the dew point temperature (T_{dp}). Table 2.3 presents commonly used decomposition models and their input parameters.

Table 2.3: Common Decomposition models

Model	Published	input parameters
Holland and Orgill [28]	1977	k_t
Erbs [29]	1982	k_t
DISC [30]	1987	k_t, α
Reindl 1 & 2 [31]	1990	k_t, α
Louche [32]	1991	k_t
DIRINT [33]	1992	$\Delta k_t, \alpha, T_{dp}$

2.2.2.2.3 Global Horizontal Irradiance (GHI)

The total solar radiation received by a horizontal surface placed on the earth' surface per unit area is known as GHI, which encompasses both direct beam and diffuse components of sunlight. Measured using a pyranometer, GHI accounts for all solar irradiance from the entire sky hemisphere, including direct sunlight, scattered light, and reflected radiation. The fraction of incident radiation that is reflected by a surface is known as albedo [34].

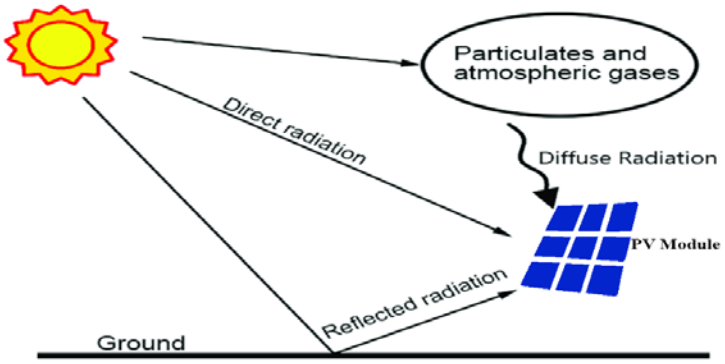

Figure 2. 10: Components of solar irradiance [25]

2.2.2.2.4 Global Plane of Array Irradiance

This term denotes the sum of solar radiation received per unit area on a tilted surface of the solar array, including both direct and diffuse components of solar radiation. PV system designers strive to maximise GPOA to enhance system performance [35].

PV system simulation software employs transposition models shown in Table 2.4 to calculate irradiance on a tilted surface based on horizontal data, with each model varying in its assumptions and required input variables [36].

Table 2.4: Common Transposition Models

Model	Input parameters
Perez [33]	DHI, DNI, GHI_{extra}, θ_T , θ_{AOI} , airmass
Isotropic [37]	DHI, θ_T
Hay-Davies [38]	DHI, DNI, GHI_{extra}, θ_T , θ_{AZ} , θ_Z, φ_s
Reindl [31]	DHI, DNI, GHI, θ_T , θ_{AZ} , θ_Z, φ_s
Klucher [39]	DHI, GHI, θ_T , θ_{AZ} , θ_Z, φ_s

2.2.2.3 Sources of solar radiation data

Typically, this refers to data acquired through ground measurements, satellite observations, or a combination of both. Ground-based data collection employs instruments like reference solar cells (silicon sensors) and pyranometers to collect irradiance data on-site. However, because of the limited availability of extensive historical data, interpolation is often used to generate long-term datasets [40]. Challenges associated with ground measurements include uncertainties in interpolated data, inconsistencies in calibration standards, maintenance issues, and varying measurement periods. Conversely, satellite data offers broader geographical and historical coverage [41]. In a comprehensive study conducted to benchmark modelled solar radiation data from various sources against ground measurements at 31 sites worldwide, the IEA-PVPS Task 16 report found that SolarGIS provided the most accurate solar radiation data compared to other sources. The study evaluated several parameters and methodologies to determine the best-performing sources, highlighting SolarGIS as the closest to ground truth in various climatic conditions and geographic locations [42]. This finding underscores SolarGIS reliability for accurate solar energy resource assessment and planning. Additionally, the average uncertainty of SolarGIS resource estimate is 5% vs. the industry average of 10% [43]. Table 2.5 provides an overview of several globally relevant solar radiation data sources.

Table 2.5: Several solar radiation data sources [44][45]

Data Source	Data Type	Coverage	Data Availability	Availability
Meteonorm	Ground	Global, most regions from 1981 to 2010	Historical and recent datasets	Paid
PVGIS	Varies on time frame and region	Global, varies by region and time frame (1981–2011)	Free historical data	Free
SolarGIS	Satellite	Global, 1994 to the present	High-resolution satellite-derived data	paid
NASA-SSE	Satellite	Global, 1983 to 2005.	Historical dataset	Free
NREL NSRDB	Satellite and Ground	United States and limited global data, from 1998 to the present	High-resolution hourly data	Free
HelioClim	Satellite	Middle East, Africa and Europe, 2004 to the present.	Provides high-frequency solar data	Paid
Renewables.ninja	Satellite & Model	Global, 1983 to present	Long-term historical and weather-based data	Free and Paid

2.2.3 Photovoltaic Plant System Components

PV plant systems have various components, each fulfilling a distinct function. This subsection highlights some key elements of PV plants which include solar PV modules, mounting structures, storage (Battery bank), charge controller, solar inverters and DC and AC cables [46].

2.2.3.1 Solar PV Modules

2.2.3.1.1 Working Principle of Solar PV Modules

PV modules are the fundamental components of a PV system, converting sunlight into electrical energy through the photovoltaic effect. In this process, photons interact with the semiconductor material in the PV cells. Each module consists of solar cells, typically made from two layers of semiconductor material, often silicon. When the n-type silicon,

with excess electrons, is combined with p-type silicon, which has an abundance of electron vacancies (holes), an electric field forms at the junction, creating the conditions necessary for electricity generation [47], as illustrated in Figure 2.11 below.

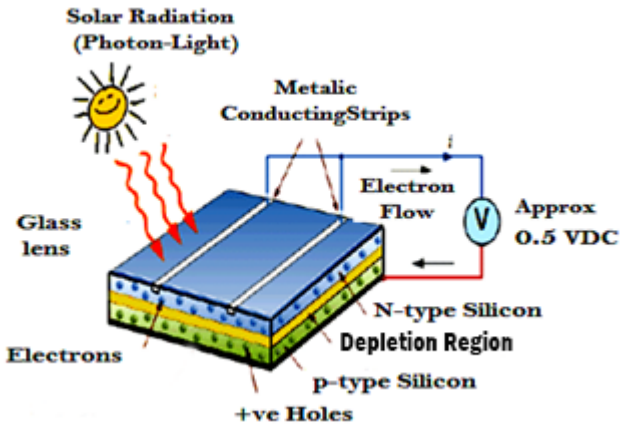

Figure 2. 11: Structure of crystalline silicon solar cell [48]**.**

In the absence of illumination, a PV cell functions like a conventional semiconductor diode, allowing current flow from the p-type to the n-type layer under forward bias. Upon light exposure, photon absorption generates electron-hole pairs, resulting in a photocurrent (I_{Ph}) that varies in proportion to the irradiance. Light-generated current is directed from the n-type to the p-type region. Theoretically, an ideal solar cell can be represented as a current source in parallel with a diode [49]. However, inherent material and design imperfections introduce additional elements, such as series resistance and shunt resistance, which influence the overall performance of the PV cell. This is illustrated in Figure 2.13 (b). In Figure 2.12, series resistance (R_s) is represented by Rseries, which is in series with the PV cell, and shunt resistance (R_{sh}) is shown as Rshunt, which provides a leakage path across the junction. In Figure 2.13 (b), the effects of these losses are visualised in the I-V curve, where series resistance losses cause a voltage drop, shifting

the curve leftward, and shunt losses reduce the current output, affecting the overall module efficiency.

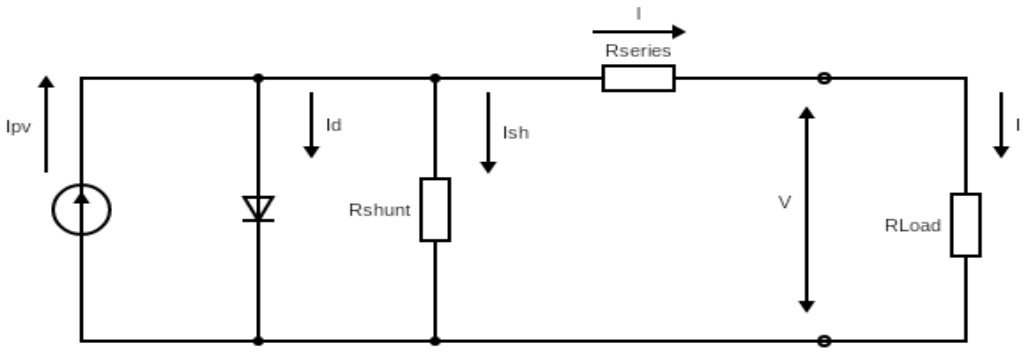

Figure 2. 12: Equivalent circuit diagram of a PV cell, illustrating series and shunt resistances with a single-diode model.

When illuminated, the output current (I) of a real PV cell can be expressed using the single-diode equation [50]:

$$I = I_{ph} - I_s(e^{\frac{q(V+IRs)}{nkT}} - 1) - (\frac{V + IR_s}{R_{sh}}) \quad \text{(eq. 13)}$$

where, I_{Ph} is the photogenerated current, V is the output voltage, I_s is the dark saturation current, q is the elementary charge, n is the diode ideality factor, k is the Boltzmann constant, and T is the absolute temperature in Kelvin.

PV cells and modules are assessed under Standard Testing Conditions (STC) [51], which consist of normal incidence of solar simulated irradiance of 1000 W/m², cell temperature 25°C and air mass 1.5 solar spectrum. These conditions provide a uniform benchmark for

comparing different PV modules. Figure 2.13 (a). illustrates the I-V curve and P-V curve for a photovoltaic module under STC.

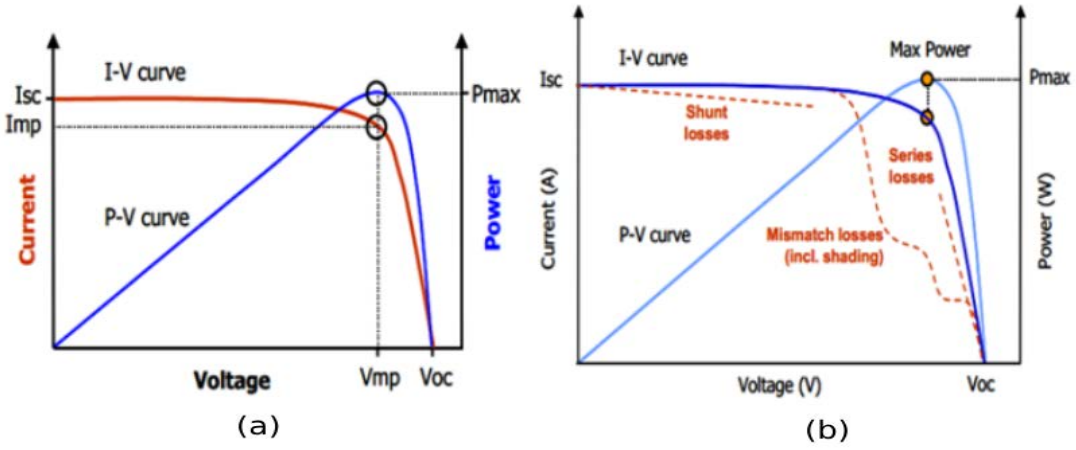

Figure 2. 13: (a)Module I-V Curve under STC versus (b)Real-World Losses [52]**.**

The I-V curve of a PV module demonstrates that no power is produced when the module is in either an open or short circuit state. The Maximum Power Point (MPP) or where output power is maximum (Pmax), is defined as [52]:

$$P_{MPP} = V_{MPP} \times I_{MPP} \quad \text{(eq. 14)}$$

where V_{MPP} and I_{MPP} are the voltage and current at the maximum power point, respectively. The MPP is the point on the IV curve of a PV module where the product of I and V is maximised, resulting in the highest possible power output.

The performance of a PV module is influenced by both irradiance and module temperature. At constant irradiance, an increase in module temperature results in a decrease in maximum power output, as higher temperatures reduce the module's voltage, thereby decreasing its overall efficiency. This relationship is shown in Figure 2.14. Conversely, when module temperature is constant and irradiance increases, the maximum

power output rises. This is because higher irradiance supplies more energy for conversion, leading to an increase in current. Figure 2.14 illustrates these effects, demonstrating the positive correlation between irradiance and power output [53].

It is essential to consider these factors when designing and optimizing PV systems to ensure maximum energy yield under varying environmental conditions.

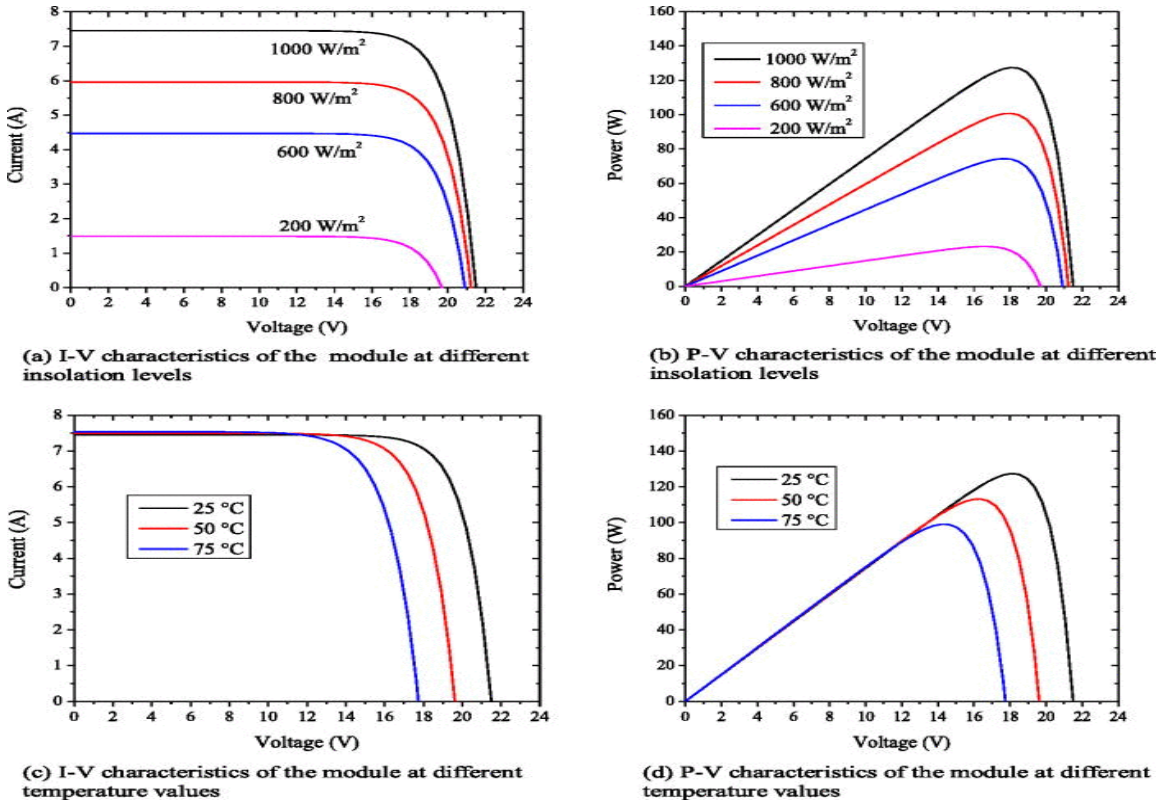

Figure 2. 14: IV and Power Curves for varying irradiance and temperature [53]**.**

2.2.3.1.2 Photovoltaics Module Technologies

PV panels are constructed from various semiconductor materials. These modules can be broadly classified into several categories, the most prominent being crystalline silicon, thin-film, and advanced technologies such as c-Si bifacial and half-cut solar cell modules.

Each type possesses unique electrical and optical characteristics, making them suitable for different environments and applications [54].

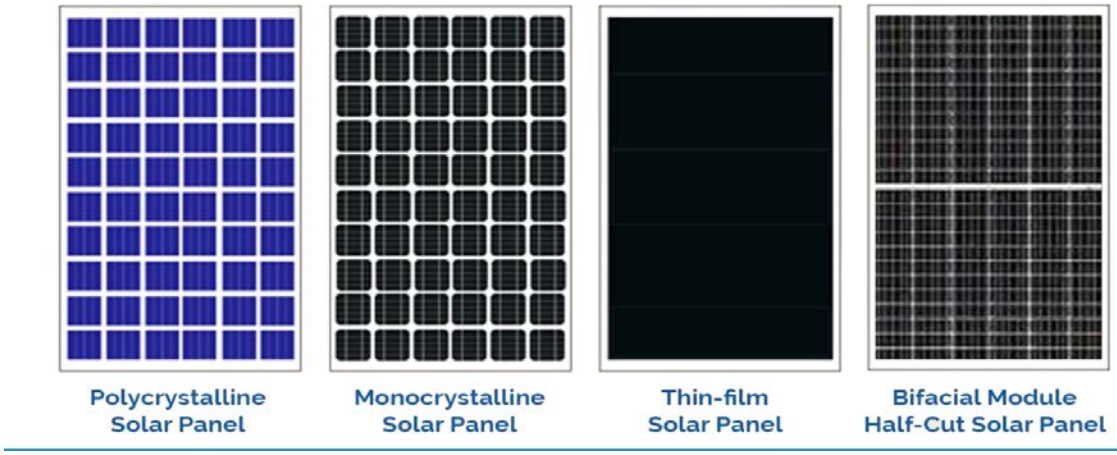

Figure 2. 15: Different Types of Solar Panels

Crystalline Silicon Solar Panels

- Crystalline silicon solar panels, which include monocrystalline and polycrystalline types, are known for their high efficiency, typically ranging from 15% to 23%, as shown in Figure 2.16. Monocrystalline panels, the most used panels shown in Figure 2.17 are produced using the Czochralski method, where a single continuous crystal structure, called an ingot, is formed. This method offers higher efficiency but comes at a higher cost due to its complex production techniques. Poly-c-Si panels are made from silicon crystals that are melted together and poured into a square mould. They are more cost-effective but slightly less efficient. These c-Si panels possess a long operational lifespan, often exceeding 30 years. They dominate the market due to their reliability and performance, typically supported by a manufacturer's performance warranty of 25 years. After this period, it

declines every year from day one. However, they continue to function beyond the warranty period [55][56].

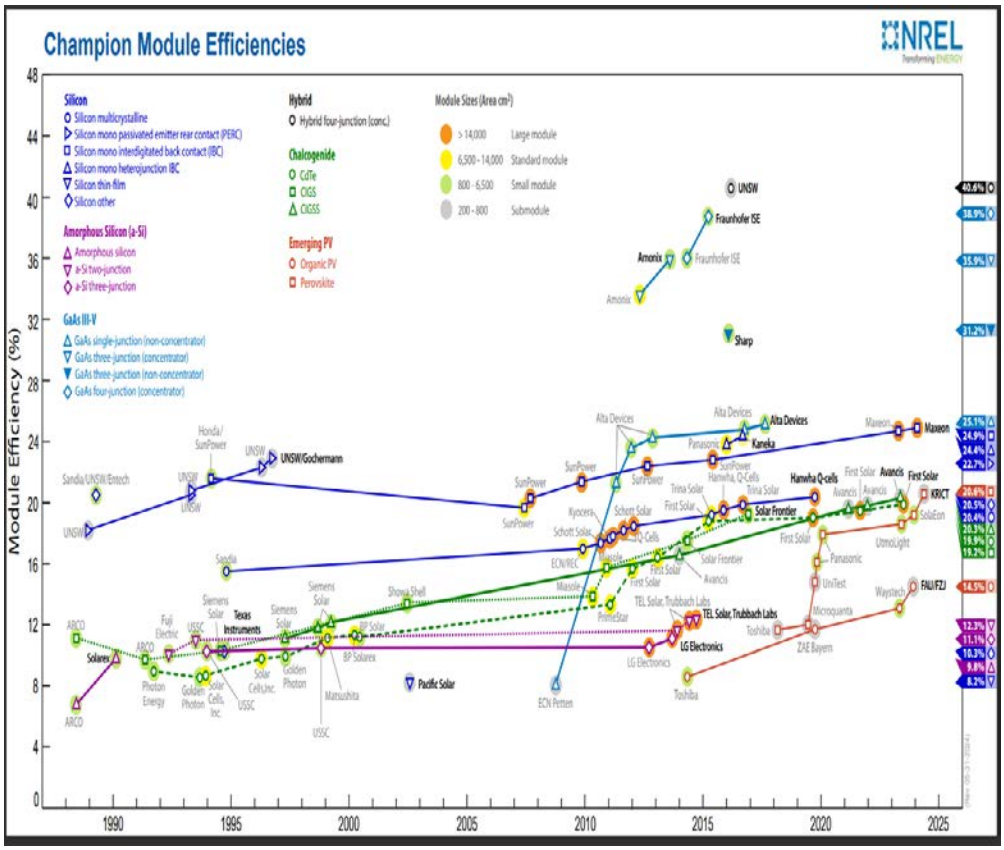

Figure 2. 16: Module Technology Efficiencies and their improvement over the years [57]

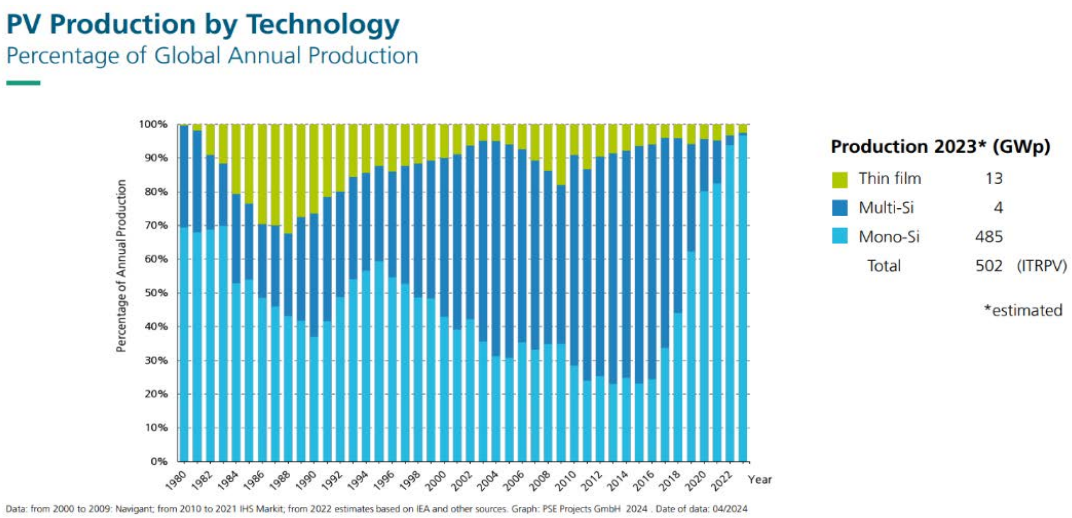

Figure 2. 17 PV Production by Technology and Year [57]

Thin Film Solar Panels

- PV panels manufactured by depositing photovoltaic materials such as cadmium telluride, amorphous silicon, or copper indium gallium selenide onto substrates like glass, metal, or plastic are known as Thin Film solar panels. They have lower efficiencies, ranging from 10% to 12%, though advanced models can reach up to 18%. These panels have lower production costs and perform better in low-light conditions and elevated temperatures. However, they typically have a shorter lifespan of 10-20 years and because of their lower efficiencies they require more space to generate the same power output compared to crystalline silicon panels [58].

Bifacial Half-Cut Cell Solar Panels

- Bifacial half-cut cell solar panels combine the benefits of bifacial and half-cut cell technologies, achieving efficiencies that can exceed 22%. Bifacial panels capture light from both sides, increasing the energy yield, while half-cut cells reduce resistive losses by halving the current, the power losses are reduced to one-quarter of those

experienced by full-sized cells. Additionally, the smaller size of half-cut cells makes them less prone to cracking, enhancing the overall reliability of the module. Furthermore, the module is divided into two parallel sections. Instead of all cells being in series, the module contains two parallel subpanels that divide and recombine at the module terminals (Figure 2.18), which improves shade tolerance, allowing the module to maintain higher energy output even when partially shaded. Although these panels have higher initial costs due to advanced manufacturing techniques, they offer higher energy yields, improved durability, and better performance in various conditions [59][60].

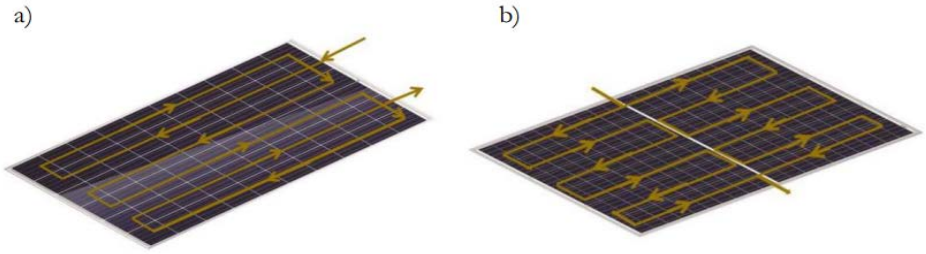

Figure 2. 18: Circuit configuration in (a). Traditional panel VS (b). Half-Cut cell panel [61]**.**

2.2.3.2 Mounting Structures

The method of installing PV modules significantly impacts both the performance and cost of a photovoltaic system. Single-axis tracking, and Fixed Tilt PV Systems are considered the most commonly used ground-mounted systems [62]:

- **Single-Axis Tracking:** Arrays are mounted with a permanent tilt angle but include a tracking mechanism that follows the sun's movement from east to west daily. Modern

single-axis trackers typically rotate around a horizontal axis, which can be aligned in a north-south or east-west orientation. Some systems also incorporate backtracking, a loss-mitigation technique that optimises the positioning of module rows to prevent inter-row shading, especially when the sun is at low elevations.

- **Fixed Tilt:** Arrays are constructed with a fixed tilt and an azimuth angle. PV designers often use the site latitude as the optimal tilt angle and orient the azimuth angle towards the equator, north for locations in the southern hemisphere and south for those in the northern hemisphere.

Figure 2.19 provides a schematic representation of these mounting methods. Additionally, Figure 2.20 compares the output power generated by a PV system with a tracking system to that of one without a tracking system [63].

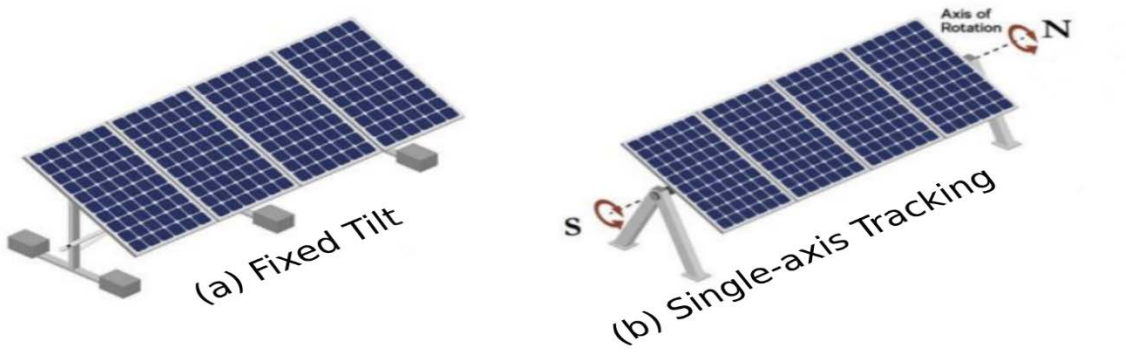

Figure 2. 19: Common Mounting Methods

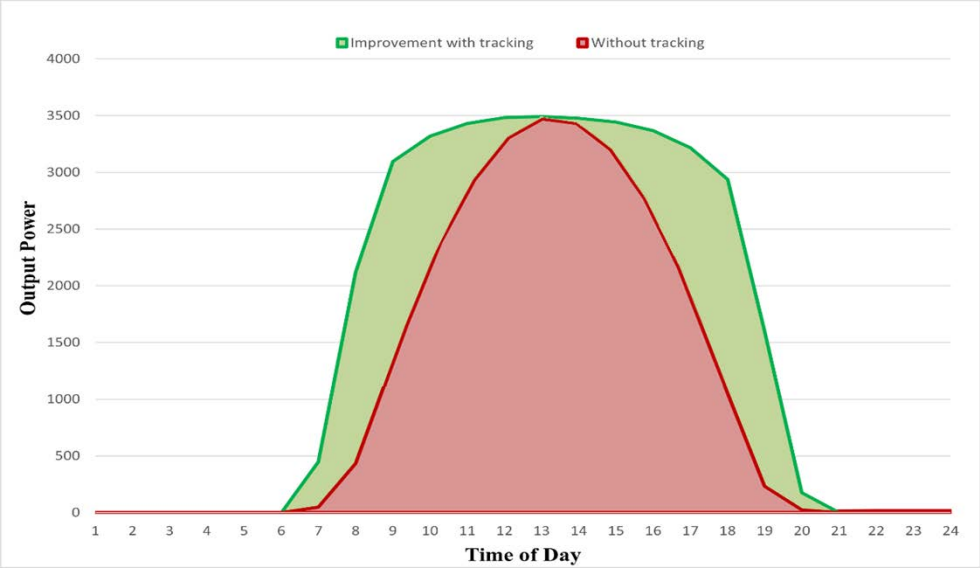

Figure 2. 20: Comparison of output power generated with single-axis tracking system and without any tracking system

2.2.3.3 Storage (Battery Technology)

Batteries, although optional and commonly known as battery banks, are becoming essential components in PV plant systems. They address the intermittent nature of solar power generation. In this research, the battery ensures that the system supplies the load demand as fully as possible. Several important battery parameters must be considered when selecting a battery [64][65][66]:

- **Capacity:** The amount of energy a battery can store is referred to as the battery's capacity, typically measured in ampere-hours (Ah). Capacity determines how long a battery can power a load before needing to be recharged.
- **Round trip Efficiency:** The ratio of the energy output to the energy input in recharging the battery, often expressed as a percentage. Greater efficiency results in reduced energy loss during both the charging and discharging processes.

- **Depth of Discharge (DoD):** The proportion of the battery's capacity that has been used relative to its total capacity. Higher DoD can shorten the battery's life but allow for more energy usage per cycle, and batteries tend to have longer life when the DoD is lower.
- **Charge/Discharge Rate:** Typically expressed in C-rate, C-rate is a relationship between charge/discharge current and time. Higher rates allow for faster energy transfer, which can be critical during peak demand periods.

2.2.3.4 Charge Controller

Charge controllers manage the voltage and current produced by PV panels to ensure efficient and safe battery charging, while also preventing overcharging and deep discharging. By optimising the charging process according to the battery's state of charge, charge controllers extend battery life and improve the stability of the energy storage system. Charge controllers can have PWM (Pulse Width Modulation) or MPPT (Maximum Power Point Tracking) capability. PWM charge controllers are simpler and more affordable, but they are less efficient as they reduce the voltage from the panels to match the battery's voltage. On the other hand, MPPT charge controllers are more advanced and efficient, as they adjust the voltage to maximise the power output from the solar panels, especially in varying weather conditions [67][68].

Table 2.6: Advantages and Disadvantages of MPPT and PWM charge controllers.

Controller Type	Advantages	Disadvantages
MPPT	High charging efficiency.	It is more expensive compared to PWM controllers.
	It can be used with 60-cell panels.	Shorter lifespan due to more electronic components and greater thermal stress.
	Flexible in choosing the size of the PV array.	
PWM	It is cheaper and simpler in design than MPPT.	The PV array and battery bank must be accurately sized.
	Smaller size.	

2.2.3.5 Solar Inverter

Solar inverters convert the direct current electricity generated by solar panels into alternating current electricity. Solar inverters are essential components, enabling grid connection and energy distribution of the electricity generated by the PV system. Although DC can be used within a PV plant, AC is the more practical and cost-effective choice for grid integration. In systems like the Tsau //Khaeb National Park hydrogen project, AC is preferred because it offers better control and compatibility with energy storage and grid-tied systems. Solar inverters ensure system stability, regulatory compliance, and efficient operation of electrolysers and other loads. Solar inverters in grid-connected installations must meet two key types of requirements, namely [69]:

- **Performance requirements:** installation cost, high efficiency, minimisation of leakage current and power density.
- **Legal requirements:** anti-islanding detection, galvanic isolation, and compliance with technical standards such as IEEE 1547 (for interconnection), IEC 62109 (safety), and VDE-AR-N 4105 (Germany-specific grid compliance).

2.2.3.6 DC and AC cables

In PV plant systems, DC cabling is used to connect solar modules to the inverters, facilitating the transfer of direct current generated by the panels. In contrast, AC cabling links the inverters to the other electrical equipment in the PV plant, managing the alternating current following conversion. The cables used in solar projects must adhere to both international and local standards applicable to these installations. The DC cable selection criteria can be defined by three key parameters [70]:

- **Cable voltage rating:** Chosen cables should be capable of withstanding the voltage output of the connected modules.
- **Current carrying capacity:** The cable should be appropriately sized to handle the maximum current under worst-case conditions.
- **Voltage drops:** Minimising energy losses is essential for the success of PV system projects. Therefore, minimising voltage drops in the cables is essential, a 3% drop is considered acceptable, however, achieving losses of 1% or less is feasible.

Essentially, cables used in a photovoltaic solar plant need proper protection to withstand specific site conditions, including sunlight, moisture, and heat [70].

2.2.4 Photovoltaic Plant Performance Parameters

Performance parameters in PV systems serve as key performance indicators, evaluating a PV plant's technical and financial performance. These indicators are utilised to pinpoint ways to improve the reliability and performance of a PV system, ultimately boosting yield and profitability [71]. The most important performance metrics are:

2.2.4.1 Energy Production

One of the most common methods for assessing a PV plant's performance is by measuring the energy produced over a specific period. The energy production metric is defined as the total amount of energy generated by a PV plant during a given period. Energy production is affected by various factors, such as the amount of irradiance received by the PV panels, the temperature of the panels, the PV panel's efficiency, the conversion efficiency of the inverter, and losses incurred during energy generation and transmission. In theory, energy production is determined by multiplying the total system power output by the duration of the period [72].

$$E_{AC}(kWh) = P_{sys}(kW) \times t(h) \text{ (eq.15)}$$

2.2.4.2 Specific Yield (SY)

SY compares the actual energy production of a PV system to its installed nominal capacity, standardising performance comparisons across different PV technologies and designs. SY is expressed in kWh/kWp and represents the AC energy output per unit of DC installed power. It essentially reflects the number of hours the PV plant must operate at its nominal (maximum) power output to generate the same amount of energy produced over a defined period, typically one year. Theoretically, SY is calculated as the ratio of the AC energy output to the installed nominal power under standard test conditions (STC) [73].

$$SY(kWh/kW_p) = \frac{E_{AC}(kWh)}{P_{STC}(kW_p)} \text{ (eq. 16)}$$

2.2.4.3 Performance Ratio (PR)

These parameters assesses the quality of a PV plant. PR indicates the fraction of DC energy produced from incident solar radiation that is delivered to the grid or, in the case of an off-grid system, to the user or load [74]. This is mathematically represented by:

$$PR(\%) = \frac{E_{AC}}{\eta \times (A_{mod}) \times (Energy\ incident\ on\ generator\ surface)} \quad \text{(eq.17)}$$

where E_{AC} is the energy exported to the grid (for off-grid E_{AC}, will be replaced by $E_{\text{to user}} - E_{\text{backup}}$) and is given in kWh, η is the module efficiency at STC, A_{mod} is the area of the module and is given in m^2, Energy incident on generator surface, given in kWh m^{-2}, represents the solar radiation received by modules during the assessment period.

2.2.4.4 Capacity Factor (CF)

The ratio of the actual energy output to the energy the generator would output if it ran at its design power all the time is known as the CF, and is expressed as a fraction or percentage. A higher capacity factor indicates better utilisation of the PV system's potential [75]. CF is given by:

$$CF = \frac{E_{AC}(kWh)}{P_{STC}(kW_p) \times t(h)} \quad \text{(eq.18)}$$

2.2.4.5 Levelised Cost of Energy

This serves as a comprehensive metric for comparing the cost-effectiveness of different energy generation technologies. It considers all costs incurred during a technology's lifetime and correlates them with the energy output produced during the same period. By comparing projects across various technologies, lifespans, and capacities, LCOE provides valuable insights into generation option's competitiveness and proximity to grid parity, where it desired that alternative energy sources generate power at an LCOE equal to or lower than the grid electricity price [76]. The LCOE can be obtained (eq.19):

$$LCOE = \frac{Total\ Lifetime\ Cost}{Total\ Energy\ output} = \frac{\sum_{t=0}^{n} \frac{C_{capex_t} + C_{OM_t} + F_t}{(1+d)^t}}{\sum_{t=0}^{n} \frac{E_t}{(1+d)^t}} \quad \text{(eq.19)}$$

where C_{capex_t} represents the investment cost (or capital expenditure) in year t, C_{OM_t} denotes the operational expenditure in year t, F_t is the fuel expenditure in year t, Et is the energy generated in year t and the discount rate is denoted by d.

LCOE is a critical metric for assessing the economic viability of PV systems, particularly when compared to other energy-generating technologies. The LCOE calculation is rooted in discounted cash flow analysis, which accounts for the time value of money by discounting future costs and revenues. This method incorporates the Net Present Value (NPV) of all lifetime costs associated with the system, including the initial capital investment, operations and maintenance costs, and fuel costs (if applicable). Additionally, factors such as the discount rate, which reflects the weighted average cost of capital (WACC), and considerations for inflation rates are included to provide a more accurate economic assessment [77]. LCOE serves as a comprehensive measure, enabling

stakeholders to compare renewable energy technologies with conventional power plants across various locations.

The global weighted average LCOE for large PV systems has shown a notable decline. According to a report by [78] , the LCOE for large PV systems in 2022 was 0.047 €/kWh (47 €/MWh), continuing a long-term trend of a 15% annual reduction over the past 12 years (Figure 2.30). The report highlights the variation in costs, with the 95th percentile reaching 0.114 €/kWh (114 €/MWh), reflecting differences influenced by factors such as project location, size, and specific conditions [78].

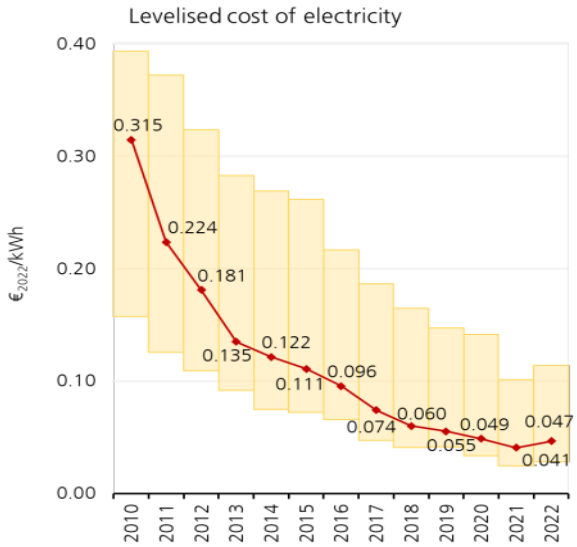

Figure 2. 21: Global Weighted Average LCOE for Large PV Systems [78]**.**

The report further shows by 2030, the cost of generating electricity with a PV and battery system is anticipated to be lower than that of a combined cycle power plant. Furthermore, by 2040, even small PV-battery systems are expected to achieve an LCOE ranging between 5 and 12 euro-cents per kilowatt-hour (€Cent/kWh), as illustrated in Figure 38 [77].

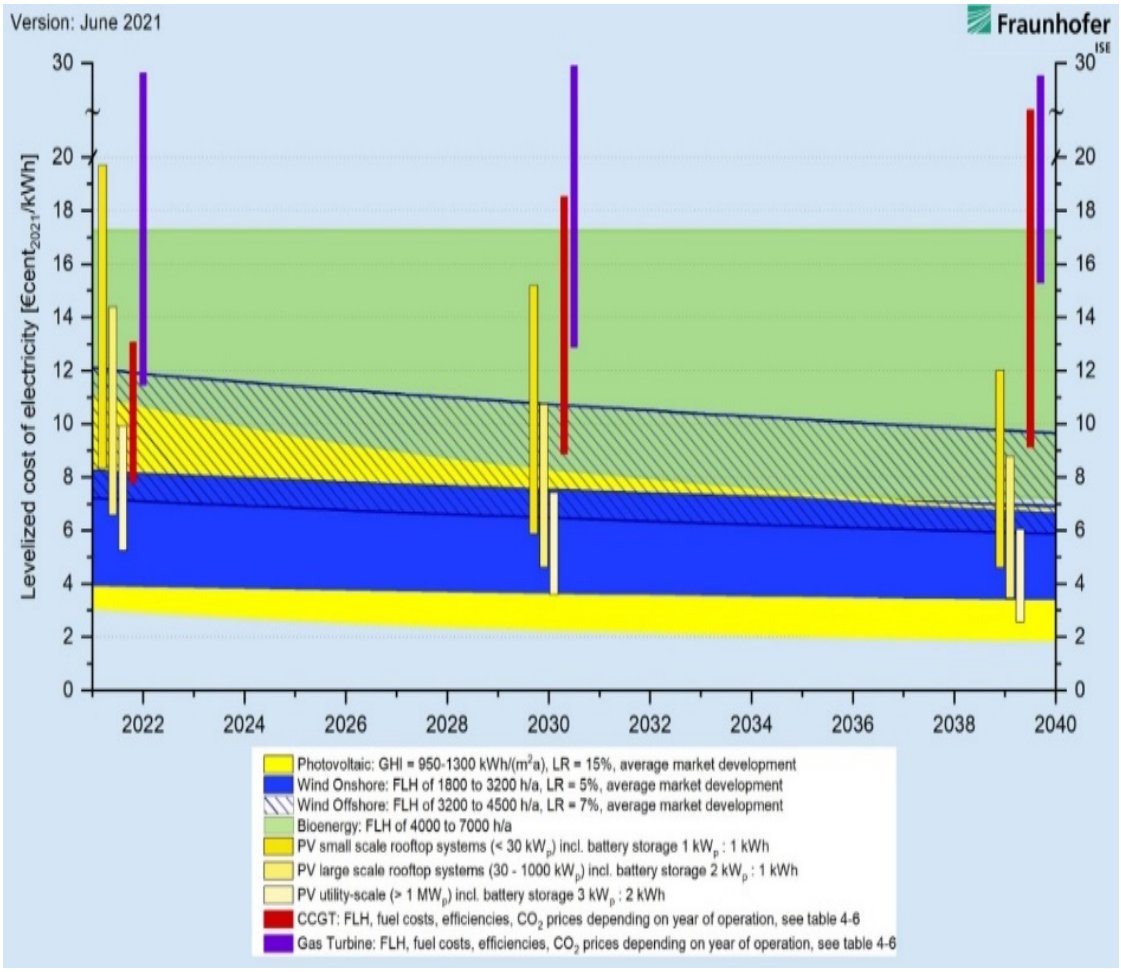

Figure 2. 22: LCOE Forecast for different energy technologies [77]**.**

In the context of the SCDI Green Hydrogen Project, which includes energy storage, understanding the LCOE of the PV system becomes essential, as it directly impacts the overall cost of hydrogen production via electrolysis. Factors influencing LCOE in PV systems are summarised in Table 2.7.

Table 2.7: Factors influencing LCOE in PV system.

Factor	Details
1. Capital Expenditure (CAPEX):	
Initial Costs	Includes costs for PV modules, inverters, mounting structures, BoS components, installation, and grid connection fees.
Financing	Interest rates and terms of loans impact overall CAPEX and LCOE. Favourable financing can reduce LCOE by lowering the cost of capital.
2. Operational Expenditure (OPEX):	
Maintenance	Ongoing costs for cleaning, repairs, and monitoring. Effective maintenance can enhance performance and longevity, reducing LCOE.
Insurance and Land Use	Costs for ensuring the PV system and leasing or purchasing land. Varies based on location and project scale.
3. System Efficiency	
PV Module Efficiency	Higher efficiency leads to greater energy output, reducing LCOE.
Inverter and System Losses	Minimising losses in inverters and system components increases efficiency and reduces LCOE. Efficient design and component selection are crucial.
4. Energy Yield	
Solar Irradiance	Directly proportional to energy yield. Higher irradiance levels result in greater energy production and lower LCOE. Accurate site assessment is essential.
Degradation Rate	Affects total energy output over time. Lower degradation rates lead to higher long-term energy production and lower LCOE.
5. Economic and Financial Factors	
Project Lifespan	Expected operational life affects total energy produced and LCOE. Longer lifespans spread initial investment over more years, reducing LCOE.
Incentives and Subsidies	Government incentives, such as tax credits or feed-in tariffs, can lower LCOE by reducing initial costs or increasing revenues.

2.2.4.6 Losses

Analysing losses is essential for evaluating the performance of a PV plant, as it helps identify incorrect configurations or faults within the system. Typically, these losses arise from suboptimal operating conditions, inadequate system design, and inherent inefficiencies of PV components.

2.2.4.6.1 Shading losses

These occur in PV systems when obstructions block sunlight from reaching the solar panels. In utility-scale PV plants, these obstructions can include nearby objects like buildings, trees, and poles, as well as self-shading from other PV panel rows or horizon shading from the surrounding terrain. Shading losses can be reduced by performing thorough due diligence during the site selection process. Minimising shading losses is challenging in areas with limited land. In regions like Europe, close row spacing is common due to high land costs, prioritising surface efficiency over peak power [79]. However, where land is abundant, designers must optimise row spacing and tilt angles to reduce inter-row shading. Typically, Industry acceptable shading loss is around 2.5%. If the loss factor exceeds this threshold, the system is considered suboptimal. While alternative methods exist to mitigate shading losses [80] and [81], optimising inter-row spacing remains the most employed approach. Equation 20 mathematically optimises inter-row spacing to minimise shading between rows.

Figure 2.23 illustrates the key variables involved, including the solar altitude angle, module tilt angle, and shading length.

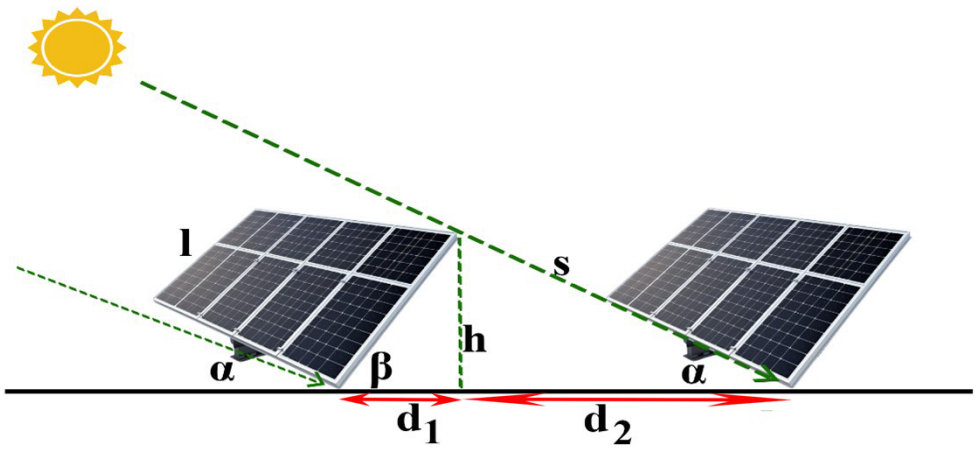

Figure 2. 23: Illustration of Key Variables in Inter-Row Spacing Optimisation for PV Arrays

$$d = d_1 + d_2 = l\,cos\beta + s\,cos\alpha = l\,cos\beta + \frac{h}{sin\alpha} = l\,cos\beta + l\,sin\beta\,cot\alpha \quad \text{(eq.20)}$$

In this analysis, the following parameters are defined:

α: Solar altitude angle.

β: Tilt angle of the PV module.

l: Length of the PV module.

h: Vertical height of the module above the ground due to the tilt.

$\boldsymbol{d_1}$**:** Horizontal distance from the base of the PV module to the point where its shadow falls on the ground, considering the solar altitude angle.

$\boldsymbol{d_2}$**:** Shading distance, which is the horizontal gap between the end of one module's shadow and the beginning of the next module.

s: Shadow length cast by the PV module on the ground.

2.2.4.6.2 Incidence Angle Modifier (IAM) Losses

These losses refer to the reduction in solar energy captured by the PV panels due to reflections caused by non-normal incidence angles. When sunlight strikes the glass cover of a PV panel at a large angle, more light is reflected away, reducing the amount of energy that reaches the cells. These losses increase as the angle of incidence deviates further from the perpendicular. To mitigate IAM losses, some PV panels are equipped with anti-reflective coatings (ARC). These coatings have a refractive index that is intermediate between the refractive indices of the glass and the silicon, which helps reduce reflections and improve light absorption. Typically, IAM losses range from 3% to 4.5% of the incident irradiance and are related to the tilt and orientation losses [82].

2.2.4.6.3 Soiling losses

Soiling losses occur when dust, dirt, snow, and other contaminants accumulate on the module surface, reducing the amount of sunlight reaching the PV cells. This reduction in sunlight leads to a direct decrease in energy production and overall efficiency. These losses can be estimated through field measurements and simulations. Regular cleaning, the use of hydrophobic coatings, and site-specific strategies are essential to minimise these losses and optimise PV system performance [83].

Current research quantifies soiling effects and develops predictive models based on soil types, climatic factors, and module characteristics [84]. An alternative, cost-effective method for estimating soiling losses involves using monthly precipitation levels. For instance, a study by [80] in South Africa used precipitation data to estimate soiling losses, demonstrating its effectiveness as a practical estimation approach.

2.2.4.6.4 Thermal losses

The efficiency of a solar module is typically specified based on STC, which assumes a cell temperature of 25°C as mentioned in Section 2.2.3 . In practice, the temperature of the cells often deviates from this standard. When modules operate at temperatures exceeding the standard, their efficiency declines. These temperature-related decreases in efficiency are known as thermal losses. Thermal losses are assessed by examining the energy balance between the module cell temperatures during operation and the ambient temperature [85].

2.2.4.6.5 Mismatch Losses (ML)

Variations in current output among modules connected in a series string result in ML. Even when using PV modules of the same model, slight differences in their electrical properties, such as I-V characteristics, are inevitable. In series configuration, the current of the entire string is determined by the module with the lowest output, leading to a decrease in total power generated. This reduction is called mismatch loss [86]. Quantifying mismatch losses can be challenging, therefore, statistical sampling is often employed, particularly when using simulation software [87].

2.2.4.6.6 DC Ohmic Losses

Resistance within the cables connecting the PV panels results in DC ohmic losses. These losses also arise from the transition resistance found in terminal connections and fuses. Furthermore, in larger PV plants, it is crucial to take into account the ohmic losses in the cables extending from the combiner boxes to the inverters, as each string usually does not connect directly to an inverter [88]. Additionally, voltage drops can occur due to

differences in cable lengths and cross-sectional areas among parallel strings. These factors can contribute to mismatch losses. As a result, it is a widespread practice to combine DC ohmic losses and mismatch losses into a single value for simplicity and clarity [89].

2.2.4.6.7 Inverter Losses

Inverters incur losses mainly from ohmic and switching losses in their semiconductor components, additionally, if they operate at lower loads like in mornings, later afternoons, and in cloudy conditions [90].

2.2.4.6.8 AC Ohmic and Transformer Losses

Energy losses in AC wiring occur during the transmission and distribution of AC electricity between the solar inverter output and the utility meter, primarily due to Ohmic losses in conductors and additional losses within transformers, which ultimately reduce the energy delivered to the grid [91]:

2.2.5 Photovoltaic System Simulation Tools

2.2.5.1 Introduction to Photovoltaic System Simulation Tools

PV system simulation software packages integrate complex algorithms, meteorological data, and component specifications to provide comprehensive analysis and forecasting. PV simulation tools are essential for accurate performance modelling and financial analysis of PV systems [92]. These software packages typically offer the following key features, which are summarised in the table 2.8.

Table 2.8: Key Features in Solar PV Software Packages [92]

Category	Key Activities
Performance Modelling	- Estimate energy output based on location-specific solar irradiance data and system design.
	- Account for various system losses, including shading, soiling, temperature effects, mismatches etc.
	- Simulate different module technologies and inverter configurations. -Simulate system performance with high temporal resolution.
Financial Analysis	- Calculate LCOE.
	- Estimate project costs, including construction, maintenance, and operational expenses.
	- Forecast potential revenue from energy sales or savings.
System Design	- Optimize module layout and string configurations.
	- Perform detailed shading analysis.
	- Provide an extensive database of appropriate inverters and a balance of system components.
Advanced Capabilities	- 3D visualisation of PV installations.
	- Integration with energy storage systems.
	- Sector-coupled energy system planning (e.g., combining PV with water pumps).

2.2.5.2 Steps for Modelling and Forecasting PV System Energy Yield

The modelling process of a photovoltaic system and the forecasting of its energy output at hourly or sub-hourly intervals within simulation software are detailed in Table 2.9:

Table 2.9: Steps for Modelling and Forecasting Energy Yield in PV Systems

Step	Description
1. Sourcing Meteorological Data	Obtain high-quality weather data (GHI, DHI, DNI, temperature, wind speed, humidity) from reliable sources and use simulation tools with built-in or custom data.
2. Data Quality Control and Gap Filling	Perform quality checks to identify errors or inconsistencies and fill data gaps to ensure a complete time series for simulation.
3. Solar Resource Assessment	Estimate missing data using decomposition models. Calculate the irradiance on the tilted PV array with transposition models and consider shading from the horizon and nearby objects.
4. PV System Design and Configuration	Define system layout (module type, inverter specs, array configuration), considering tilt angle, azimuth, and tracking systems if applicable.
5. PV Module and Inverter Modelling	Simulate PV module performance with temperature effects and spectral response, IAM and model inverter efficiency across its operational range.
6. System Loss Analysis	Evaluate loss factors: soiling, snow, mismatch, wiring, inverter and transformer losses, Light-Induced Degradation (LID), and age-related degradation.
7. Energy Yield Calculation	Perform time-step simulations (hourly or sub-hourly) for DC and AC power output, and aggregate results to determine monthly and annual energy yield.
8. Performance Ratio and Other Metrics	Calculate performance indicators like specific yield (kWh/kWp) and performance ratio.
9. Financial Modelling	Integrate energy yield predictions with financial models to calculate metrics such as LCOE.
10. Reporting and Visualization	Generate performance reports including energy yield predictions, loss diagrams, and financial metrics. Create visualisations to communicate results to stakeholders effectively.

2.2.5.3 Classification of Solar PV Simulation Software Packages

There are numerous solar PV simulation software packages available, both free and paid. Each software package offers features that make them better suited for specific tasks, and they exhibit vastly different degrees of sophistication, complexity, and capabilities. PV

system designers need to choose appropriate software that aligns with their requirements, is compatible with their platform, and remains within their budget. Additionally, the designer's competence plays a significant role in effectively utilising these tools. These design tools can be classified into five categories, as shown in Table 2.10.

Table 2.10: Solar PV Simulation Software Packages

Category	PV Simulation Software
Free Software	HOMER Legacy v.2.68, SAM, HYBRID2, SKELION, RETScreen, PVLib
Proprietary Software	PV*SOL, Fraunhofer Zenit ,PVsyst, , PV Sol Premium, PVscout 2.0 Premium, PVComplete, PV F-Chart, Homer, EasySolar, PolySun, Solarmapper, SolarPro, HELIOS 3D Solarparkplanung, Plan4Solar PV
Tools Online	**Free:** PVWATTS, DIAFEM, EASY-PV, PV*SOL, PV-GIS, SISIFO **Paid:** SolarGis PV Planner, Solar Analytics, Helioscope, SolarDesignTool, Focus Solar, SOLARPlus, Aurorasolar, PolySun, Solarmodel, EasySolar
Inverter Manufacturer Tools	SMA Sunny Design, ABB (Power One), Samil Power Design, Mastervolt, Fronius, Kaco, Ingecon Sun Planner, SolarInfo Design Software, Satcon Configurator, Goodwe EZDesigner

Chapter 3

PV System Design and Simulation

This chapter provides a detailed design of PV systems that can supply 40% of the energy demand of the electrolysers [4] needed at the Tsau //Khaebs Green Hydrogen production plant in Namibia. It includes an analysis of the criteria for component selection, followed by a presentation of the engineering and financial computations conducted. Furthermore, the chapter addresses the inherent limitations, assumptions, and simplifications in the methodological approach.

3.1 Simulation Software Selection

As introduced in section 2.2.5, several commercially available PV simulation software packages exist. This research, however, will only utilise two software packages, namely PVsyst and the Fraunhofer Zenit software. PVsyst, a widely recognised commercial software developed in Switzerland, is utilised across various scales of PV systems, from residential rooftops to large-scale installations. It offers key features such as site analysis, system sizing, and energy production evaluation, supported by extensive databases such as Meteonorm for solar irradiance and PV components. Professionals, including engineers, architects, and researchers, rely on PVsyst for tasks like assessing energy yield, optimising system configurations, and identifying suitable installation sites. The software is available with both a paid license and a free trial [93]. In contrast, the Fraunhofer Zenit software, developed by the Fraunhofer Institute, serves a specialised scientific purpose and is not accessible for general commercial use. It is primarily used by researchers at

Fraunhofer to cross-validate results from other PV simulation tools, focusing on rigorous evaluation of PV system performance beyond commercial viability. This scientific approach ensures robust analysis, making Zenit valuable for quality assurance and benchmarking [94]. Table 3.1 outlines some differences between PVsyst and Zenith.

Table 3. 1: Difference Between PVsyst and Zenith

PVsyst Version 7.4.7	**Fraunhofer Zenit software**
Meteorological Data: Typical: Meteonorm monthly values. 1-hour steps.	Meteorological Data: Typical: SolarGIS monthly values with artificial dynamics. ¼ hour steps.
Total irradiance on a tilted plane: free to choose	Total irradiance on a tilted plane is always Perez (90) compared Hay/Klucher. Ray Tracing Model
Module model: 1-diode model	Module model: MPP based
Soiling: monthly values	Soiling: estimation based on climate zone
Snow: seasonal soiling	No snow calculated
Storage	No Storage capabilities
Parameters: PAN and OND files	Not applicable
View Factor Model for bifacial panels	Not applicable

PVsyst version 7.4.7 was selected for this study due to its comprehensive capabilities in simulating fixed tilt and tracking technology systems[95], additionally, the software can simulate grid-tied PV systems with battery storage, using three different dispatch strategies: peak shaving, self-consumption, and weak grid. Peak shaving refers to storing excess PV energy during high-generation periods and releasing it during low-generation periods to reduce peak grid injection. Self-consumption focuses on minimising grid reliance by using stored energy to meet demand when PV generation is low, maximising the use of PV energy over the grid. Weak grid provides backup during grid outages by maintaining a reserve battery charge to support critical loads, ensuring stability in weak grid conditions[96]. Lastly, PVsyst has demonstrated competitive accuracy in predicting energy output, with results within 2% of real data for fixed tilt monofacial systems [97] and within 5% for tracking systems[98]. In this study, in addition to Fraunhofer Zenit,

PVSyst's self-consumption strategy and its unlimited sheds and trackers models are utilised. The self-consumption strategy prioritises electrolyser demand over grid injection.

3.2 Site and Horizon

The exact location of the proposed project site was obtained from [3]. However, detailed information about the site is limited. The study conducted a computational site investigation of the proposed site. This investigation included determining the precise coordinates of the two proposed PV system sites, namely the Springbok and Dolphin sites, as well as calculating the total area of each site, the proximity of the sites to the load (electrolyser), the distance between the two sites and determining the topology of the sites, to determine whether far shading will be experienced at the sites. The map provided in Figure 1.1, which had the marked location of the three sites served as a reference for this investigation, which was conducted using Quantum Geographic Information System (QGIS) software [99].

The study began by adjusting the scale of the map provided in [3], by overlaying it onto the actual map of Namibia. The coordinate reference system was set to UTM Zone 33S with the WGS84 datum to ensure alignment between the provided map and the actual geographic data within QGIS. This step was crucial for accurately georeferencing the map, maintaining consistent scale, and ensuring precision when calculating distances and analysing the topography of the site. This is illustrated in Figure 3.1.

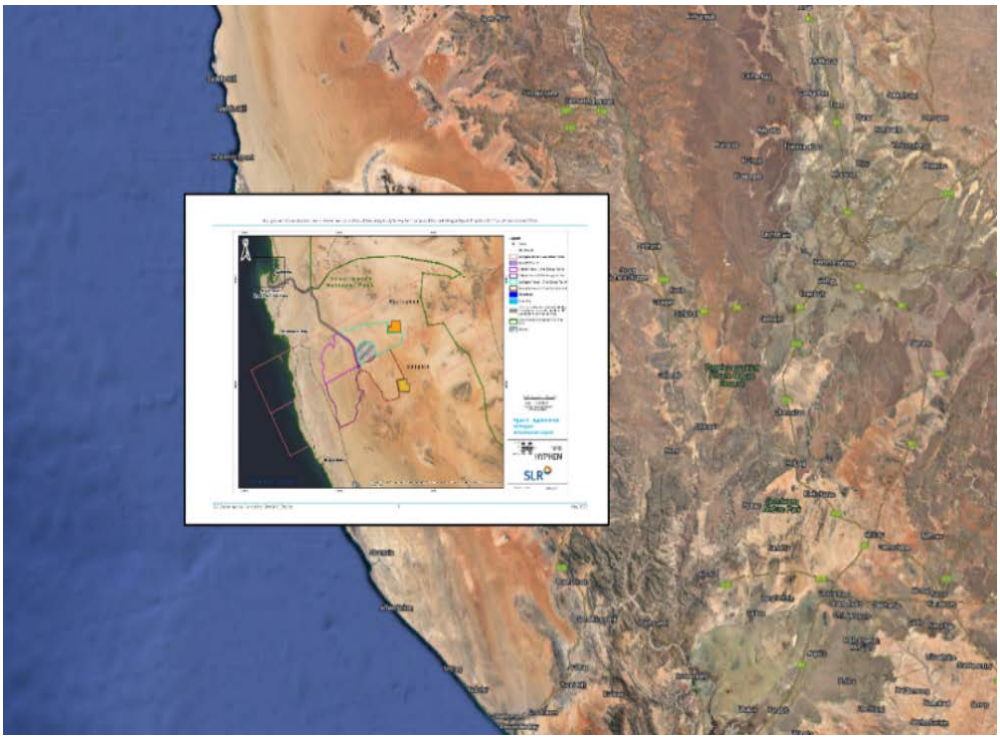

Figure 3. 1: Georeferencing and Scale Adjustment of the Provided Map Using QGIS

The investigation determined the approximate coordinates of the two proposed PV system sites and the electrolyser site. These findings are illustrated in Figure 3.2 and summarised in Table 3.2. As shown in Figure 3.2, mountains are present on the eastern side of the PV plant site. To assess their impact, horizon data from PVGIS were overlaid onto the sun path diagram in Figure 3.3. The resulting red horizon line indicates minimal obstructions, confirming that far shading from these mountains will not significantly affect the plant's performance, so will not be considered in the simulation.

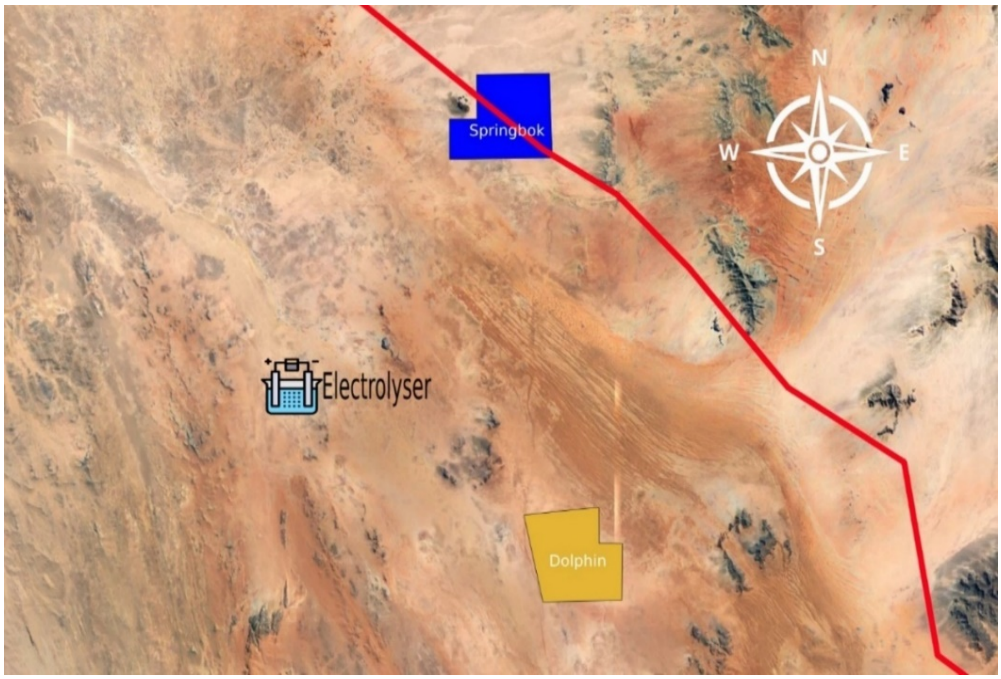

Figure 3. 2: Location of PV System Sites and Electrolyser Site

Table 3. 2: Investigation outcome

Proposed PV system site:	**Coordinates**	**Area Size (km^2) approx.**	**Type of Climate**	**Type of Topology**	**Far Shading**
Springbok Site	Lat: -26.888418° Long:15.800220°	33	Desert	Flat	Minimal
Dolphin	Lat: -27.151717° Long:15.863645°	33	Desert	Flat	Minimal
		Distance from PV sites: approx.			
Electrolyser	Lat: -27.062459° Long:15.614712°	Springbok: 24 km Dolphin: 21.5 km			
Distance between the two sites		23 km			

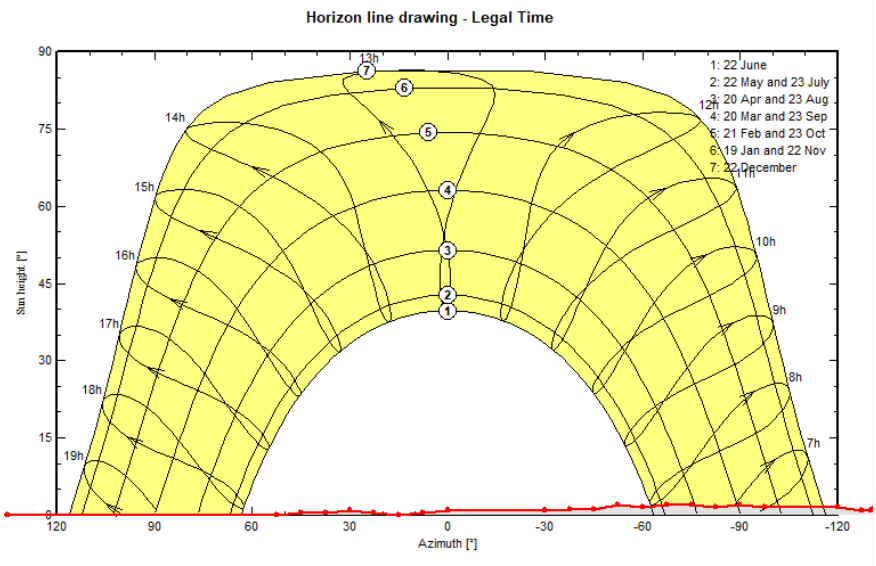

Figure 3. 3: Sun Path Diagram with Horizon Line Overlay for Springbok

3.3 Solar Resource Analysis

Accurate solar resource analysis is vital for reliable PV project simulations, as data quality directly impacts yield predictions. Although ground-based measurements are generally the most precise, the recent installation of weather equipment at Tsau//Khaeb Park has insufficient data, to be used for simulation. Therefore, this research will use satellite-derived data instead.

This study's solar resource data is sourced from SolarGIS for reasons outlined in section 2.2.2.3. To ensure the high quality and reliability of the data, the SolarGIS dataset is compared with other well-established sources, such as Meteonorm, PVGIS, and the Global Solar Atlas. The different solar radiation data sets from various sources for the proposed PV site are shown in Figure 3.4.

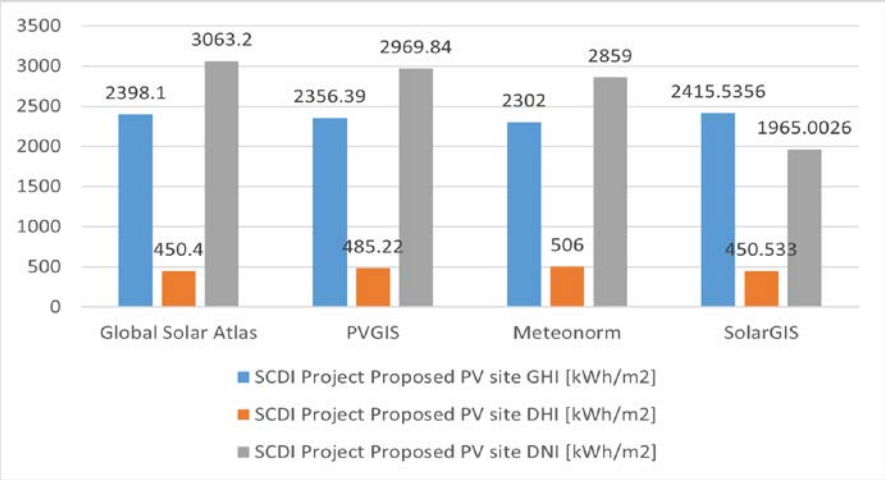

Figure 3. 4: Different Sources of Average Daily Solar Radiation Data for Springbok Site

This cross-verification process helps validate the accuracy and quality of the satellite data and provides confidence in the subsequent performance simulations. The quality data assurance ratio standard, as defined by the Fraunhofer Institute for Solar Energy Systems, states that if the Coefficient of Variation (CV) of GHI data between different solar resources GHI exceeds 4%, the data is considered to be of low quality. Since the available data points are few a table calculation was utilised as shown in Table 3.3, in which the calculation found the standard deviation for GHI (indicated in yellow) to be under 4%, indicating that the quality of the SolarGIS Meteo data to be used in the assessment is of high quality, The mathematical representation for CV used is shown below:

$$CV[\%] = \frac{\sqrt{\frac{1}{n}\sum_{i=1}^{n}(x_i-\mu)^2}}{\mu} \times 100 \quad \text{(eq. 21)}$$

where CV[%] is the standard deviation expressed as a percentage, μ is the mean of the data set (calculated as the average of all data points), x_i represents each data point, n is the total number of points.

Table 3. 3: Coefficient of Variation for various Sources of Solar Radiation Data for PV Site

Irradiation Data origin:						
Data origin:	Global Solar Atlas	Meteonorm 8	PVGIS	Solargis	Average	CV [%]
Global radiation [kWh/m2]:	2398.1	2302	2356.39	2415.5356	2350.5814	2.15
Direct radiation (I_hor) [kWh/m2]:	3063.2	2859	2969.84	1965.0026	1990.37315	25.44
Diffuse radiation (D_hor) [kWh/m2]:	450.4	506	485.22	450.533	360.20825	7.61
Diffuse radiation/ global radiation:	0.19	0.22	0.21	0.19	0.20	7.76
temperature [°C]:	19.9	21.8	19.78	19.3549	21.01391644	5.17

Since the SCDI project involves two sites, as detailed in section 3.2, the study will conduct a solar resource analysis for both the Springbok and Dolphin sites using SolarGIS Meteo data. This analysis aimed to determine if there are significant differences in solar resources between the two sites. This was accomplished using column charts, shown in Figure 3.5. The chart shows that the solar resource values are similar, indicating that the irradiance at both sites is relatively consistent.

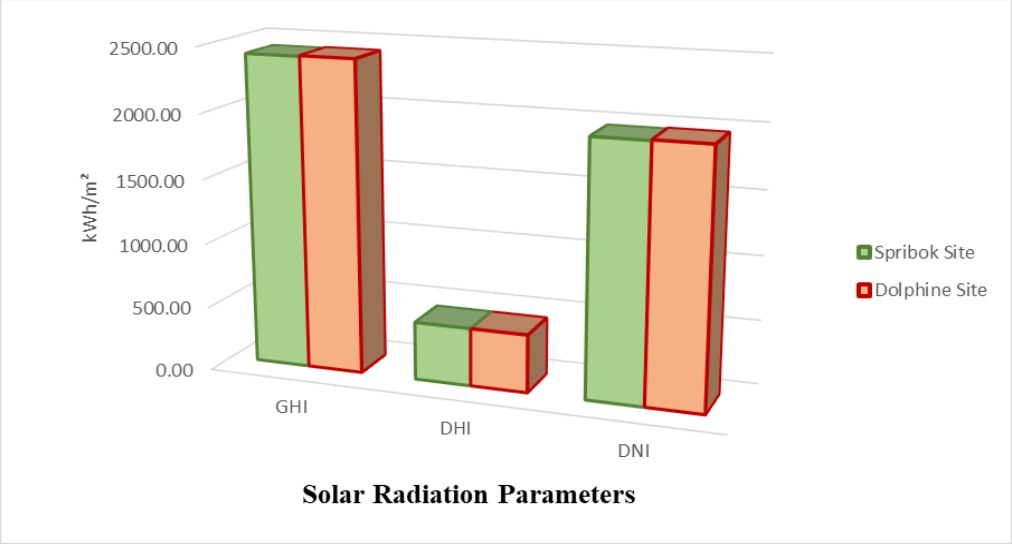

Figure 3. 5: Average daily GHI, DHI and DNI Data for PV Sites

Lastly, monthly albedo values were obtained from the NASA POWER/DAV and SolarGIS databases. The difference between the two datasets was notable, with NASA reporting an average albedo of 29% and SolarGIS reporting an average of 32%. To ensure a conservative approach and given that the default PVsyst value of 30% lies between these

two, this value was selected for the study. This is illustrated in Figure 3.6. This data will help enhance the precision of performance simulations for the system configurations.

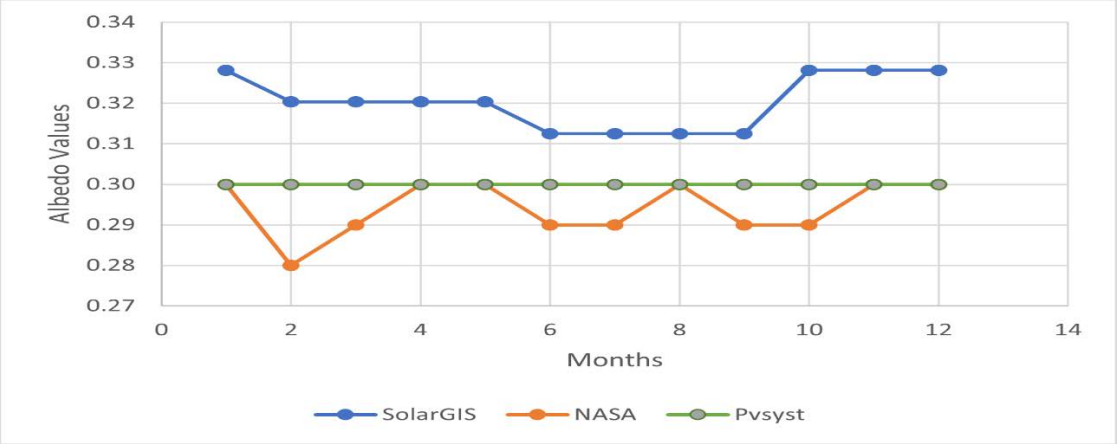

Figure 3. 6 Monthly Albedo Values

3.4 Selection of Electrolyser

In this research, an alkaline electrolyser, specifically the DQ1000 model by John Cockerill Renewables, is selected, as shown in Figure 3.7.

Figure 3. 7: : Photo of the DQ1000 Alkaline Electrolyser

This electrolyser offers efficient and reliable production of green hydrogen, making it suitable for large-scale hydrogen production as the literature indicates [8]. This alkaline

electrolyser is assumed to be the preferred choice for the reasons outlined in Section 2.2, including its cost-effectiveness, technological maturity, and suitability for integration with renewable energy sources, these reasons make it a logical choice for this project. Since the PV plant is expected to supply 40% of the total energy required for hydrogen production, the analysis focuses on this 40% portion which is about 18,082,240 kWh per day, the safety factors are not included in the total amount. The exact total energy demand of the electrolyser remains unknown, and only the energy contribution from the PV system is considered and analysed. This approach allows for a detailed assessment of the PV system's role in meeting the hydrogen production energy requirements. The specifications of the selected electrolyser are presented in Table 3.4 below.

Table 3. 4: Selected Electrolyser Specifications

Specification	Details
Hydrogen Production Capacity	1000 Nm^3/h (2136 kg/day)
Flow Range	40% - 100%
Hydrogen Delivery Pressure	30 bar (g) without compression
Hydrogen Purity Before Purification	99.8%
Hydrogen Purity After Purification	99.999%
Power Consumption (AC)	5000 kW
Stack Consumption (DC)	4.0 – 4.3 kWh/Nm^3 H2
Electrical Converter Power Factor	≥ 95%
Primary Voltage	3.3 – 20 kV (typical 10 kV) (optional up to 34 kV)
Demineralised Water Consumption	0.92 l/Nm^3 H2
Electrolyte	30% KOH aqueous solution
Stack Dimensions (L×W×H)	6.9 m x 2.2 m x 2.2 m
Stack Weight	58,000 kg

3.5 Project Capacity Requirement

The power capacity requirement for the project is determined based on the planned peak hydrogen production target. Various sources provide different estimates for the planned annual hydrogen production, with some suggesting 350,000 tons per year [100] and others

indicating 300,000 tons per year [4]. For this study, the more conservative estimate of 300,000 tons per year has been selected as the basis for calculating the required power capacity to meet 40% of the energy demand from the PV system.

The calculation process is as follows:

1. **Annual to Daily Hydrogen Production:**
    - The annual hydrogen production target of 300,000 tons is divided by 365 days to determine the daily hydrogen production:

$$DailyH_2 = \frac{300\,000\ tons}{365\ days} = 821.92\ tons/day \qquad \text{(eq. 22)}$$

2. **Energy Requirement Calculation:**
    - The energy required to produce one kilogram of hydrogen is multiplied by the daily hydrogen production in kilograms to obtain the total daily energy requirement. The production of one kilogram of hydrogen via electrolysis requires a minimum energy input of 50 to 55 kWh [8]. For this analysis, the upper bound of 55 kWh was selected:

$$Total\ Energy\ (kWh/day) = DailyH_2 \times Energy\ per\ kg\ H_2 = 45205600\ kWh/day$$

(eq. 23)

    - Since only 40% of the total energy is to be supplied by the PV system, this fraction is applied to find the energy required from the PV system:

$$E_{PV\ req}\ (kWh/day) = Total\ Energy\ (kWh/day) \times 0.4 = 18082240\ kWh/day$$

(eq. 24)

3. **Peak-sun-hours Calculation:**
    - To determine the power capacity required, the sun peak hours for the site are calculated by dividing the total irradiance (approximated to $6kWh/m^2$, instead of the $6.4kWh/m^2$ from SolarGIS as a safety factor for any uncertainties the data might have) at the site by the standard test condition irradiance (1,000 W/m²):

$$Sun\ Peak\ Hours\ (hours/day) = \frac{Total\ Insolation\ (Wh/m^2\ day)}{1000\ W/m^2} = 6 \text{ hours/day} \quad \text{(eq. 25)}$$

4. **Power Capacity Rating:**
    - The power capacity rating for the PV system is then calculated by dividing the energy required from the PV system by the peak-sun hours:

$$Power\ Capacity\ (kW) = \frac{E_{PV\ req}\ (kWh/day)}{Sun\ Peak\ Hours\ (hours/day)} = 3013706.67kW \quad \text{(eq. 26)}$$

This systematic approach ensures that the PV system is appropriately sized to meet the project's hydrogen production requirements, considering the project's load demands.

3.6 Components Selection

3.6.1 PV Module

The research considered several key parameters when selecting the optimal module for the proposed project [101]:

- **Low-Temperature Coefficient (Tk P_{mpp})**: Modules with a low-temperature coefficient for maximum power point (P_{mpp}) ensure efficiency across a range of temperatures.
- **High Stability in Hot Temperatures**: Modules that maintain consistent performance and stability in high-temperature conditions to ensure reliability and efficiency.
- **Tier 1 Module Suppliers**: Modules from Tier 1 suppliers to safeguard the warranty. Tier 1 suppliers are generally more stable and less likely to go out of business, thus protecting your investment.

The research selected a module from Jinko Solar, which is recognised as one of the top five module providers worldwide. The chosen module has a -0.29%/°C power temperature coefficient, which is lower than the average and within the acceptable range for high temperatures. This makes it particularly suitable for the desert climate at the proposed site. The selected module is also available in a bifacial configuration. The complete specifications of the module are listed in table 3.5 below.

Table 3. 5: Selected Module Specifications

Manufacturer:	Jinko Solar
Model:	JKM610N- 66HL4M
Technology:	MONO-FACIAL MODULE
Cells:	N type Mono-crystalline 132 (2×66)
Maximum power at STC, P_{mpp}:	610Wp
Module efficiency:	22.58%
Open-circuit voltage, V_{oc}:	48.63V
Max. power point voltage, V_{mpp}:	40.56V
Short-circuit current, I_{sc}:	16.01A
Max. power point current, I_{mpp}:	15.04A
P_{mpp} temperature coefficient:	-0.29%/°C
V_{oc} temperature coefficient:	-0.25%/°C
I_{sc} temperature coefficient:	0.045%/°C
NOCT	45±2°C

3.6.2 Inverter

The inverter for this study was selected from Sungrow, one of the leading inverter manufacturers, with a market share of over 40% [102]. The chosen inverter is specifically engineered for large-scale PV systems, providing full grid support capabilities. A key feature of this inverter is its integrated MV transformer, which simplifies installation and reduces system costs. Additionally, the inverter meets international standards such as IEC 61727 and IEC 62116, ensuring compliance with grid connection and safety requirements. The primary characteristics of the selected inverter include high efficiency (up to 99%), robust performance in diverse environmental conditions, and advanced active and reactive power control. The main characteristics of the inverter shown in Table 3.6:

Table 3. 6: Selected Inverter Specifications

Parameter	Value
Type of inverter	Central inverter
Maximum input voltage	1500 V
Maximum PV input current	4178 A
Nominal output power	3125 kW (at 50 ºC)
Nominal AC voltage	600 V (Low Voltage side of the transformer)
Min. PV input voltage / Startup input voltage	875 V / 915 V
Maximum inverter output current	3458 A
Maximum efficiency	99%
European (Euro.) efficiency	98.7%
Dimensions	6058 x 2896 x 2438 mm
Weight	17 T
Transformer Specifications:	
Rated power	3125 kVA

3.6.3 Trackers

The horizontal single-axis tracker from Ideematec was selected for its robust design and innovative features. This tracker was compared to alternatives in the industry, but its ability to handle heavy wind loads and its decoupled drive system provided an advantage.

Like many modern trackers, it includes backtracking capability and a stow function for protection during extreme weather. The tracker's modular design allows for easy scalability, making it suitable for utility-scale projects. The Ideematec system can efficiently support up to 28 modules per row and 8 strings per tracker, maximising the energy yield while optimising space [103]. The tracker details are summarised in Table 3.7, and an illustration is provided in Figure 3.9.

Table 3. 7: Specifications of the Selected Tracker for the Study

Parameter	Value
Manufacturer	Ideematec
Model	Horizon L
Tracker length	Up to 260m (853') in length; coherent string conforms tables
Type	Independent-row single-axis 1P tracker
Tracking Range	±60°
Motor type	DC and AC are available
Row length	28-224 modules
Warranty	Structural components: 15 years Electronic components: 5 years
Features	Backtracking capability, night-time stows, modular design, decoupled drive

Figure 3. 8: Ideematec Horizon L: TEC 1P tracker, sourced from [103]

3.6.4 Battery

The BYD Battery-Box Premium LVL15.4 (2021) was selected as the energy storage solution for this study. This model is designed for a large-scale PV system with high self-consumption requirements. It boasts a maximum capacity of 983 kWh when scaled across multiple units, making it highly suitable for large installations to optimise energy consumption and reduce reliance on the grid. The LVL15.4 battery is compatible with leading three-phase inverters, ensuring seamless integration into different system configurations. Its lithium iron phosphate cells provide excellent safety, longevity, and reliability. Moreover, it can operate in both on-grid and off-grid scenarios, providing energy storage for night-time consumption and grid independence. In this study, the battery primarily functions as a storage system, allowing excess solar energy to be utilised at night rather than serving purely as a backup system. In addition to offering high power performance, the battery system's space-saving design and floor-standing installation make it ideal for projects where footprint is a concern. The unit's advanced communication and protection systems, coupled with a round-trip efficiency of over 95%, ensure optimal energy storage and retrieval, contributing to the overall efficiency of the PV plant. Key characteristics of the selected battery system are shown in Table 3.8 below:

Table 3. 8: Selected Battery Specifications

Parameter	Value
Usable energy	15.36 kWh (per unit)
Maximum continuous output current	250 A
Peak output current (5 seconds)	375 A
Nominal voltage	51.2 V
Maximum capacity	983 kWh
Round-trip efficiency	≥ 95%
Operating temperature	-10°C to +50°C
Protection rating	IP20
Battery type	Lithium Iron Phosphate (LiFePO4)
Certifications	IEC 62619 / CE / CEC / UN38.3
Dimensions (H/W/D)	660 x 650 x 575 mm (per unit)
Warranty	10 Years
Weight	168 kg (per unit)

3.7 Plant Sizing

A preliminary design study was conducted to assess and optimise various configuration parameters for the solar PV plant. These parameters included tilt angles, row spacing, the number of modules per string, the number of strings per inverter, and the Inverter Loading Ratio (ILR). Assumptions from existing literature were also considered to estimate system losses and assist in sizing the battery storage system. The study began with a single inverter setup, which was then scaled up. The main goal of this design phase was to identify the most effective configurations, summarise them, and use these configurations as inputs for PVsyst and Fraunhofer Zenit software to compare yield differences.

3.7.1 Determining and Configuring String Sizes

The first step involved determining the maximum and minimum number of modules that could be connected in series within a string. This required identifying the site's lowest ambient temperature and estimating the highest expected module temperature to account for the absolute voltage limits. According to SolarGIS TMY data, the lowest recorded

ambient temperature was 1.2°C. However, for a more conservative approach, the study assumed a minimum temperature of 0°C. Equations 27 and 28 were used to calculate the maximum number of modules per string. For the minimum number of modules, a high ambient temperature of 40°C and strong irradiance of 1000 W/m^2 were assumed, based on the site's climate. This estimate was used to calculate the highest expected module temperature and the corresponding voltage at the maximum power point under these conditions. Equations 29, 30, and 31 were then used to determine the minimum number of modules per string.

$$V_{max} = V_{oc} \cdot \left(1 + \frac{\left((T_{mod} - 25°C) \cdot \beta\right)}{100}\right) \quad \text{(eq.27)}$$

where V_{max} represents the maximum PV module output voltage, T_{mod} is the lowest possible module temperature during the day (assumed to be 0°C), and β stands for the module temperature coefficient.

$$n_{mod,max_{str}} = \frac{V_{inv,max}}{V_{max}} \quad \text{(eq.28)}$$

where $n_{mod,max_{str}}$ is the number of PV modules required in series to match the maximum inverter voltage $V_{inv,max}$ and V_{max} is the maximum PV module output voltage.

$$T_{cell} = T_{amb} + \frac{(NOCT - 20) \cdot G}{G_{NOCT}} \quad \text{(eq.29)}$$

where T_{cell} is the temperature of the PV cell, T_{amb} is the ambient temperature, NOCT is the nominal operating cell temperature, G is the actual irradiance (1000 W/m^2), and G_{NOCT} is the irradiance at NOCT (800 W/m^2).

$$V_{mpp}(°C) = V_{mpp_{mod}} \left(1 + \frac{\left((T_{cell} - 25) \cdot \beta\right)}{100}\right) \quad \text{(eq.30)}$$

where V_{mpp}(°C) is the voltage at the MPP of the module at the given cell temperature, $V_{mpp_{mod}}$ is the MPP voltage of the module at 25°C.

$$n_{mod,min_{str}} = \frac{V_{inv,min}}{V_{mpp(°C)}} \quad \text{(eq.31)}$$

where $n_{mod,min_{str}}$ is the number of PV modules required in series to match the minimum inverter voltage $V_{inv,min}$.

Although PVsyst can automatically perform this calculation, the study opted to manually compute the value to ensure consistent basis input values for comparison between the two-simulation software. The results are shown in Table 3.9 below, the preliminary design incorporates 28 modules in series to meet the system's voltage requirements, optimise performance, and stay within the inverter's allowable voltage range, thus enhancing efficiency and reducing potential losses.

Table 3. 9: Module Output Voltage and Number of Modules per String

Parameters	Values
V_{max} at 0°C	51.6 V
V_{mpp} at 71.25 °C	35.9 V
Max. number of modules in a string for 1500V	29
Min. number of modules in a string for 875V	25
The optimal number of modules in series selected in the preliminary design.	28

The next phase of the study focused on determining the optimal number of strings that could connect to the inverter. The maximum allowable number of strings per inverter was determined using Equations 32 and 33. The study employed a scaling factor approach, beginning with a single system configuration consisting of one inverter and its connected modules, which were later scaled up to identical subsystems. The optimal Inverter Loading Ratio (ILR) was chosen by first determining the best subsystem configuration. This involved selecting the most suitable number of modules in series per string and the optimal number of strings connected to each inverter input.

$$I_{mpp}(°C) = I_{mpp_{mod}}\left(1 + \frac{((T_{cell}-25)\cdot\beta_I)}{100}\right) \quad \text{(eq.32)}$$

where $I_{mpp}(°C)$ is the MPP current at a given cell temperature, in this case 70°C, $I_{mpp_{mod}}$ is the MPP current of the module at 25°C, β_I is the temperature coefficient for current.

$$n_{inv,max_{str}} = \frac{I_{DC\ max,inv\ input}}{SF \times I_{mpp(°C)}} \quad \text{(eq.33)}$$

where $n_{inv,max_{str}}$ is the number of strings per inverter input, $I_{DC\ max,inv\ input}$ is the maximum allowable DC input current per inverter input, SF is the safety factor (1.25) for inverter sizing for grid-connected PV systems.

Once this configuration was established as shown in Table 3.10, the ILR was calculated by dividing the nominal DC power (kW) of the array by the AC power rating of the inverter (kW), shown in Equation 34. To ensure high-efficiency operation of the inverter, the target ILR range was set between 0.85 and 1.26, and after evaluating site-specific factors such as climate and irradiance, an ILR of 1.11 was selected as the most appropriate for the system. This choice ensures optimal performance and efficiency, particularly considering the proposed project location's environmental conditions.

$$ILR = \frac{P_{DC,array}}{P_{AC,inv}} \quad \text{(eq.34)}$$

where ILR is the Inverter Loading Ratio, $P_{AC,inv}$ is the AC power output of the inverter, and $P_{DC,array}$ is the DC power output of the PV array.

Table 3. 10: Chosen Subsystem Configuration and Performance Parameters

Parameters	Values
Inverter Loading Ratio	1.1
Subsystem Number of Inverter	1
Max. number of String per Inverter	218
The optimal chosen number of strings per Inverter	204
Total Number of Modules per Subsystem	5712
Subsystem Nominal power	3484.3 kWp

3.7.2 Configuration of PV Modules

One of the most important factors when designing a utility-scale PV system is the module tilt angle and the row distance between the rows, therefore a computational optimising tool was used to determine and validate the chosen parameters. The optimisation is further discussed in the next chapter. The study added a 20% buffer to the required land area to account for inverters, access routes between rows of panels, and other infrastructure necessary for system operation and maintenance. The system's orientation was selected based on its location in the southern hemisphere, where the optimal orientation for a fixed system is north-facing. The tracker's rotational axis is aligned north-south, allowing the panels to rotate from east to west throughout the day and follow the sun's movement.

The fixed system consists of six modules stacked in a landscape configuration. This arrangement was chosen Because of the way bypass diodes are arranged in the modules, which minimises shading losses. The configuration layout and side view are illustrated in Figure 3.9. The system's pitch was optimised using the simple winter solstice rule, applied within the computational optimisation tool, as given by Equation 20.

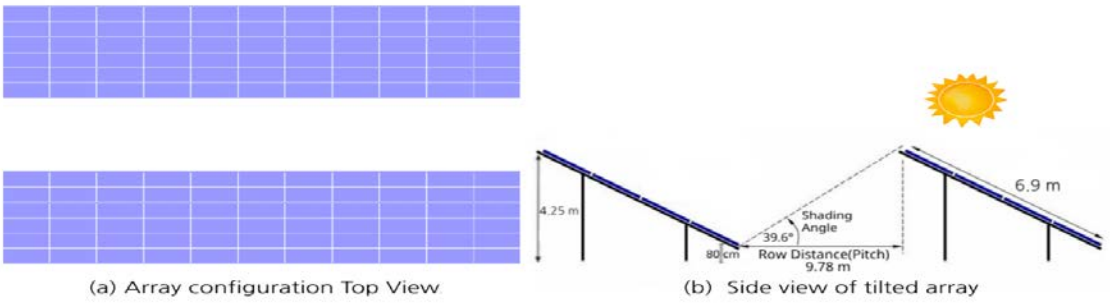

Figure 3. 9: Module mounting configuration for fixed system.

The tracked system is configured in a portrait orientation, with every array row fitted with a tracker. This layout is supported by the tracker’s backtracking capability, which prevents

row-to-row shading by enabling the backtracking algorithm, making shading losses negligible. The array height when modules are horizontal was set to 1.80 m, a conservative choice that ensures mechanical stability, as taller systems can face structural challenges. Additionally, a shorter table height allows for more strings to be interconnected, with each tracker capable of handling up to eight strings, offering maximum flexibility. The configuration is illustrated in Figure 3.10 below. All configuration parameters for both fixed and tracked are shown in Table 3.11.

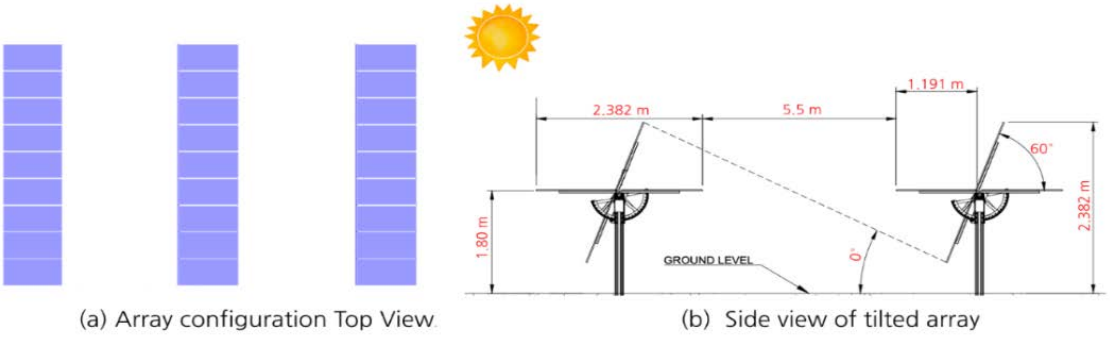

Figure 3. 10: Module mounting configuration for single-axis tracked system.

Table 3. 11: System Configuration Parameters for Fixed and Tracked PV Systems

System Type:	Fixed	Tracked
Orientation	0°	180°
Tilt	25°	0°
Row distance (Pitch)	9.78 m	5.5 m
Table length	6.9 m	2.38
$\varphi_{min}, \varphi_{min}$	N/A	-60°,60°
Tracker sensitive	N/A	2.38
Backtracking	N/A	Enabled

3.7.3 Determining and Configuring Battery Storage System Sizes

The study adopted the assumption from [96], which suggests that the optimal battery capacity for a system using a self-consumption dispatch strategy in a desert climate is approximately 2 kWh per MWh/year. The methodology outlined below was employed to determine the battery storage system size for the proposed PV system.

First, the study converted the daily expected energy requirement to yearly production:

$$E_{PV,yr_{req}} MWh/yr = \frac{E_{PV\,req}\ (kWh/day) \times 365\ days/year}{1000} \quad \text{(eq.35)}$$

where $E_{PV\,req}$ (kWh/day) is the expected year energy production in MWh/yr.$E_{PV,yr_{req}}$ is the total expected energy production over a year, expressed in kWh/year.

The study then applied the optimal battery capacity ratio from [96] to determine the required battery capacity for the self-consumption system:

$$C_{opt} = E_{PV,yr_{req}} MWh/yr \times 2\ \text{kWh}/(\text{MWh/yr}) \quad \text{(eq.36)}$$

where C_{opt} is the optimal battery capacity in kWh based on the yearly energy requirement. The factor of 2 represents the battery capacity ratio, which scales the energy requirement for the self-consumption system.

To ensure that the storage system adequately meets the energy demands of the load during periods of low solar generation, a safety factor is applied to C_{opt}. This is expressed as follows:

$$Adjusted_{C_{opt}} = \frac{C_{opt} \times D.O.A}{D.O.D} \text{ (eq.37)}$$

where D.O.A refers to the days of autonomy, which, in this case study, is set to 2 days. D.O.D represents the selected battery depth of discharge, with a theoretical maximum of 100%. However,

for this study, 80% is used, as recommended by PVsyst for optimal battery performance and longevity.

Finally, the number of batteries required for the system was calculated as:

$$N_{batr} = \frac{Adjusted_{C_{opt}}}{C_{unit}kWh} \qquad \text{(eq.38)}$$

where N_{batr} is the number of batteries required. C_{unit} is the capacity of a single battery unit.

This study opts for operation near the maximum input voltage of the inverter, as the proposed PV system is in a desert climate, where high temperatures are common. Operating near the maximum voltage enhances system efficiency, as inverters perform optimally when the DC input is close to their upper voltage limit, reducing conversion losses. Additionally, high temperatures can reduce battery efficiency, but by maintaining a higher voltage, the risk of voltage drops due to heat and ageing is minimised. Configuring the system with more batteries in series ensures continuous and stable operation, even under load or during battery discharge, by reducing the likelihood of voltage drops. The number of batteries connected in series at maximum voltage input can be calculated by using equations 39 and 40, The optimal battery configuration is provided in section 3.8.

$$N_{batr,series} = \frac{inv_{DC\ Input\ Voltage\ Range\ (MPPT)}}{Nominal\ Battery\ Voltage} \qquad \text{(eq.39)}$$

$$N_{batr,parallel} = \frac{N_{batr}}{N_{batr,series}} \qquad \text{(eq.40)}$$

3.7.4 PV System Losses

When designing a PV system, various losses must be anticipated, as discussed in Section 2.2.4.6. This subsection outlines the specific loss parameters that were manually adjusted for the simulation.

3.7.4.1 Soiling

Soiling losses were set to 3.0%, based on a study that correlated soiling losses with monthly precipitation. At the proposed site, precipitation levels range from 0-20 mm per month, which corresponds to a 3.0% loss factor. Although [80] focused on fixed systems, the same loss factor was applied to tracked systems for simulation purposes, as no specific research comparing soiling losses between tilted fixed and tracking systems was available. Therefore, the same soiling figures were assumed for both configurations.

3.7.4.2 Degradation

Degradation in modules refers to the gradual decline in the energy output of the module over time. Fraunhofer ISE studies show that crystalline silicon module degradation rates are within measurement uncertainty for the first 10 years. On average, PV systems with these modules experience a capacity decrease of 0.25% per year [104]. However, due to the variability in system performance and the short duration of some measurements, this rate may not apply universally. Other studies report annual degradation rates between 0.23% and 0.59% [105]. For this study, a rate of 0.25% per year is assumed.

3.7.4.3 Other Losses

The remaining detailed loss inputs for simulation are presented in Table 3.12. The wind-dependent heat loss factor and the constant heat loss factor, which together comprise the field thermal loss factor, were sourced from [106]. The study faced a limitation in accurately predicting cable ohmic losses, as both the total cable length and cable cross-sections were considered unknown variables. Consequently, standard values were assumed for DC and low AC 1 losses. For AC 2, an estimate was made based on the site distance to the load, including the estimated losses due to combiner boxes and AC distribution boxes. The final input parameter considered in this study was the various losses due to the PV system's self-consumption such as the trackers, inverters, electrical fences, fans etc. A fixed Fraunhofer constant consumption ratio was used throughout the analysis, with differences in values observed between the tracked and fixed systems, as outlined in the table 3.12 and can be calculated as:

$$System\ Self\ Consumption(S) = 5 \times yr\left(\frac{P_{system}\ (kW_p)}{1000}\right) \quad \text{(eq.41)}$$

where S represents the system self-consumption (in kWh/year), the value of 5 is a scaling factor for a fixed system, while a value of 10 applies to a tracked system.

All other input losses were left on default during the simulation.

Table 3. 12: Assumed Input Loss Parameters in the Study

Constant thermal loss factor (U_c)	25.0 $W \cdot m^{-2} \cdot K^{-1}$
Wind loss factor (U_v)	1.2 $W \cdot m^{-2} \cdot K^{-1} \cdot (m/s)^{-1}$
DC ohmic losses	1.50%
AC ohmic losses (Low Voltage)	0.05%
AC ohmic losses (Medium Voltage)	2.19%
Fixed constant consumption (Fixed system)	5 kWh/MW/year
Fixed constant consumption (Tracked system)	10 kWh/MW/year

3.7.5 PV System Lifetime

Historically, the system lifetime was aligned with the module warranty period, typically set at 25 years. However, modern developers are increasingly adopting longer lifetimes of 30, 35 years, or even more[107], to reduce the LCOE and enhance the attractiveness of investments. In this thesis, a default system lifetime of 30 years was used, as recommended by the IEA-PVPS Task 12 report [108].

3.8 Optimised PV System, Electrolyser, and Battery Sizing: Simulation Inputs

3.8.1 Optimisation Based on Row Distance and Tilt Angle for Fixed and Tracked Systems

The optimisation tool aimed to analyse the most efficient row distance for the fixed and tracked systems. The results are presented in Figures 3.11 and 3.12. The graphs show energy production, energy gain, land usage, and tilt angle dependence on the row distance. The fixed system graph illustrates the relationship between energy per inverter and the tilt angle as the row distance varies from 9.44 m to 10.22 m. It highlights that energy production peaks around a row distance of 9.78 m and a tilt angle of 25°, after which it starts declining. It was also observed that as the tilt angle increased linearly, energy output per inverter declined, indicating diminishing returns due to suboptimal sun exposure and increased shading between rows. The optimal row distance for the fixed system was chosen to be 9.78 m, with an optimal tilt angle of 25°. This configuration was selected based on its ability to maximise energy output.

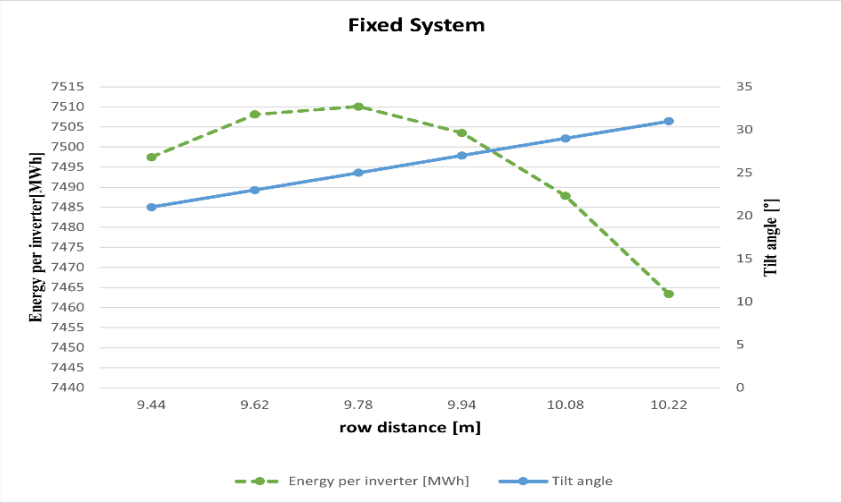

Figure 3. 11: Energy Output and Tilt Angle Optimisation for Fixed Solar System

In contrast, the tracked system graph depicts the relationship between land required and energy gain as row distance increases from 5 m to 10 m. As the distance between rows increases, the required land area expands substantially. In contrast, the associated energy gain exhibits only marginal increases with greater row spacing. For this reason, an optimal row distance of 5.5 m was selected for our tracked system. This choice not only adheres to established practices but also minimises the required land area, given that increasing the row distance yields negligible gains in energy production.

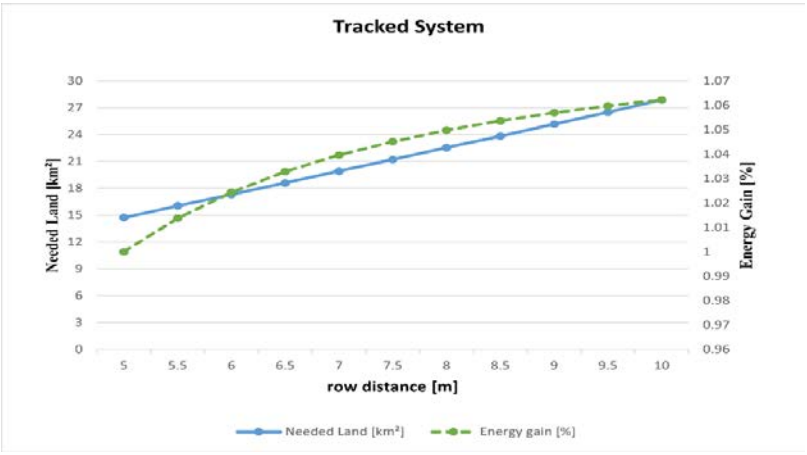

Figure 3. 12: Land Usage and Energy Gain Optimisation for Tracked Solar System

3.8.2 Electrolyser selection Results

Alkaline electrolysers, a mature and cost-effective technology used in large-scale applications such as the Namibian Green Hydrogen project, are best suited for continuous operation. While they are cheaper than PEM electrolysers, their efficient performance depends on stable, uninterrupted running, rather than frequent on/off cycling or ramping. According to the literature [7], operating alkaline electrolysers under part-load or intermittent conditions increases the risk of contamination, reduces safety, and accelerates equipment degradation. Therefore, to maintain both performance and longevity, it is crucial that the PV system provides a consistent energy supply at stable voltage levels, minimizing fluctuations or interruptions.

3.8.3 Project System Sizing Results

The key characteristics of the PV plant system design requirement to meet the required 40% of the load demand for the electrolyser are detailed in the tables 3.13 for both the Springbok and Dolphin sites.

Table 3. 13: Technical Specifications of the PV Plant at Springbok Site.

Site: Springbok	Coordinates: Lat: -26.888418°, Long:15.800220°	
Parameters:	**Fixed System**	**Tracked System**
Orientation	0°	180°
Tilt	25°	0°
Row distance (Pitch)	9.78 m	5.5 m
System Nominal Power	1.404 GWp	1.275 GWp
DC: AC power ratio	1.115	1.115
Total number of modules	2 301 936 units	2 090 592 units
Total number of Inverters	403 units	366 units
Total number of 1d Tracker	N/A	10248
Number of modules in series	28	28
Number of strings	82212 strings	74664 strings
Occupied land	10.9 km²	16.1 km²

Table 3. 14: Technical Specifications of the PV Plant at Dolphin Site.

Site: Dolphin	Coordinates: Lat: -27.151717°, Long:15.863645°	
Parameters:	**Fixed System**	**Tracked System**
Orientation	0°	180°
Tilt	25°	0°
Row distance (Pitch)	9.78 m	5.5 m
System Nominal Power	1.394 GWp	1.275 GWp
DC: AC power ratio	1.115	1.115
Total number of modules	2 284 800 units	2 090 592 units
Total number of Inverters	400 units	366 units
Total number of 1d Tracker	N/A	10248 units
Number of modules in series	28	28
Number of strings	81600 strings	74664 strings
Occupied land	10.8 km²	16.1 km²

Table 3. 15: Needed Battery Capacity and Unit Parameters

Parameters	Values
Total optimal battery capacity	32 991 792.5 kWh
Number of battery units	2 147 903
Number of batteries in series at 1300V	26
Number of batteries in parallel at 1300V	82 611

A limitation in the PVsyst simulation software was encountered, as it restricts the number of batteries that can be connected in parallel. To address this issue, the study scaled down the simulation to a single subsystem. This subsystem is required to produce 9027.7 MWh/year to meet the specified portion of the total load demand for the electrolyser. The methodology described in Section 3.7.3 was applied to determine the optimal battery capacity, the number of battery units, and the configuration of batteries in series and parallel for the subsystem. It is important to note that for simulation purposes, the battery capacity was assumed to remain consistent across all configurations. Input results are shown in table 3.16.

Table 3. 16: Needed Battery Capacity and Unit Parameters for one Sub System

Parameters	Values
Total optimal battery capacity	45138.5 kWh
Number of battery units	2939
Number of batteries in series at 1300V	26
Number of batteries in parallel at 1300V	113

3.9 Summary and Conclusion

This chapter presented the methodological framework for designing and evaluating the photovoltaic (PV) systems used in the study. The selection of sites, system components, and simulation tools was detailed, with a focus on comparing fixed and tracked PV configurations. Additionally, the integration of battery storage was addressed, highlighting the challenges and assumptions made in modelling energy storage.

Key methodologies included using PVsyst and Zenit for performance simulation and comparative analysis of efficiency, energy yield, and losses. A structured approach to battery sizing and load distribution ensured realistic modelling, although PVsyst's restriction on parallel battery connections required a scaled-down subsystem model.

In conclusion, the methodologies applied in this chapter provide a strong foundation for analysing system performance and economic feasibility. The modelling approach was carefully chosen to align with industry standards while accounting for software constraints.

Chapter 4

Techno-Economic Evaluation

This chapter presents the energy output and system performance assessment of the proposed PV systems for the Springbok and Dolphin sites, Furthermore, a comprehensive economic evaluation is performed using the LCOE approach to assess the cost-effectiveness and overall energy performance of the systems.

4.1 Energy Output and System Performance Assessment

The simulation process included fixed and tracked configurations at two sites, without energy storage, to enable a fair comparison between the two software packages, since the Zenit software does not support storage. In total, eight simulations were conducted. Additionally, simulations incorporating energy storage were performed exclusively using PVsyst.

4.1.1 Springbok Site Simulation Performance Analysis

The simulation results for the Springbok site, comparing fixed and tracked PV systems, are shown in Figure 4.1. The performance ratio (PR) for the fixed-tilt system obtained with PVsyst was 83.6% while the Zenith simulation resulted in a PR of 75.5%. The tracked systems showed closer results, with PVsyst reporting a PR of 82.4% and Zenit reporting 81.4%. PVsyst's highest PR for the fixed system was in June (86.8%), while Zenit's was in December (79%). This discrepancy is likely due to differences in how the software tools model seasonal variations. PVsyst may account for higher irradiance levels

and lower temperatures in June, improving PR, whereas Zenit could apply different loss factors or averaging methods, leading to an improved peak in December. A more detailed loss breakdown and input validation would be required to confirm which trend is more accurate, which could be explored in future work. The tracked systems showed more consistent results, peaking in June and July, with the lowest PR during the summer months for both software.

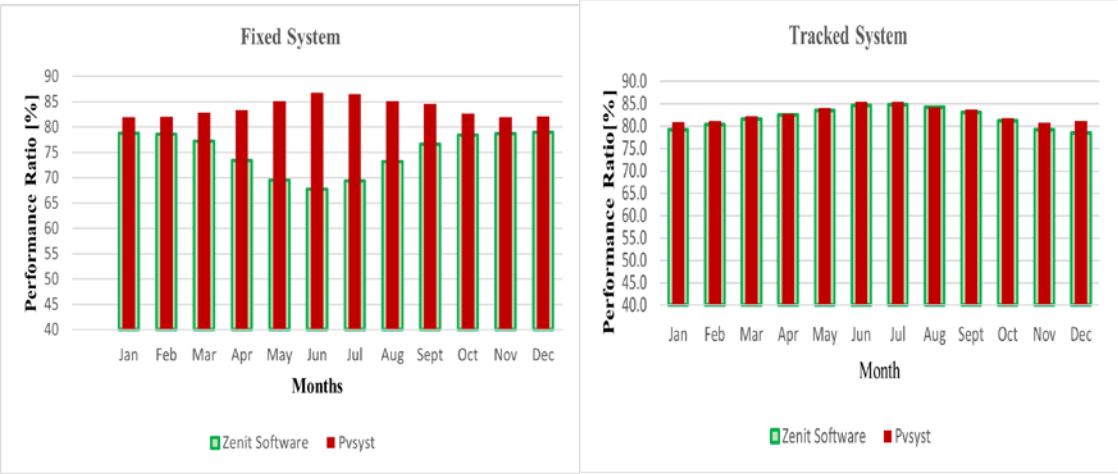

Figure 4. 1: PR comparative software simulation results for the Springbok site

Table 4.5 and Figure 4.2 present a Comparison of the Specific Yield (SY) for Fixed and Tracked Systems at Springbok sites using PVsyst and Zenit.

Table 4. 1: Specific Yield Comparison for Fixed and Tracked Systems at Springbok Site

Simulation Software	Configuration	SY [kWh/kWp/year]	Highest SY [Month][kWh/kWp]	Lowest SY [Month][kWh/kWp]
PVsyst	Fixed	2210	October: 207.08	June: 145.2
Zenit	Fixed	2355	December: 231.2	June: 139.6
PVsyst	Tracked	2621	December: 282.72	June: 134.1
Zenit	Tracked	2591	December: 286.1	June: 137.5

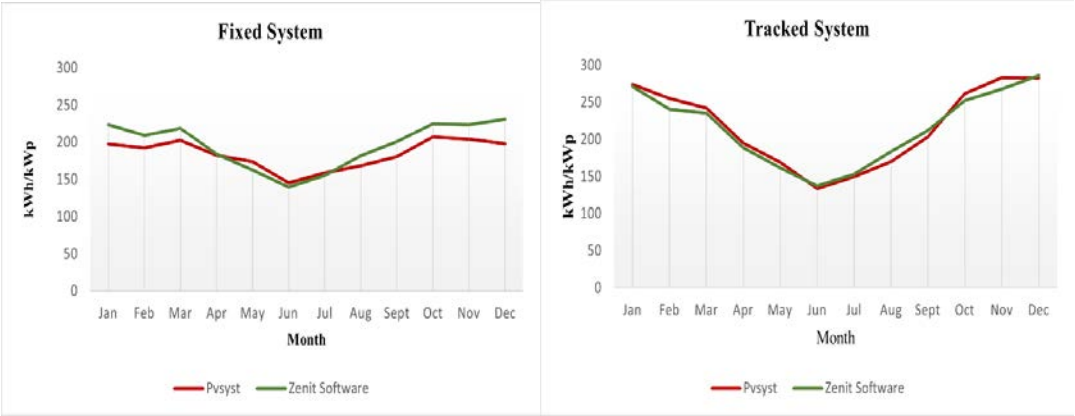

Figure 4. 2: SY comparative software simulation results for the Springbok site

The annual energy output, performance ratio, and specific yield of the Springbok site without storage are summarised below. The loss diagrams are available in the appendix.

Table 4. 2: PVsyst and Zenit Simulation Results for Springbok Site.

Simulation Software	Configuration	Nominal Power, [GW]	Annual Production, [GWh]	Performance Ratio, [%]	Specific Yield, [kWh/kWp/year]
PVsyst	Fixed	1.404	3150.454	83.55	2210
	Tracked	1.275	3421.417	82.42	2621
Zenit Software	Fixed	1.404	3306.367	75.5	2355
	Tracked	1.275	3304.142	81.4	2591

4.1.2 Dolphin Site Simulation Performance Analysis

The simulation results for the Dolphin site, comparing fixed and tracked PV systems, are shown in figure 4.3. For the fixed system, PVsyst reported a PR of 84%, while Zenit gave 76.1%. The tracked systems were closer, with PVsyst at 82.7% and Zenit at 81.6%. PVsyst highest PR for the fixed system was in June with 87%, whereas Zenit's was in December with 79.9%, likely due to differences mentioned in the above results. The

tracked systems showed more consistent results, peaking in June and July, with the lowest PR during the summer months for both software.

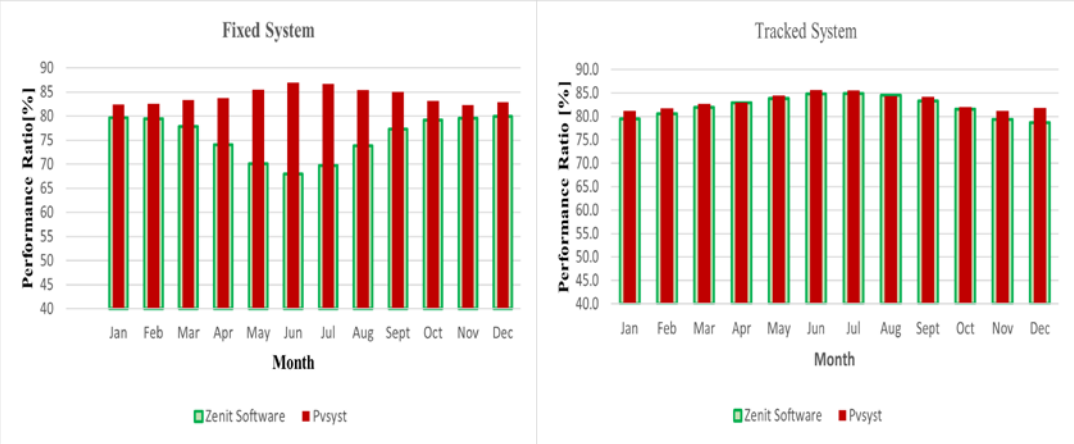

Figure 4. 3: PR comparative software simulation results for the Dolphin site

Table 4.7 and Figure 4.4 present a Comparison of the Specific Yield for Fixed and Tracked Systems at Dolphin sites using PVsyst and Zenit.

Table 4. 3 SY Comparison for Fixed and Tracked Systems at Dolphin Site

Simulation Software	Configuration	SY [kWh/kWp/year]	Highest SY [Month][kWh/kWp]	Lowest SY [Month][kWh/kWp]
PVsyst	Fixed	2253	October: 210.18	June: 144.9
Zenit	Fixed	2373.1	December: 234.3	June: 138.4
PVsyst	Tracked	2692	December: 306.59	June: 132.9
Zenit	Tracked	2594.2	December: 287.4	June: 135.6

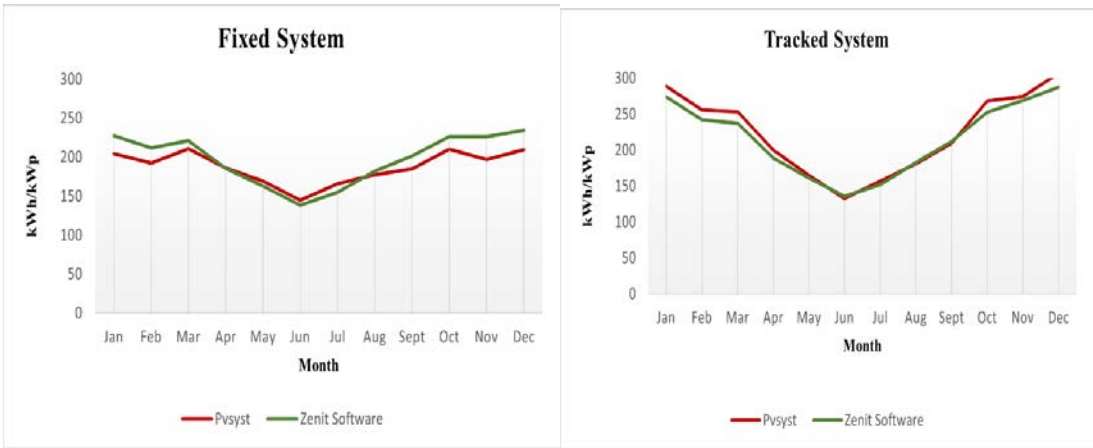

Figure 4. 4: PR comparative software simulation results for the Dolphin site

The annual energy output, performance ratio, and specific yield for the Dolphin site without storage are summarised in Table 4.4, below. The loss diagrams are available in the appendix.

Table 4. 4: PVsyst and Zenit Simulation Results for Dolphin Site.

Simulation Software	Configuration	Nominal Power, [GW]	Annual Production, [GWh]	Performance Ratio, [%]	Specific Yield, [kWh/kWp/year]
PVsyst	**Fixed**	1.394	3140.601	83.99	2253
	Tracked	1.275	3432.621	82.75	2692
Zenit Software	**Fixed**	1.394	3307.450	76.1	2373.1
	Tracked	1.275	3308.307	81.6	2594.2

4.1.3 Subsection Summary

The comparison between PVsyst and Zenit simulations for the Springbok and Dolphin sites reveals notable differences in PR and SY due to their distinct modelling approaches. For fixed systems, PVsyst consistently reported higher PR values, particularly in winter, likely due to its detailed loss modelling and temperature correction, which may result in a more stable performance ratio. In contrast, Zenit showed a higher SY, possibly due to differences in how irradiation and system losses are accounted for, suggesting a higher

estimated energy yield despite lower PR values. For tracked systems, both PVsyst and Zenit produced comparable results in Performance Ratio (PR) and Specific Production (SP), indicating consistency in their simulation methodologies. This agreement suggests that the modelling of dynamic tracking algorithms and irradiance capture in both tools is well-calibrated. The consistency can be attributed to the ability of tracking systems to optimise solar incidence angles throughout the day, reducing losses due to shading and mismatch. Additionally, tracking systems inherently mitigate seasonal variations, leading to more stable performance predictions across different simulation platforms.

Overall, PVsyst appears to provide more detailed predictions for system stability in fixed configurations, as reflected by its higher PR values. In contrast, Zenit's consistently higher specific energy yields may result from differences in how the software models system losses and irradiation, rather than indicating a higher actual energy conversion efficiency.

4.2 Simulation Result for a Subsystem with Storage with Self-consumption Storage Strategy (PVsyst)

The simulation results for both sites, using PVsyst for PV subsystems with storage, demonstrated consistent performance ratio (PR) across all configurations. The fixed system at the Springbok site recorded a PR of 77.6%, while the Dolphin site reported 77.9%. Similarly, for the tracked system, Springbok achieved a PR of 77%, and Dolphin yielded 77.3%. The highest PR for the fixed system was observed in June, and for the tracked system, it peaked in April. However, the data indicates that the PR remains stable throughout the year, with minimal month-to-month variation.

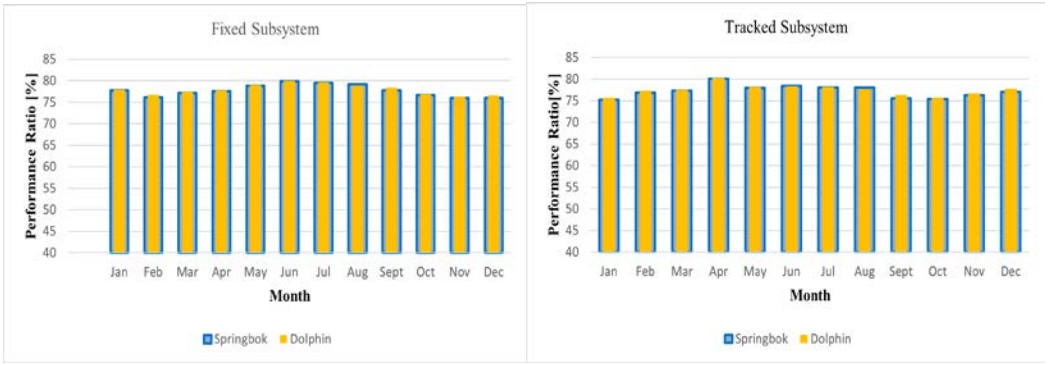

Figure 4. 5: Springbok and Dolphin site comparative simulation results, of performance ratio (PR), With Storage

The simulation results for Specific Yield (SY) were also consistent across both sites, with notable differences based on the configuration type. The tracked systems outperformed the fixed systems in terms of SY. At the Springbok site, the fixed system achieved an SY of 2084 kWh/kWp, while Dolphin reported 2090 kWh/kWp. For the tracked systems, Springbok yielded an SY of 2506 kWh/kWp, and Dolphin reached 2516 kWh/kWp. Both configurations exhibited peak SY during the summer months, with a decline observed in the winter months.

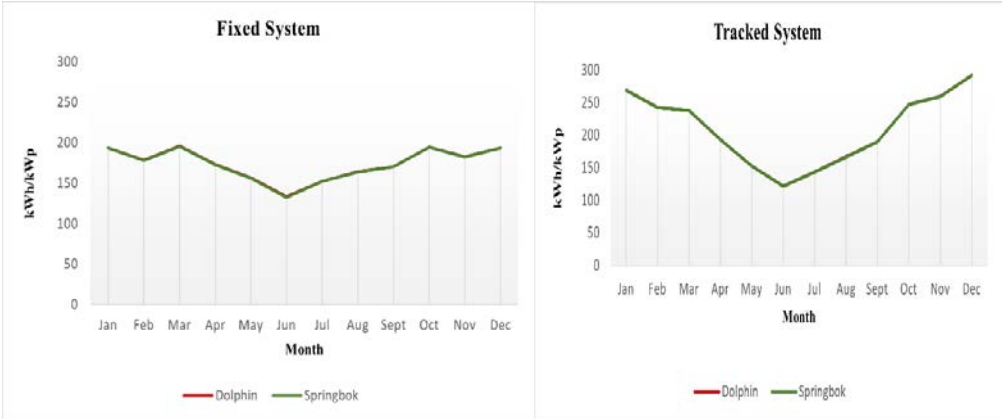

Figure 4. 6: Springbok and Dolphin site comparative simulation results for SP With Storage

The annual energy output, performance ratio, and specific yield for the Dolphin site and Springbok site with battery storage are summarised in Table 4.5 below. The loss diagrams are available in the appendix.

Table 4. 5: PVsyst Simulation Results for Springbok and Dolphin Site Subsystem with Storage.

Site	Configuration	Nominal Power, [MW]	Annual Production, [kWh]	Performance Ratio, [%]	Specific Yield, [kWh/kWp/year]
Springbok	**Fixed**	3.48	7261145	77.6	2084
	Tracked	3.48	8732697	77	2506
Dolphin	**Fixed**	3.48	7280597	77.9	2090
	Tracked	3.48	8766092	77.3	2516

4.2.1 Monthly Interaction Between PV System, Storage, and Grid Results

This subsection of the simulations offers an analysis of the monthly interaction between the PV system, energy storage, and the grid. The focus was on understanding how the PV system, in different configurations, interacted with the utility grid throughout the year. For both the fixed systems at Springbok and Dolphin sites, the results were similar, showing a continuous need for grid support annually, especially during the winter months when solar generation is lower. The Springbok site system drew 1,765,521 kWh annually from the grid, while at the Dolphin site, it pulled 1,746,149 kWh. Notably, both systems did not inject any excess (0 kWh) energy back into the grid for the winter and summer months. These results are illustrated in Figure 4.7 below.

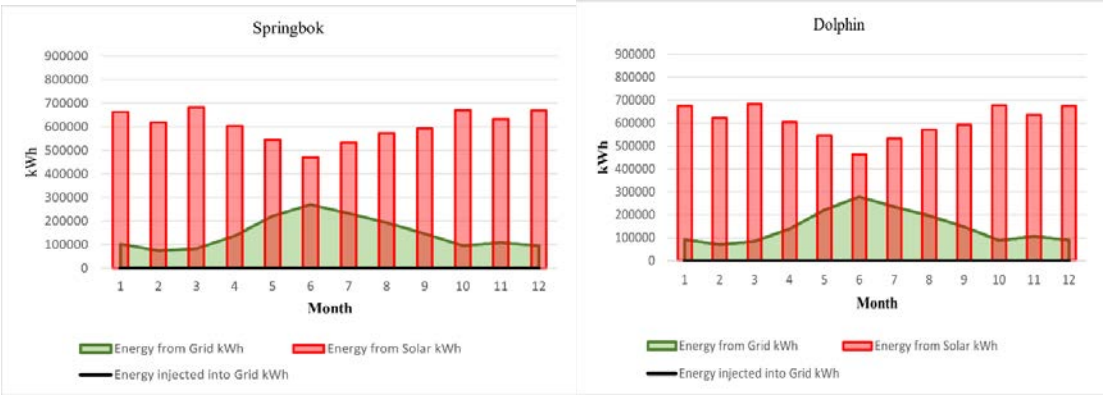

Figure 4. 7: Energy Storage Comparison for Fixed Systems at Springbok and Dolphin

The tracked configurations produced different results compared to the fixed systems. For both the Springbok and Dolphin sites, the tracked systems still required grid support, particularly during winter months when solar generation was lower. However, during the summer months, these systems generated surplus energy and injected it into the grid without requiring any grid assistance. At the Springbok site, the system drew 1,136,654 kWh annually from the grid and injected 842,495 kWh, resulting in a net consumption of 294,159 kWh/year. Similarly, at the Dolphin site, the system drew 1,153,656 kWh from the grid, injected 893,070 kWh, and was liable for only 260,586 kWh annually. This demonstrates the advantages of the tracked configurations in reducing grid dependency during periods of high solar generation. The results are illustrated in Figure 4.8 below.

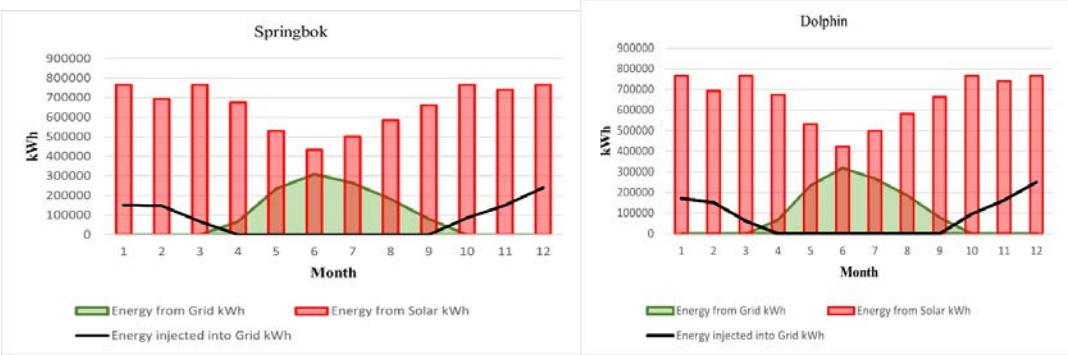

Figure 4. 8: Energy Storage Comparison for Tracked Systems at Springbok and Dolphin

The annual grid consumption, Self-consumption, Grid Injection, battery stored and battery direct use for the Dolphin site and Springbok site with battery storage are summarised in Table 4.6 below.

Table 4. 6: Monthly Interaction Between PV System, Storage, and Grid Results

Site	Configuration	Grid Consumption [kWh]	Self Consumption [kWh]	Grid Injection [kWh]	Battery Stored [%]	Battery Direct Use [%]
Springbok	**Fixed**	1765521	7261145	0	52.6	47.4
	Tracked	1136654	7890012	842684	48	52
Dolphin	**Fixed**	1746149	7280597	0	52.7	47.3
	Tracked	1153657	7873012	893080	47.6	52.4

4.2.2 Daily Interaction Between PV System, Storage, and Grid Results

This subsection of the simulations offers an analysis of the daily interaction between the PV system, energy storage, and the grid. The focus was on understanding how the PV system, in different configurations, behaves on both high-energy production days (HPD) and low-energy production days (LPD). The results provide insights into system performance on a low-energy production day (15 June 2023) and a high-energy

production day (15 December 2023). The year 2023 was selected as it represents the most recent available data. As shown in Figure 4.9 at the Springbok site, the fixed configuration shows a greater reliance on grid support (indicated in green) during a low production day, especially in the morning hours to meet the electrolyser's load demand (indicated in red). In contrast, on a high-production day, the system requires significantly less grid energy. This is illustrated in Figure 4.9 below. To enhance the clarity of figures, a legend explaining the meaning of each colour is provided in Table 4.11.

Table 4. 7 Legend for Subsection figures

Parameters	Colour Representation
Available Energy at Inverter Output (kWh)	
Energy supplied to the user (kWh)	
Energy injected into grid (kWh)	
Energy from the grid (kWh)	
Battery Charging Energy (kWh)	
Battery Discharging Energy (kWh)	

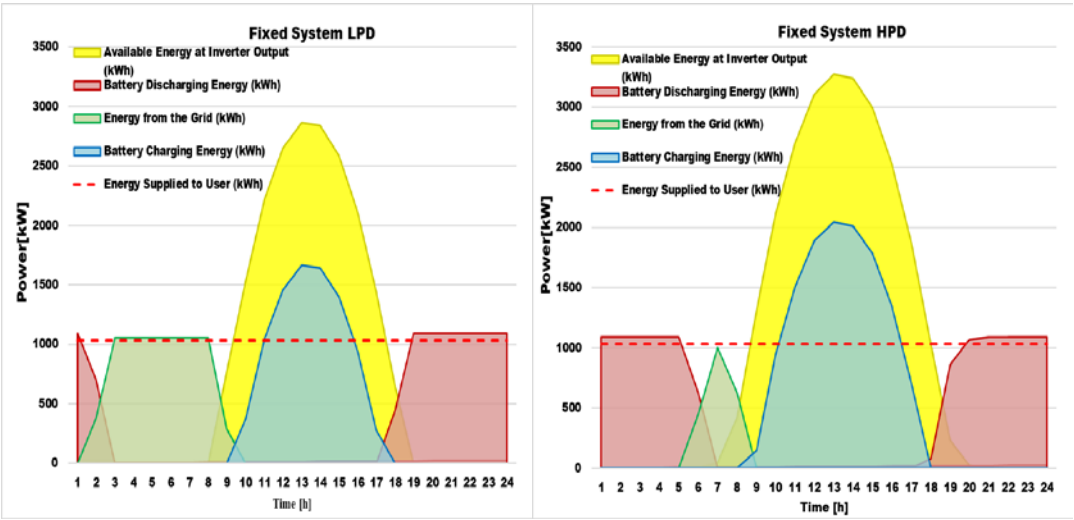

(a) low-energy production days (LPD), (b) high-energy production days (HPD)

Figure 4. 9: Springbok Fixed Configuration with Storage Results

Similarly, the tracked configuration shows greater reliance on grid support during a low production day, particularly in the morning to meet the electrolyser's load demand. However, on a high-production day, the system requires no grid energy and injects surplus energy into the grid, as indicated in purple. This is illustrated in Figure 4.10 below.

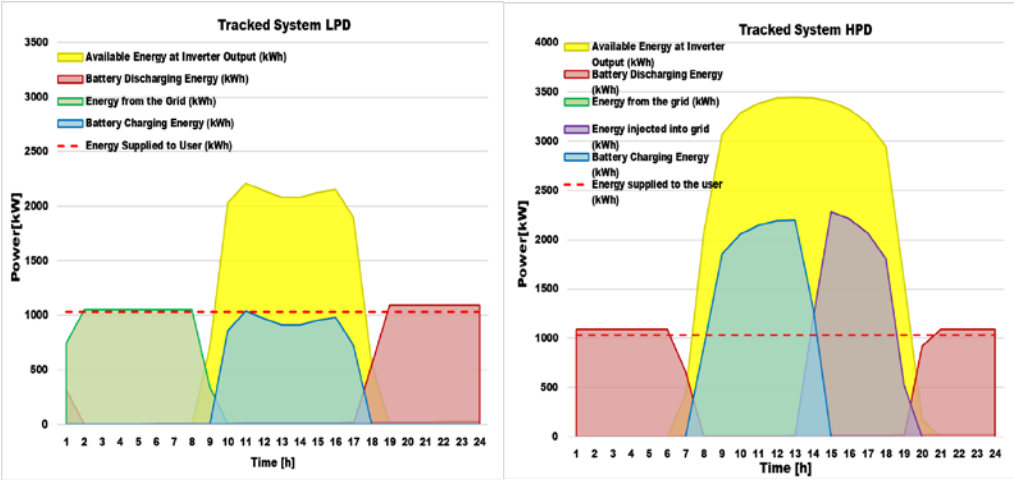

(a) low-energy production days (LPD) (b) high-energy production days (HPD)

Figure 4. 10: Springbok Tracked Configuration with Storage Results

The Dolphin site exhibits similar outcomes, with the key difference being that on a high-energy production day, the tracked system requires grid support an hour earlier compared to the Springbok site. Dolphin results are highlighted in Figures 4.11 and 4.12 below.

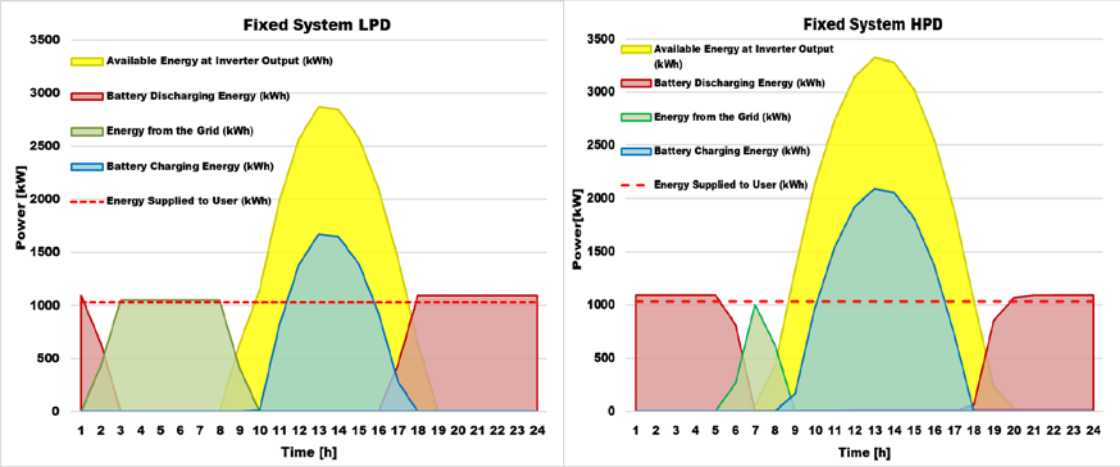

(a) low-energy production days (LPD) **(b) high-energy production days (HPD)**

Figure 4. 11: Dolphin Fixed Configuration with Storage Results

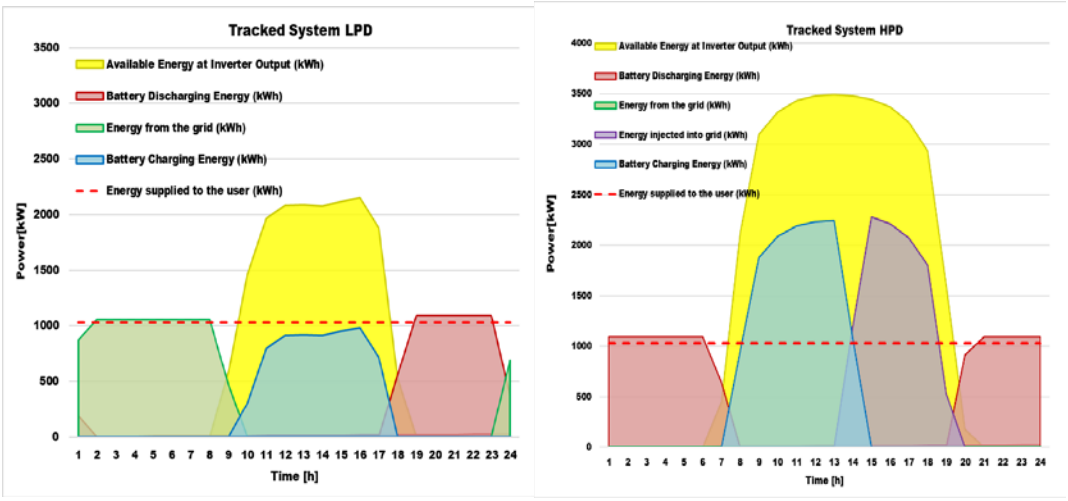

(a) low-energy production days (LPD) **(b) high-energy production days (HPD)**

Figure 4. 12: Dolphin Tracked Configuration with Storage Results

4.2.3 Subsection Summary

The simulations highlighted distinct performance differences between fixed and tracked PV systems with energy storage and grid interaction. Fixed systems required consistent grid support, particularly during winter, with no surplus energy injection. Tracked systems, however, reduced grid reliance by generating surplus energy in summer, which

was fed back into the grid. While both systems needed grid support on low-production days, tracked systems outperformed in terms of self-consumption and grid interaction, particularly on high-production days. These findings align with existing research that shows the superior efficiency of tracked systems in maximising energy yield [63]. However, limitations such as potential higher maintenance costs for tracking mechanisms and regional variations in solar irradiance should be considered. Overall, the improved self-consumption and reduced grid dependency of tracked systems highlight their potential for enhanced PV performance when integrated with energy storage.

4.3 Economic evaluation of PV systems

This study utilised the LCOE to evaluate the economic performance of the proposed PV system, for fixed systems with battery storage, and tracked systems with battery storage. Due to the significant financial uncertainties and the complex nature of the proposed project, this study opted for a more straightforward approach by employing the turnkey method for LCOE calculations. The LCOE was determined by aggregating all the relevant system costs expected to be incurred throughout the project's lifetime. These total costs were then divided by the expected total discounted energy output of the system over its operational lifespan, as outlined in Equation 19. The annual energy output projections were derived from the PVsyst simulation results, which were then scaled up using appropriate scaling factors. This was necessary as each complete system had to be adjusted to account for the battery input limitation in PVsyst, as discussed in 3.8. Assumptions on system cost were made based on [109], [110]and [77]. These Assumptions are shown in Table 4.12. Component replacements were not considered due to significant uncertainties surrounding the proposed mega project. Microsoft Excel was

used to analyse, aggregate, and scale the system data for each site configuration. The NPV of the CAPEX, OPEX, and annual energy output values were input into a Python-based LCOE model, for the final calculation of LCOE. The model was pre-programmed with a discount rate (WACC), inflation rate, and module degradation factors, with NPV CAPEX, OPEX, and annual energy output as the primary input parameters.

Table 4. 8: Assumed economic parameters.

Parameters	Values
Capital Expenditure (CAPEX)	1030 USD$/kW
Battery 10hr	139 USD$/kWh
1d Trackers	200 USD $/kW
Operational Expenditure (OPEX)	13 USD$/kW
Land Lease	28,555,800 USD$
Discount rate (WACC)	10%
Inflation Rate	4%
Module Degradation	0.25 %/yr.
System Lifetime	30 years
First-year energy output	PVsyst Simulation with Storage Result

The costs of the battery and tracking systems are added to the total capital CAPEX because the initial CAPEX ratio only considers fixed systems without storage. These additional costs must be accounted for and added to the overall CAPEX calculation to provide an accurate total CAPEX for systems that include trackers and energy storage.

4.3.1 Economic Analyses for Both Sites

As previously stated, the annual energy outputs from the PVsyst simulations for each subsystem are utilised in this section. The economic analyses for both sites are summarised in Tables 4.9 and 4.10 below, and Figure 4.13 illustrates the financial and energy output performance differences between tracked and fixed systems, specifically comparing the OPEX and energy output behaviour over a 30-year period. The observed

decrease in OPEX over time, as depicted in Figure 4.13, is attributable to the discounting of future costs. Although nominal OPEX increases with inflation, the economic evaluation applies a discount rate, typically reflecting the project's Weighted Average Cost of Capital that exceeds the inflation rate. This results in the net present value of future OPEX decreasing over time, which is why they appear lower in the long-term economic analysis..

Table 4. 9: Economic Evaluation for the Springbok Site

Site	Configuration With Storage	Nominal Power, GW	Total CAPEX [US$]	Total OPEX [US$]	Energy output [kWh/yr.]	LCOE $/kWh
Springbok	**Fixed**	1.394	3 913 884 859	46 808 476	2 926 241 435	0.168
	Tracked	1.275	3 809 574 355	45 132 672	3 196 167 102	0.149

Table 4. 10: Economic Evaluation for the Dolphin Site

Site	Configuration With Storage	Nominal Power, GW	Total CAPEX [US$]	Total OPEX [US$]	Energy output [kWh/yr.]	LCOE $/kWh
Dolphin	**Fixed**	1.394	3 884 749 240	46 672 600	2 912 238 800	0.167
	Tracked	1.275	3 809 574 355	45 132 672	3 208 389 672	0.149

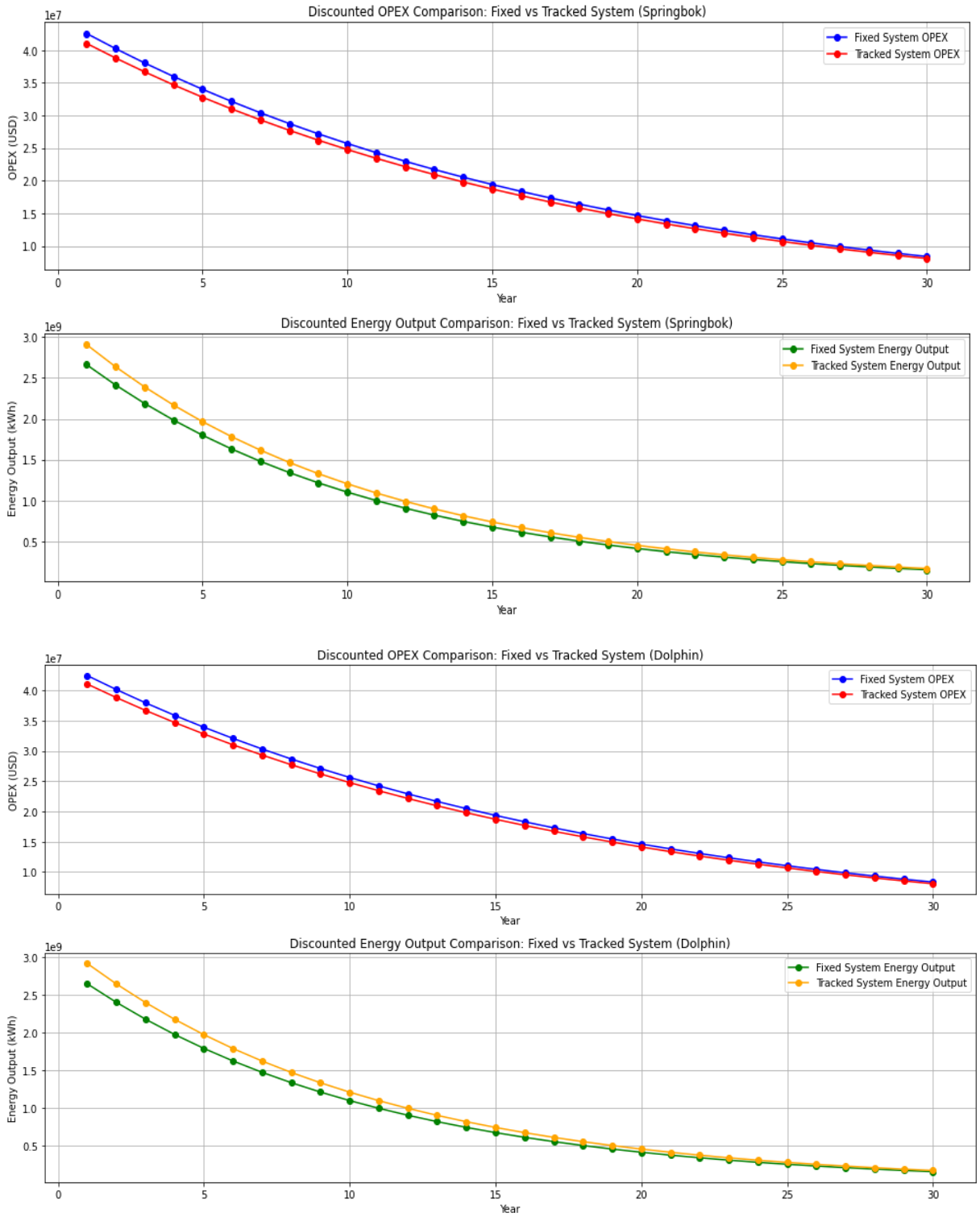

Figure 4. 13: Comparison of OPEX and Energy Output over the 30 years

According to [111] and [77], the calculated LCOE values for the two sites fall within the typical range for grid-connected PV systems with battery storage. However, the replacement costs of the batteries, inverters and trackers were not included in this analysis. Incorporating these factors would lead to an increase in the LCOE for the system. The results indicate that a tracking system with storage has a lower LCOE compared to a fixed system with storage. Furthermore, the simulations show that the tracked system has a slightly lower CAPEX and OPEX, as well as a higher first-year energy output, compared to the fixed system for both sites. The fixed system requires approximately 10.11% more subsystems at the Springbok site and 9.29% more at the Dolphin site compared to the tracked system to meet the same load demand. This difference leads to higher CAPEX and OPEX for the fixed system, as the simulations showed (Figure 4.13) it does not also produce surplus energy for the grid. In contrast, the tracked system meets the demand with fewer subsystems while generating more energy overall.

Chapter 5

Conclusion and Recommendations

5.1 Introduction

This chapter summarises the key conclusions of the research, presents recommendations, discusses the limitations encountered, and suggests areas for further research.

This study aimed to conduct an independent techno-economic assessment of the photovoltaic component of the proposed SCDI Namibian Green Hydrogen project. It provided insights into the approximate system cost, performance metrics and optimisation of the PV system required to power the electrolysers. This study carried out a detailed analysis of site conditions, component selection, PV system design and operational simulations, and economic feasibility, offering an objective assessment to complement company-sourced data, and ensuring transparency in the proposed project.

5.2 Summary of the Study

The Specific details of the proposed PV sites of the SCDI Namibia Green Hydrogen project were not extensively disclosed, aside from graphical representations marking its location. To address this, a comprehensive site investigation was conducted to determine suitable site's coordinates, area, topography, and solar resources, using tools such as QGIS, Google Earth, and SolarGIS. Preliminary decisions regarding input parameters, such as safety factors, system sizing, orientation, and component selection, were made to ensure accurate simulations and enable a robust comparative analysis between PVsyst and Fraunhofer Zenit software. The input parameters were standardised across both software

platforms for consistent and reliable comparison of results. Energy storage was added and simulated only with PVsyst to determine the impact of battery storage on system performance, particularly in terms of energy self-consumption, grid interaction and cost. This clarified how both fixed and tracked systems operate when integrated with storage and the grid, monthly and daily. Lastly, an economic analysis was performed using the LCOE metric for both the fixed system with storage and grid support and the tracked system.

5.3 Analysis of Key Findings

The study revealed that the proposed 33 km² area by Hyphen for both sites is oversized, even when accounting for a 20% safety margin. The presence of mountains to the east of the proposed plant location does not introduce any significant shading effects on the system. Additionally, although the two sites are located 23 km apart, they experience remarkably similar solar resource availability throughout the year. Furthermore, the analysis identified a 66 kV transmission line passing through the Springbok site, which could potentially ease grid connection for the project.

The analysis indicates that the total system must generate 18.08 GWh per day at its peak capacity to meet the daily load demand for producing a conservative estimate of 300,000 tonnes of hydrogen per year. Both sites are expected to contribute equally, with each required to deliver 9.04 GWh per day.

It was observed that the tracked system, despite requiring fewer subsystems, yields higher energy output compared to the fixed system. Additionally, the analysis shows that both configurations will interact with the utility grid for supplemental support, even when operating in a self-consumption mode with energy storage. This interaction is especially

notable after midnight during the winter months when both systems draw more energy from the grid. The tracked system is projected to inject surplus energy into the grid during the summer months due to higher production. Moreover, the analysis assessed that all configurations would incorporate battery storage, which will be used both for storing and directly supplying energy to the electrolysers. For the fixed system configurations, the storage system is projected to achieve a self-consumption rate of 80%, with the remaining 20% supplemented by the grid. The tracked system will have a slightly higher self-consumption rate of 87%, requiring only 13% support from the grid. This highlights the crucial role of the grid in the Green Hydrogen project, ensuring a consistent energy supply to the electrolyser when battery storage is insufficient. Additionally, the grid lowers OPEX by allowing excess energy to be fed back through net metering, reducing reliance on battery storage and offsetting electricity costs. The study estimated that the cost of implementing a fixed PV system with storage would be approximately US$ 3.91 billion, representing 39% of the total known investment of US$ 10 billion [2]. In comparison, the tracked system is estimated to cost US$ 3.80 billion, which represents 38% of the total investment. Furthermore, the annual operating costs for all configurations are projected to start at approximately US$ 46 million and increase over time due to inflation.

The analysis determined that the LCOE for the tracked system with storage is US$ 0.149/kWh. While this is higher than Namibia's current electricity tariff of US$ 0.12/kWh [112], the difference may be due to grid subsidies or cost structures that favour conventional electricity sources. Despite PV's global cost competitiveness, the addition of storage increases costs, making hydrogen production less economically viable under current conditions.

The findings of this study have significant implications for future renewable energy projects in other regions of Namibia that also enjoy similar solar irradiance.

The study concludes that producing cost-effective H_2 in Namibia using photovoltaics alone is currently unachievable. This is due to several factors being excluded from the techno-economic analysis, such as component replacements and miscellaneous costs, which contributed to an incomplete assessment. Despite conservative estimates, the LCOE remained high, additionally, the OPEX needs to be significantly reduced to make hydrogen production economically viable. However, with the ongoing decline in renewable energy costs, the prospect of producing hydrogen at a lower cost in the near future remains promising. A comprehensive techno-economic evaluation that incorporates both PV and wind systems could also potentially reduce the LCOE.

5.4 Recommendations

Based on the findings of the research, the following recommendations are made for the successful implementation of the proposed PV system:

5.4.1 Optimising System Design for Space Efficiency

The research revealed that both the site's proposed areas are oversized for the fixed and tracked systems, even when factoring in a 20% safety margin. It is recommended to optimise the land use by resizing the project footprint to align more closely with the actual space required, this would reduce unnecessary costs related to construction, such as fencing cost, and land works and will result in lower maintenance costs. Prioritising the tracked system over the fixed system will reduce the number of subsystems required, enhancing overall project performance.

5.4.2 Leveraging Grid Interaction for Energy Management

Given the findings that both fixed and tracked systems interact with the grid, particularly during winter months or after midnight, it is recommended that grid integration be carefully managed. Implementing advanced demand-side management strategies could help reduce grid reliance during low production periods.

5.4.3 Adopting the Tracked System as the Preferred Configuration

While both fixed and tracked configurations are viable for the proposed project, the tracked system consistently demonstrated a higher performance and greater energy generation with lower reliance on the grid. Therefore, the tracked system is recommended as the preferred configuration for this project, especially considering the potential to achieve higher self-consumption rates of 87% and inject surplus energy into the grid during peak energy production months. This choice would lead to improved economic performance over the project’s lifecycle.

5.4.4 Utilisation of Tier One Equipment

Given that the proposed project will incur an annual operating cost of over US$46 million, it is recommended that the plant design incorporates Tier One equipment. The use of Tier One equipment, which offers extended warranties and meets industry standard testing protocols, will ensure greater reliability and longer operational lifespans. By selecting high-quality components, the likelihood of equipment failure or costly maintenance can be minimised, reducing long-term operational costs. Furthermore, the robust performance of Tier One equipment will support the system's efficiency and stability, contributing to the overall economic feasibility and success of the project.

5.5 Limitations

While the simulation results indicate that the tracked system outperforms the fixed system in terms of energy production and LCOE, several limitations of this research must be acknowledged. Firstly, although satellite data from SolarGIS is regarded as high-quality, inherent uncertainties remain, particularly in the accuracy of long-term solar irradiance predictions and localised meteorological variations. Furthermore, given the scale of the proposed system, additional challenges related to land use, shading, and topographical effects may not have been fully captured in the simulations. The reliance on simulation tools such as PVsyst and Fraunhofer Zenit, though widely accepted in the industry, introduces a level of uncertainty, as these tools depend on assumptions regarding meteorological inputs and system component behaviour. Real-world performance may deviate due to factors such as equipment downtime, unforeseen weather conditions, and operational inefficiencies. Additionally, the economic assumptions made in the analysis, such as CAPEX and OPEX estimations, do not fully account for market fluctuations in material costs, government incentives, unforeseen interest rates, or exchange rate volatility could affect the long-term economic viability of the project, especially since most hydrogen off-takers are international entities rather than Namibian.

5.6 Areas of further research

While this study has provided valuable insights into system costs, performance, and optimisation, several information gaps remain. Future research should focus on refining LCOE calculations, particularly to account for unforeseen costs, as current literature does not extensively address LCOE in the Southern African context. Special attention should be given to systems incorporating newer battery technologies or hybrid configurations.

Additionally, further investigation into the Levelised Cost of Hydrogen (LCOH) in conjunction with the PV system is recommended to fully assess the economic feasibility of green hydrogen production. Studies on advanced energy storage solutions and their potential to reduce grid dependence would also enhance system optimisation and cost-efficiency. Moreover, site-specific research is crucial, particularly on the impact of soiling on PV modules, the effects of wind speed on the mounting systems, and the influence of temperature on the BESS.

References

[1] A. Roshini, A. Chokri, B. Luisa, and F. López González, “Green Hydrogen Production in Namibia.” Accessed: Jun. 24, 2024. [Online]. Available: https://dechema.de/green_hydrogen_namibia_report.html

[2] The Southern Corridor Development initiative, “Namibia Green Hydrogen Projects,” 2023.

[3] Hyphen Hydrogen Energy (Pty) Ltd, “ENVIRONMENTAL AND SOCIAL SCREENING STUDY,” May 2022.

[4] Andreas Glockner, “HYPHEN: First Gigawatt-scale Green Ammonia Project in Namibia.” Accessed: Mar. 07, 2024. [Online]. Available: https://hyphenafrica.com/wp-content/uploads/2022/05/Hyphen-World-Economic-Forum-Presentation-24-May-2022.pdf

[5] J. Manna, “Overview on application of hydrogen,” *Towards Hydrogen Infrastructure: Advances and Challenges in Preparing for the Hydrogen Economy*, pp. 401–430, Jan. 2024, doi: 10.1016/B978-0-323-95553-9.00006-6.

[6] S. Shiva Kumar and V. Himabindu, “Hydrogen production by PEM water electrolysis – A review,” Dec. 01, 2019, *KeAi Communications Co.* doi: 10.1016/j.mset.2019.03.002.

[7] Rob Cockerill, “PEM vs Alkaline electrolysis,” 2019. Accessed: Jul. 12, 2024. [Online]. Available: https://www.h2-view.com/

[8] D. M. F. Santos, C. A. C. Sequeira, and J. L. Figueiredo, “HYDROGEN PRODUCTION BY ALKALINE WATER ELECTROLYSIS,” 2013. doi: 10.1590/s0100-40422013000800017.

[9] Seyed Ehsan Hosseini, “50 shades of (grey and blue and green) hydrogen,” *energy cities*, Mar. 2021, Accessed: Apr. 01, 2024. [Online]. Available: Http://energycities.eu/50-shades-of grey-and-blue-and-green-hydrogen/

[10] A. Mohamed Elshafei and R. Mansour, “Green Hydrogen as a Potential Solution for Reducing Carbon Emissions: A Review,” *Journal of Energy Research and Reviews*, vol. 13, no. 2, pp. 1–10, Feb. 2023, doi: 10.9734/jenrr/2023/v13i2257.

[11] S. A. Grigoriev, V. I. Porembsky, and V. N. Fateev, “Pure hydrogen production by PEM electrolysis for hydrogen energy,” in *International Journal of Hydrogen Energy*, Feb. 2006, pp. 171–175. doi: 10.1016/j.ijhydene.2005.04.038.

[12] S. N. M. Abdalla and H. Özcan, “Design and simulation of a 1-GWp solar photovoltaic power station in Sudan,” *Clean Energy*, vol. 5, no. 1, pp. 57–78, Mar. 2021, doi: 10.1093/ce/zkaa030.

[13] U. Subramaniam, S. Vavilapalli, S. Padmanaban, F. Blaabjerg, J. B. Holm-Nielsen, and D. Almakhles, “A hybrid PV-battery system for ON-grid and off-grid applications-controller-in-loop simulation validation,” *Energies (Basel)*, vol. 13, no. 3, 2020, doi: 10.3390/en13030755.

[14] H. Nakayama, E. Hiraki, T. Tanaka, N. Koda, N. Takahashi, and S. Noda, “Stand-alone Photovoltaic Generation System with Combined Storage using lead Battery and EDLC,” Aug. 2008, pp. 1877–1883. doi: 10.1109/EPEPEMC.2008.4635539.

[15] M. Consulting Services, “Namibia Renewable Energy Grid Code: Final Prepared for the Electricity Control Board (ECB) By Mutschler Consulting Services and subconsultants Contents Final RE Grid Code,” 2020.

[16] Global Sustainable Energy Solutions, “GRID-CONNECTED PV SYSTEMS SYSTEM DESIGN GUIDELINES,” 2019.

[17] R. Srivastava and V. K. Giri, “Design of Grid Connected PV System Using Pvsyst,” *African Journal of Basic & Applied Sciences*, vol. 9, no. 2, pp. 92–96, 2017, doi: 10.5829/idosi.ajbas.2017.92.96.

[18] A. Singh, S. K. Sinha, K. Pandey, and S. Hans, “An optimized smart switch hybrid renewable system with battery storage system,” in *2017 4th IEEE Uttar Pradesh Section International Conference on Electrical, Computer and Electronics (UPCON)*, IEEE, Oct. 2017, pp. 162–168. doi: 10.1109/UPCON.2017.8251041.

[19] W. S. Ebhota and P. Y. Tabakov, “Assessment and performance analysis of roof-mounted crystalline stand-alone photovoltaic (SAPV) system at selected sites in South Africa,” *Bull Natl Res Cent*, vol. 46, no. 1, Aug. 2022, doi: 10.1186/s42269-022-00929-3.

[20] J. Hurtt and K. Baker, “Sensitivity Analysis of Photovoltaic System Design Parameters to Passively Mitigate Ramp Rates,” *IEEE J Photovolt*, vol. 11, no. 2, pp. 545–551, Mar. 2021, doi: 10.1109/JPHOTOV.2020.3045679.

[21] A. B. Sproul, “Derivation of the solar geometric relationships using vector analysis,” *Renew Energy*, vol. 32, no. 7, pp. 1187–1205, Jun. 2007, doi: 10.1016/j.renene.2006.05.001.

[22] A. K. Yadav and H. Malik, “Optimization of tilt angle for installation of solar photovoltaic system for six sites in India,” in *2015 International Conference on Energy Economics and Environment (ICEEE)*, IEEE, Mar. 2015, pp. 1–4. doi: 10.1109/EnergyEconomics.2015.7235078.

[23] H. Terzioɬlu, F. A. Kazan, and C. Sungur, “The irrigation system fed from biaxial PV panels,” in *Proceedings - 2015 2nd International Conference on Information Science and Control Engineering, ICISCE 2015*, Institute of Electrical and Electronics Engineers Inc., Jun. 2015, pp. 981–987. doi: 10.1109/ICISCE.2015.222.

[24] C.Honsberg and S.Bowden, “Terrestrial Solar Radiation.” Accessed: Aug. 26, 2024. [Online]. Available: https://www.pveducation.org/pvcdrom/properties-of-sunlight/declination-angle

[25] A. Al-Helaly and I. J. Muhsin, “Gaussian Equation to Describe the Percent of Shadow Length in Satellite Image.”

[26] A. Carballar, R. Rodríguez-Garrido, M. Jerez, J. Vera, and J. Granado, “Measuring DNI with a New Radiometer Based on an Optical Fiber and Photodiode,” *Sensors*, vol. 24, no. 11, p. 3674, Jun. 2024, doi: 10.3390/s24113674.

[27] W. Yao, Z. Li, T. Xiu, Y. Lu, and X. Li, “New decomposition models to estimate hourly global solar radiation from the daily value,” *Solar Energy*, vol. 120, pp. 87–99, Oct. 2015, doi: 10.1016/j.solener.2015.05.038.

[28] J. F. Orgill and K. G. T. Hollands, “Correlation equation for hourly diffuse radiation on a horizontal surface,” *Solar Energy*, vol. 19, no. 4, pp. 357–359, 1977, doi: 10.1016/0038-092X(77)90006-8.

[29] D. G. Erbs, S. A. Klein, and J. A. Duffie, “Estimation of the diffuse radiation fraction for hourly, daily and monthly-average global radiation,” *Solar Energy*, vol. 28, no. 4, pp. 293–302, 1982, doi: 10.1016/0038-092X(82)90302-4.

[30] E. L. Maxwell, “A Quasi-Physical Model for Converting Hourly Global Horizontal to Direct Normal lnsolation,” 1987.

[31] P. G. Loutzenhiser, H. Manz, C. Felsmann, P. A. Strachan, T. Frank, and G. M. Maxwell, “Empirical validation of models to compute solar irradiance on inclined surfaces for building energy simulation,” *Solar Energy*, vol. 81, no. 2, pp. 254–267, Feb. 2007, doi: 10.1016/j.solener.2006.03.009.

[32] A. Louche, G. Notton, P. Poggi, and G. Simonnot, “Correlations for direct normal and global horizontal irradiation on a French Mediterranean site,” *Solar Energy*, vol. 46, no. 4, pp. 261–266, 1991, doi: 10.1016/0038-092X(91)90072-5.

[33] R. Perez, “Dynamic global-to-direct irradiance conversion models,” 1992. [Online]. Available: https://www.researchgate.net/publication/279868352

[34] H.-M. Zuo, J. Qiu, and F.-F. Li, “Ultra-short-term forecasting of global horizontal irradiance (GHI) integrating all-sky images and historical sequences,” *Journal of Renewable and Sustainable Energy*, vol. 15, no. 5, Sep. 2023, doi: 10.1063/5.0163759.

[35] J. S. Stein and C. W. Hansen, “Irradiance on the Plane of the Array,” in *Photovoltaic Solar Energy*, Wiley, 2024, pp. 25–38. doi: 10.1002/9781119578826.ch4.

[36] L. Deville, M. Theristis, B. H. King, T. L. Chambers, and J. S. Stein, “Comparison of Open-Source Photovoltaic Performance Models Against Multi-Year Field Data,” in *2023 IEEE 50th Photovoltaic Specialists Conference (PVSC)*, IEEE, Jun. 2023, pp. 1–3. doi: 10.1109/PVSC48320.2023.10359971.

[37] B. Y. H. Liu and R. C. Jordan, “The interrelationship and characteristic distribution of direct, diffuse and total solar radiation,” *Solar Energy*, vol. 4, no. 3, pp. 1–19, Jul. 1960, doi: 10.1016/0038-092X(60)90062-1.

[38] J. E. Hay, “Calculating solar radiation for inclined surfaces: Practical approaches,” *Renew Energy*, vol. 3, no. 4–5, pp. 373–380, Jun. 1993, doi: 10.1016/0960-1481(93)90104-O.

[39] T. M. Klucher, “Evaluation of models to predict insolation on tilted surfaces,” *Solar Energy*, vol. 23, no. 2, pp. 111–114, 1979, doi: 10.1016/0038-092X(79)90110-5.

[40] L. C. Segado-Moreno, J. A. Ruiz-Arias, and J. P. Montávez, “Surface solar radiation trends over Europe assessed from ground-based measurements and satellite imagery and their comparison with climate models,” Mar. 2023. Accessed: Jun. 06, 2024. [Online]. Available: https://meetingorganizer.copernicus.org/EGU23/EGU23-15554.html

[41] G. M. Foody, “Ground Truth in Classification Accuracy Assessment: Myth and Reality,” *Geomatics*, vol. 4, no. 1, pp. 81–90, Feb. 2024, doi: 10.3390/geomatics4010005.

[42] Anne Forstinger, Adam R. Jensen, and Stefan Wilbert, *Worldwide Benchmark of Modelled Solar Irradiance Data 2023 Task 16 Solar Resource for High Penetration and Large Scale Applications*. IEA PVPS TCP, 2023. [Online]. Available: www.iea-pvps.org

[43] R. Pacudan, “Implications of applying solar industry best practice resource estimation on project financing,” *Energy Policy*, vol. 95, pp. 489–497, Aug. 2016, doi: 10.1016/j.enpol.2016.02.021.

[44] C. Budig, J. Orozaliev, and K. Vajen, “Comparison of Different Sources of Meteorological Data for Central Asia and Russia,” in *Proceedings of the EuroSun 2010 Conference*, Freiburg, Germany: International Solar Energy Society, 2010, pp. 1–8. doi: 10.18086/eurosun.2010.13.01.

[45] T. Bravo Mahachi, A. Johan Rix, T. Mahachi, and A. Rix, “COMPARISON OF VARIOUS LONG TERM AVERAGED METEOROLOGICAL DATA SOURCES FOR A SITE IN SOUTH AFRICA COMPARISON OF VARIOUS LONG TERM AVERAGED METEO-ROLOGICAL DATA SOURCES FOR A SITE IN SOUTH AFRICA.” [Online]. Available: https://www.researchgate.net/publication/313249254

[46] C. Vlad and C. V. Lungu, “Considerations regarding PV systems,” *Annals of the ”Dunarea de Jos” University of Galati Fascicle II Mathematics Physics Theoretical Mechanics*, vol. 45, no. 2, pp. 126–132, Dec. 2022, doi: 10.35219/ann-ugal-math-phys-mec.2022.2.14.

[47] N. M. Kumar *et al.*, “Solar PV module technologies,” in *Photovoltaic Solar Energy Conversion*, Elsevier, 2020, pp. 51–78. doi: 10.1016/B978-0-12-819610-6.00003-X.

[48] M. T. Makhloufi, Y. Abdessemed, and M. S. Khireddine, “A Feed forward Neural Network MPPT Control Strategy Applied to a Modified Cuk Converter,” *International Journal of Electrical and Computer Engineering (IJECE)*, vol. 6, no. 4, p. 1421, Aug. 2016, doi: 10.11591/ijece.v6i4.pp1421-1433.

[49] N. A. Zainal, Ajisman, and A. R. Yusoff, “Modelling of Photovoltaic Module Using Matlab Simulink,” *IOP Conf Ser Mater Sci Eng*, vol. 114, p. 012137, Feb. 2016, doi: 10.1088/1757-899X/114/1/012137.

[50] T. A. Chandel, M. Y. Yasin, and M. A. Mallick, “Modeling and Simulation of Photovoltaic Cell using Single Diode Solar Cell and Double Diode Solar Cell Model,” *International Journal of Innovative Technology and Exploring Engineering*, vol. 8, no. 10, pp. 558–565, Aug. 2019, doi: 10.35940/ijitee.J8863.0881019.

[51] C. M. Whitaker and J. D. Newmiller, “Photovoltaic Mg. dule Energy Rating Procedure Final Subcontract Report,” 1998.

[52] Solmetric, “Application Note PVA-600-1 Guide To Interpreting I-V Curve Measurements of PV Arrays,” 2011. [Online]. Available: http://www.solmetric.com

[53] S. Bhattacharjee and B. J. Saharia, “A comparative study on converter topologies for maximum power point tracking application in photovoltaic generation,” *Journal of Renewable and Sustainable Energy*, vol. 6, no. 5, Sep. 2014, doi: 10.1063/1.4900579.

[54] V. Benda and L. Černá, “PV cells and modules – State of the art, limits and trends,” *Heliyon*, vol. 6, no. 12, p. e05666, Dec. 2020, doi: 10.1016/j.heliyon.2020.e05666.

[55] S. W. Glunz, R. Preu, and D. Biro, “Crystalline Silicon Solar Cells,” in *Comprehensive Renewable Energy*, Elsevier, 2012, pp. 353–387. doi: 10.1016/B978-0-08-087872-0.00117-7.

[56] N. Kumari, S. Kumar Singh, and S. Kumar, “A comparative study of different materials used for solar photovoltaics technology,” *Mater Today Proc*, vol. 66, pp. 3522–3528, 2022, doi: 10.1016/j.matpr.2022.06.403.

[57] F. Ise and P. Projects GmbH, “Photovoltaics Report-Fraunhofer Institute for Solar Energy Systems, ISE with the support of PSE Projects GmbH,” 2024. [Online]. Available: www.ise.fraunhofer.de

[58] T. D. Lee and A. Ebong, “Thin film solar technologies: a review,” in *2015 12th International Conference on High-capacity Optical Networks and Enabling/Emerging Technologies (HONET)*, IEEE, Dec. 2015, pp. 1–10. doi: 10.1109/HONET.2015.7395441.

[59] G. Beardsworth, & Amir, and A. Shishavan, “QUANTIFYING YOUR BIFACIAL GAINS Using Calibrated PVsyst Model Input Parameters to Accurately Predict In-Field Performance.”

[60] J.M. Kroon and B.R. Newman, “Photovoltaics International Interconnection | PV Modules.” [Online]. Available: www.pv-tech.org

[61] K. Hofmeister, “Webinar-Half-Cut Cell Modules,” 2018. Accessed: Sep. 07, 2024. [Online]. Available: www.trinasolar.com

[62] A. Bhalkar, A. Wadekar, M. Wagh, and S. Dengle, “Issues, challenges, and current lacunas in design, and installation of ground mounted solar PV module mounting structure (MMS),” *Mater Today Proc*, vol. 58, pp. 128–134, 2022, doi: 10.1016/j.matpr.2022.01.093.

[63] S. S. Hosseini, “A comprehensive review of the use of pleasant energy in Europe,” 2016, doi: 10.1387/ieee.0142154.

[64] R. Lipták and I. Bodnár, “Optimal sizing of battery storage for photovoltaic systems,” in *2023 24th International Carpathian Control Conference (ICCC)*, IEEE, Jun. 2023, pp. 236–241. doi: 10.1109/ICCC57093.2023.10178928.

[65] A. O. M. Maka and T. N. Chaudhary, “Performance investigation of solar photovoltaic systems integrated with battery energy storage,” *J Energy Storage*, vol. 84, p. 110784, Apr. 2024, doi: 10.1016/j.est.2024.110784.

[66] Z. Šimić, D. Topić, G. Knežević, and D. Pelin, “Battery energy storage technologies overview,” *International journal of electrical and computer engineering systems*, vol. 12, no. 1, pp. 53–65, Apr. 2021, doi: 10.32985/ijeces.12.1.6.

[67] M. Deepika *et al.*, “MPPT-Based Charge Controller for Battery Fast Charging,” in *2023 9th International Conference on Advanced Computing and Communication Systems (ICACCS)*, IEEE, Mar. 2023, pp. 449–453. doi: 10.1109/ICACCS57279.2023.10112852.

[68] B. Pooja, S. Rajanna, N. L. Varaprasad, M. Ramesh, G. R. Sowmya, and S. R. Rakshitha, "Design of a Battery Charge Controller Through MPPT Based Solar Photovoltaic System," in *2022 Fourth International Conference on Emerging Research in Electronics, Computer Science and Technology (ICERECT)*, IEEE, Dec. 2022, pp. 1–6. doi: 10.1109/ICERECT56837.2022.10060581.

[69] A. Dhaneria and H. Khambhadiya, "Hardware Implementation of Grid connected Solar PV Inverter," in *2020 International Conference on Power Electronics & IoT Applications in Renewable Energy and its Control (PARC)*, IEEE, Feb. 2020, pp. 28–32. doi: 10.1109/PARC49193.2020.236551.

[70] International Finance Corporation, "Utility-Scale Solar Photovoltaic Power Plants In partnershIp wIth a project Developer's GuIDe," 2015. Accessed: May 06, 2024. [Online]. Available: https://hdl.handle.net/10986/22797

[71] A. Al-Subhi, M. I. Mosaad, and T. A. Farrag, "PV parameters estimation using optimized deep neural networks," *Sustainable Computing: Informatics and Systems*, vol. 41, p. 100960, Jan. 2024, doi: 10.1016/j.suscom.2024.100960.

[72] A. Elamim, B. Hartiti, A. Haibaoui, A. Lfakir, and P. Thevenin, "Performance evaluation and economical analysis of three photovoltaic systems installed in an institutional building in Errachidia, Morocco," *Energy Procedia*, vol. 147, pp. 121–129, Aug. 2018, doi: 10.1016/j.egypro.2018.07.041.

[73] S. Gulkowski, "Specific Yield Analysis of the Rooftop PV Systems Located in South-Eastern Poland," *Energies (Basel)*, vol. 15, no. 10, May 2022, doi: 10.3390/en15103666.

[74] M. O. Dioha, A. Kumar, M. Mathew, and J. Hossain, "Comparative Performance Analysis of Different Silicon-based Photovoltaic Technologies in Nigeria," in *2018 International Conference on Power Energy, Environment and Intelligent Control (PEEIC)*, IEEE, Apr. 2018, pp. 578–584. doi: 10.1109/PEEIC.2018.8665460.

[75] A. Boretti and S. Castelletto, "Cost and performance of CSP and PV plants of capacity above 100 MW operating in the United States of America," *Renewable Energy Focus*, vol. 39, pp. 90–98, Dec. 2021, doi: 10.1016/j.ref.2021.07.006.

[76] M. S. Adaramola, "Techno-economic analysis of a 2.1 kW rooftop photovoltaic-grid-tied system based on actual performance," *Energy Convers Manag*, vol. 101, pp. 85–93, Sep. 2015, doi: 10.1016/j.enconman.2015.05.038.

[77] F. Ise, "LEVELIZED COST OF ELECTRICITY RENEWABLE ENERGY TECHNOLOGIES," 2021. [Online]. Available: www.ise.fraunhofer.de

[78] F. Ise and P. Projects GmbH, "Photovoltaics Report-Fraunhofer Institute for Solar Energy Systems, ISE with the support of PSE Projects GmbH," 2024. [Online]. Available: www.ise.fraunhofer.de

[79] S. H. Khader, A.-K. K. Daud, and A. A. Abu-aisheh, "Studying the Shading Effect of PV System on Energy Performances in Restricted Spaces," *Renewable Energies, Environment and Power Quality Journal*, vol. 2, pp. 51–59, Jul. 2024, doi: 10.24084/reepqj24.232.

[80] Arup, “First Solar Energy Yield Simulations Module Performance Comparison for Four Solar PV Module Technologies,” 2015.

[81] C. Deline, A. Dobos, S. Janzou, J. Meydbray, and M. Donovan, “A simplified model of uniform shading in large photovoltaic arrays,” *Solar Energy*, vol. 96, pp. 274–282, Oct. 2013, doi: 10.1016/j.solener.2013.07.008.

[82] S. Boppana, K. Passow, J. Sorensen, B. H. King, and C. Robinson, “Impact of Uncertainty in IAM Measurement on Energy Predictions,” in *2018 IEEE 7th World Conference on Photovoltaic Energy Conversion (WCPEC) (A Joint Conference of 45th IEEE PVSC, 28th PVSEC & 34th EU PVSEC)*, IEEE, Jun. 2018, pp. 2276–2281. doi: 10.1109/PVSC.2018.8548024.

[83] M. L. Adekanbi, E. S. Alaba, T. J. John, T. D. Tundealao, and T. I. Banji, “Soiling loss in solar systems: A review of its effect on solar energy efficiency and mitigation techniques,” *Cleaner Energy Systems*, vol. 7, p. 100094, Apr. 2024, doi: 10.1016/j.cles.2023.100094.

[84] J. G. Bessa, L. Micheli, J. Montes-Romero, F. Almonacid, and E. F. Fernández, “Estimation of Photovoltaic Soiling Using Environmental Parameters: A Comparative Analysis of Existing Models,” *Adv Sustain Syst*, vol. 6, no. 5, May 2022, doi: 10.1002/adsu.202100335.

[85] B. R. Paudyal and A. G. Imenes, “Investigation of temperature coefficients of PV modules through field measured data,” *Solar Energy*, vol. 224, pp. 425–439, Aug. 2021, doi: 10.1016/j.solener.2021.06.013.

[86] D. G. Lorente, S. Pedrazzi, G. Zini, A. Dalla Rosa, and P. Tartarini, “Mismatch losses in PV power plants,” *Solar Energy*, vol. 100, pp. 42–49, Feb. 2014, doi: 10.1016/j.solener.2013.11.026.

[87] K. A. K. Niazi, T. Kerekes, A. Dolara, Y. Yang, and S. Leva, “Performance Assessment of Mismatch Mitigation Methodologies Using Field Data in Solar Photovoltaic Systems,” *Electronics (Basel)*, vol. 11, no. 13, p. 1938, Jun. 2022, doi: 10.3390/electronics11131938.

[88] P. Lluch, O. Farrerons, and V. Co-Director, “DESIGN AND VALIDATION OF A PHOTOVOLTAIC PLANT Volume I. Memory and annexes.”

[89] T. Mahachi and A. J. Rix, “Energy yield analysis and evaluation of solar irradiance models for a utility scale solar PV plant in South Africa,” 2016. [Online]. Available: https://scholar.sun.ac.za

[90] S. Manat, V. Yugay, and N. Kaliaskarov, “Analysis of power losses in multilevel pulse-width modulation inverters,” *Eastern-European Journal of Enterprise Technologies*, vol. 2, no. 5 (116), pp. 31–42, Apr. 2022, doi: 10.15587/1729-4061.2022.252771.

[91] M. Iwakuma *et al.*, “AC loss properties of a 1 MVA single-phase HTS power transformer,” *IEEE Transactions on Appiled Superconductivity*, vol. 11, no. 1, pp. 1482–1485, Mar. 2001, doi: 10.1109/77.920054.

[92] Dr. R. M. Sumsudeen, “ANALYSIS AND DESIGN OF SOLAR PV SYSTEM USING PVSYST SOFTWARE,” in *Futuristic Trends in Electrical Engineering Volume 3 Book 2*,

Iterative International Publishers, Selfypage Developers Pvt Ltd, 2024, pp. 1–16. doi: 10.58532/V3BDEE2P1CH1.

[93] A. Grover, A. Khosla, and D. Joshi, “Design and simulation of 20MW photovoltaic power plant using PVSyst,” *Indonesian Journal of Electrical Engineering and Computer Science*, vol. 19, no. 1, p. 58, Jul. 2020, doi: 10.11591/ijeecs.v19.i1.pp58-65.

[94] B. Müller and A. Armbruster, “INNOGY-YIELD CALCULATION WORKSHOP YIELD SIMULATION SOFTWARE,” May 2020. [Online]. Available: www.ise.fraunhofer.de

[95] A. Mermoud and B. Wittmer, “YIELD SIMULATIONS FOR HORIZONTAL AXIS TRACKERS WITH BIFACIAL PV MODULES IN PVSYST,” 2018.

[96] A. Mermoud, A. Villoz, and B. Wittmer, “SIMULATION OF GRID-TIED PV SYSTEMS WITH BATTERY STORAGE IN PVSYST.”

[97] D. L. Guittet and J. M. Freeman, “Validation of Photovoltaic Modeling Tool HelioScope Against Measured Data,” 2018. [Online]. Available: https://www.nrel.gov/docs/fy19osti/72155.pdf.

[98] N. Riedel-Lyngskær *et al.*, “Validation of Bifacial Photovoltaic Simulation Software against Monitoring Data from Large-Scale Single-Axis Trackers and Fixed Tilt Systems in Denmark,” *Applied Sciences*, vol. 10, no. 23, p. 8487, Nov. 2020, doi: 10.3390/app10238487.

[99] QGIS Development Team, “QGIS Geographic Information System.,” 2024, Open Source Geospatial Foundation Project. http://qgis.org. Accessed: Jul. 23, 2024. [Online]. Available: http://qgis.org

[100] Hyphen, “Hyphen SCDI Project.” Accessed: Sep. 15, 2024. [Online]. Available: https://hyphenafrica.com/projects/

[101] Andrew Blok, “Most Efficient Solar Panels for 2024: New Record-Setting Panel Tops the List,” cnet. Accessed: Sep. 15, 2024. [Online]. Available: https://www.cnet.com/home/energy-and-utilities/most-efficient-solar-panels/

[102] Y. Park, “Sungrow Power Supply (300274 CH/Buy/Initiate).”

[103] ideematec, “Horizon L_TEC 1P Datasheet,” 2024, Accessed: Sep. 15, 2024. [Online]. Available: https://www.ideematec.com/products-services/solar-trackers/ltec-1p

[104] N. H. Reich, A. Goebel, D. Dirnberger, and K. Kiefer, “System performance analysis and estimation of degradation rates based on 500 years of monitoring data,” in *Conference Record of the IEEE Photovoltaic Specialists Conference*, 2012, pp. 1551–1554. doi: 10.1109/PVSC.2012.6317890.

[105] D. C. Jordan and S. R. Kurtz, “Photovoltaic Degradation Rates—an Analytical Review,” *Progress in Photovoltaics: Research and Applications*, vol. 21, no. 1, pp. 12–29, Jan. 2013, doi: 10.1002/pip.1182.

[106] L. Ghabuzyan, K. Pan, A. Fatahi, J. Kuo, and C. Baldus-Jeursen, “Thermal effects on photovoltaic array performance: Experimentation, modeling, and simulation,” *Applied Sciences (Switzerland)*, vol. 11, no. 4, pp. 1–15, Feb. 2021, doi: 10.3390/app11041460.

[107] P. Benalcazar, A. Komorowska, and J. Kamiński, “A GIS-based method for assessing the economics of utility-scale photovoltaic systems,” *Appl Energy*, vol. 353, p. 122044, Jan. 2024, doi: 10.1016/j.apenergy.2023.122044.

[108] R. Frischknecht, *Methodology Guidelines on Life Cycle Assessment of Photovoltaic Task 12 PV Sustainability*, 4th edition. 2020. [Online]. Available: www.iea-pvps.org

[109] TMP Public, “Least-cost energy investment study for Namibia,” 2023. [Online]. Available: www.internationalrivers.org

[110] P. Denholm, J. Eichman, and R. Margolis, “Evaluating the Technical and Economic Performance of PV Plus Storage Power Plants,” 2017. [Online]. Available: www.nrel.gov/publications.

[111] Lazard, “LEVELIZED COST OF ENERGY ANALYSIS-VERSION 17.0,” Jun. 2024. Accessed: Aug. 26, 2024. [Online]. Available: https://www.lazard.com/media/xemfey0k/lazards-lcoeplus-june-2024-_vf.pdf

[112] “Media Statement THE NEWS EDITOR FOR IMMEDIATE RELEASE NAMPOWER BULK TARIFF APPROVAL FOR THE FINANCIAL PERIOD 2024/2025,” 2024.

Appendices

List of Appendices

Appendix A:	Ethical Clearance Certificate
Appendix B:	Research Permission Letter
Appendix C:	Electrolyser datasheet
Appendix D:	Module datasheet
Appendix E:	Inverter datasheet
Appendix F:	Tracker datasheet
Appendix G:	Battery datasheet
Appendix H:	Simulation Loss diagram report Without Storage: fixed System
Appendix I:	Simulation Loss diagram report Without Storage: Tracked System
Appendix J:	Simulation Loss diagram report With Storage: fixed System
Appendix K:	Simulation Loss diagram report With Storage: Tracked System
Appendix L:	LCOE Scaling Sheets

Appendix A: Ethical Clearance Certificate

UNAM
UNIVERSITY OF NAMIBIA

ETHICAL CLEARANCE CERTIFICATE

Ethical Clearance Reference Number: SOS-0233 **Date: 23AUGUST 2024**

This Ethical Clearance Certificate is issued by the University of Namibia Ethics Committee (REC) in accordance with the University of Namibia's Research Ethics Policy and Guidelines. Ethical approval is given in respect of undertakings contained in the Research Project outlined below. This Certificate is issued on the recommendations of the ethical evaluation done by the ethics committee.

Title of Project:	ASSESSMENT OF THE PERFORMANCE OF A PHOTOVOLTAIC (PV) SYSTEM FOR POWERING ELECTROLYSERS IN THE GREEN HYDROGEN PROJECT AT TSAU//KHAEBS NATIONAL PARK USING MODELING AND SIMULATION APPROACH
Student:	JEREMIA PETRUS
Student Number:	201310573
Supervisor(s):	DR. PETJA DOBREVA DR. MATTHEW BERWIND

Centre for Research Services

Take note of the following:

1. Any significant changes in the conditions or undertakings outlined in the approved Proposal must be communicated to the ethics committee. An application to make amendments may be necessary.
2. Any breaches of ethical undertakings or practices that have an impact on ethical conduct of the research must be reported to the ethics committee.
3. The Principal Researcher must report issues of ethical compliance to the ethics committee (through the Chairperson) at the end of the Project or as may be requested by the ethics committee.
4. The ethics committee retains the right to:

i) Withdraw or amend this Ethical Clearance if any unethical practices (as outlined in the Research Ethics Policy) have been detected or suspected,

ii) Request for an ethical compliance report at any point during the course of the research.

The ethics committee wishes you the best in your research.

Prof. Ezekeil Gwinyai Kwembeya (Chairperson Ethics Committee)

Prof. Davis Mumbengegwi (Head, Multidisciplinary Research)

Appendix B: Research Permission Letter

CENTRE FOR RESEARCH SERVICES
Office of the Pro-Vice Chancellor: Research, Innovation & Development
University of Namibia, Private Bag 13301, Windhoek, Namibia
340 Mandume Ndemufayo Avenue, Pioneers Park, Office F223 - Fblock, Second Floor
☎ +264 61 206 4673; E-mail:kmbulu@unam.na; URL.: http//www.unam.edu.na

UNAM
UNIVERSITY OF NAMIBIA

RESEARCH PERMISSION LETTER

Date: 28/10/2024

Student Name: JEREMIA PETRUS

Student Number: 201310573

Programme: Master of science in Renewable energy

Approved Research Title: ASSESSMENT OF THE PERFORMANCE OF A PHOTOVOLTAIC (PV) SYSTEM FOR POWERING ELECTROLYSERS IN THE GREEN HYDROGEN PROJECT AT TSAU//KHAEBS NATIONAL PARK USING MODELING AND SIMULATION APPROACH

TO WHOM IT MAY CONCERN:

I hereby confirm that the above-mentioned student is registered at the University of Namibia for the programme indicated. The proposed study met all the requirements as stipulated in the University guidelines and has been approved by the relevant committees.

The proposal adheres to ethical principles as per attached Ethical Clearance Certificate. Permission is hereby granted to carry out the research as described in the approved proposal.

Best Regards

Dr. AEE Shikongo
Head: Postgraduate Research Support Services
Tel: +264 61 206 3129
E-mail: aeshikongo@unam.na

CENTRE FOR RESEARCH SERVICES
Office of the Director
2024 -10- 28
University of Namibia
UNAM

Appendix C: Electrolyser datasheet

DQ1000
Alkaline Electrolyser

1000 Nm^3/h

H2
Green Hydrogen

h2.johncockerill.com

John Cockerill

DQ1000, Alkaline Electrolyser | 1000 Nm^3/h

Large Scale Applications

Leader in the energy transition

John Cockerill Hydrogen offers efficient and reliable solutions for the production of green hydrogen. We meet the needs of major players in the industry, mobility, and energy sectors.

Driven by its pioneering spirit, John Cockerill Hydrogen has already delivered electrolysers to nearly 1,000 satisfied customers in a wide range of industries. Today, we offer some of the most powerful electrolysers on the market, capable of producing up to 1,000 Nm^3 per hour (5 MW of power consumption).

Pressure

Green hydrogen is delivered at 30 bar (g).

Scalability

The DQ1000 is a 5 MW stack easily duplicable to reach large scale plants.

High H_2 purity

Our purification system enables 99.999% of H_2 purity and the using in fuel cell vehicles.

The purification system is autonomous and does not consume any gases.

	DQ1000 ELECTROLYSER
H_2 gas production	
Nominal H_2 flow	1000 Nm^3/h (2136 kg/day)
Flow range	40% - 100%
Delivery pressure	30 bar (g) without compression
H_2 purity before purification system	99.8%
H_2 purity after purification system	99.999% suitable for fuel cell application
Electrical requirements	
Plant power consumption (AC)	5000 kW
Stack consumption (DC)	4.0 – 4.3 kWh/Nm^3 H_2
Electrical converter power factor	≥ 95%
Primary voltage	3.3 – 20 kV (typical 10 kV) (optional up to 34 kV)
Feed water and electrolyte	
Water conductivity required	< 1 µS/cm (demineralization process available in option)
Demineralized water consumption	0.92 l/Nm^3 H_2
Electrolyte	30% KOH aqueous solution
Dimensions & weight	
Plant footprint	Approx. 400 m^2
Stack dimensions (LxWxH)	6.9 m x 2.2 m x 2.2 m
Stack weight	58 000 kg
Norms & standards	
Marking	CE
Norms compliancy	European PED, ATEX, EMC

John Cockerill Renewables
hydrogen@johncockerill.com
h2.johncockerill.com

Appendix D: Module datasheet

www.jinkosolar.com

Tiger Neo

66HL4M-(V)

610-635 Watt

MONO-FACIAL MODULE

N-type

N-Type Technology

N-Type modules with Tunnel Oxide Passivating Contacts (TOPcon) technology offer lower LID/LeTID degradation and better low light performance.

HOT 3.0 Technology

N-type modules with JinkoSolar's HOT 3.0 technology offer better reliability and efficiency.

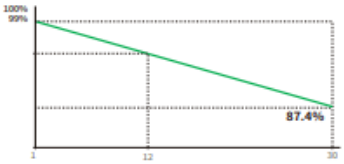

12 Year Product Warranty | **30** Year Linear Power Warranty | **1**% First-year Degradation | **0.4**% Annual Degradation Over 30 Years

Durability Against Extreme Environment

High salt mist and ammonia resistance.

Mechanical Load Enhanced

Certified to withstand:
5400 Pa front side max static test load
2400 Pa rear side max static test load

- IEC61215:2021 / IEC61730:2023
- IEC61701 / IEC62716 / IEC60068 / IEC62804
- ISO9001:2015: Quality Management System
- ISO14001:2015: Environment Management System
- ISO45001:2018: Occupational health and safety management systems

SMBB Technology

Better light trapping and current collection to improve module power output and reliability.

Anti-PID guarantee

Minimizes the chance of degradation caused by PID phenomena through optimization of cell production technology and material control.

EU-JKM610-635N-66HL4M-(V)-F2-EN

66HL4M-(V) 610-635 Watt

Mechanical Characteristics

Cell Type	N -type Mono-crystalline
No. of cells	132 (66×2)
Dimensions	2382×1134×35 mm
Weight	28.2 kg
Front Glass	3.2 mm,Anti-Reflection Coating, High Transmission, Low Iron, Tempered Glass
Frame	Anodized Aluminium Alloy
Junction Box	IP68 Rated
Protection Class	Class II
IEC Fire Type	Class C
Output Cables	4.0 mm² (+): 400 mm , (-): 200 mm or Customized Length

Packaging Configuration

Pallet Dimensions	2396×1110×1251 mm
Packing detail (Two pallets=One stack)	31 pcs/pallets, 62 pcs/stack, 620 pcs/ 40'HQ Container

Specifications (STC)

Maximum Power – Pmax [Wp]	610	615	620	625	630	635
Maximum Power Voltage – Vmp [V]	40.56	40.73	40.90	41.07	41.23	41.39
Maximum Power Current – Imp [A]	15.04	15.10	15.16	15.22	15.28	15.34
Open-circuit Voltage – Voc [V]	48.63	48.79	48.95	49.11	49.27	49.43
Short-circuit Current – Isc [A]	16.01	16.08	16.15	16.22	16.29	16.36
Module Efficiency STC [%]	22.58	22.77	22.95	23.14	23.32	23.51
Power Tolerance	0 ~ +3%					
Temperature Coefficients of Pmax	-0.29 %/°C					
Temperature Coefficients of Voc	-0.25 %/°C					
Temperature Coefficients of Isc	0.045 %/°C					

STC: Irradiance 1000W/m², Cell Temperature 25°C, AM=1.5

Application Conditions

Operating Temperature	-40 °C ~ +70 °C
Maximum System Voltage	1000/1500 VDC (IEC)
Maximum Series Fuse Rating	30 A

Engineering Drawings

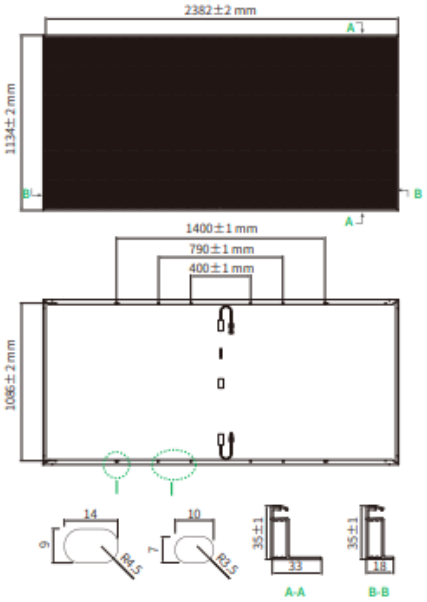

Note: For specific dimensions and tolerance ranges, please refer to the corresponding detailed module drawings.

Electrical Performance

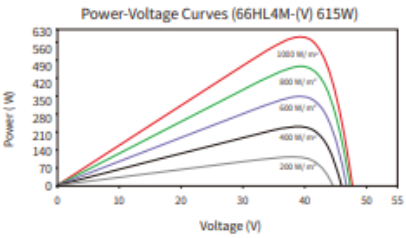

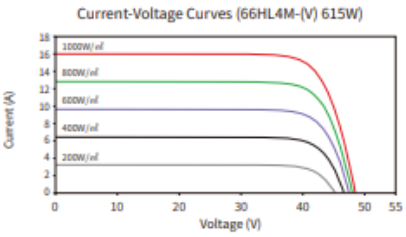

Note: Please read the safety and installation manual before using the product. We reserve the right of final interpretation. The specifications in this datasheet are subject to change without notice.

Appendix E: Inverter datasheet

SG3400/3125/2500HV-MV-20

SUNGROW
Clean power for all

MV Turnkey Station for 1500 Vdc System - MV Separate Transformer + RMU

HIGH YIELD
- Advanced three-level technology, max. inverter efficiency 99 %

EASY O&M
- Integrated current, voltage and MV parameters monitoring function for online analysis and fast trouble shooting
- Modular design, easy for maintenance
- Convenient external touch screen

SAVED INVESTMENT
- Low transportation and installation cost due to 20-foot container design
- DC 1500 V system, low system cost Integrated MV transformer and switchgear
- Q at night function optional

GRID SUPPORT
- Compliance with standards: IEC 61727, IEC 62116
- Low/High voltage ride through (L/HVRT)
- Active & reactive power control and power ramp rate control

CIRCUIT DIAGRAM

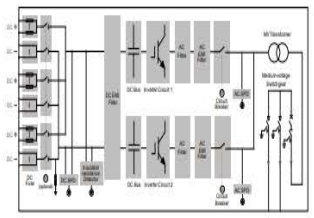

EFFICIENCY CURVE (SG3400HV-20)

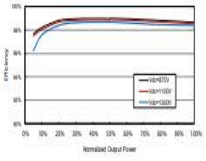

Type designation	SG3400HV-MV-20	SG3125HV-MV-20	SG2500HV-MV-20
Input (DC)			
Max. PV input voltage		1500 V	
Min. PV input voltage / Startup input voltage	875 V / 915 V	875 V / 915 V	800 V / 840 V
MPP voltage range for nominal power	875 - 1300 V	875 - 1300 V	800 - 1300 V
No. of independent MPP inputs		1	
No. of DC inputs	21 (optional: 24 negative grounding or floating; 28 negative grounding)		18 - 24
Max. PV input current	4178 A	4178 A	3508 A
Output (AC)			
AC output power	3593 kVA@ 25 °C / 3437 kVA@ 45 °C	3593 kVA@ 25 °C / 3437 kVA@ 45 °C / 3125 kVA@ 50 °C	2750 kVA@ 45 °C / 2500 kVA@ 50 °C
Max. AC output current	3458 A	3458 A	2886 A
AC voltage range		10 - 35 kV	
Nominal grid f requency / Grid f requency range		50 Hz / 45 - 55 Hz, 60 Hz / 55 - 65 Hz	
THD		< 3 % (at nominal power)	
DC current injection		< 0.5 % In	
Power factor at nominal power / Adjustable power factor		> 0.99 / 0.8 leading - 0.8 lagging	
Feed-in phases / Connection phases		3 / 3	
Efficiency			
Inverter Max. efficiency		99.0 %	
Inverter Euro. efficiency		98.7 %	
Transformer			
Transformer rated power	3437 kVA	3125 kVA	2500 kVA
Transformer max. power	3593 kVA	3593 kVA	2750 kVA
LV / MV voltage	0.6 kV / 10 - 35 kV	0.6 kV / 10 - 35 kV	0.55 kV / 10 - 35 kV
Transformer vector		Dy11	
Transformer cooling type		ONAN (Oil Natural Air Natural)	
Oil type		Mineral oil (PCB free) or degradable oil on request	
Protection and Function			
DC input protection		Load break switch + fuse	
Inverter output protection		Circuit breaker	
AC MV output protection		Circuit breaker	
Overvoltage protection		DC Type I + II / A C Type II	
Grid monitoring / Ground fault monitoring		Yes / Yes	
Insulation monitoring		Yes	
Overheat protection		Yes	
Q at night function		Optional	
General Data			
Dimensions (W*H*D)		6058 * 2896 * 2438 mm	
Weight	17T	17 T	18T
Degree of protection	IP54 (Inverter: IP55)	IP54 (Inverter: IP55)	IP54
Auxiliary power supply	415 V, 15 kVA (Optional: max. 40 kVA)	415 V, 15 kVA (Optional: max. 40 kVA)	415 V, 5 kVA (Optional: max. 40 kVA)
Operating ambient temperature range	-35 to 60 °C (> 45 °C derating)	-35 to 60 °C (> 50 °C der ating)	-35 to 60 °C (> 50 °C derating)
Allowable relative humidity range (non-condensing)		0 - 95 %	
Cooling method		Temperature controlled forced air cooling	
Max. operating altitude		1000 m (standard) / > 1000 m (optional)	
Display		Touch screen	
Communication		Standard: RS485, Ethernet; Optional: optical fiber	
Compliance		CE, IEC 62109, IEC 62116, IEC 61727	
Grid support		Q at night function (optional), L / HVRT, active & reactive power control and power ramp rate control	

Appendix F: Tracker datasheet

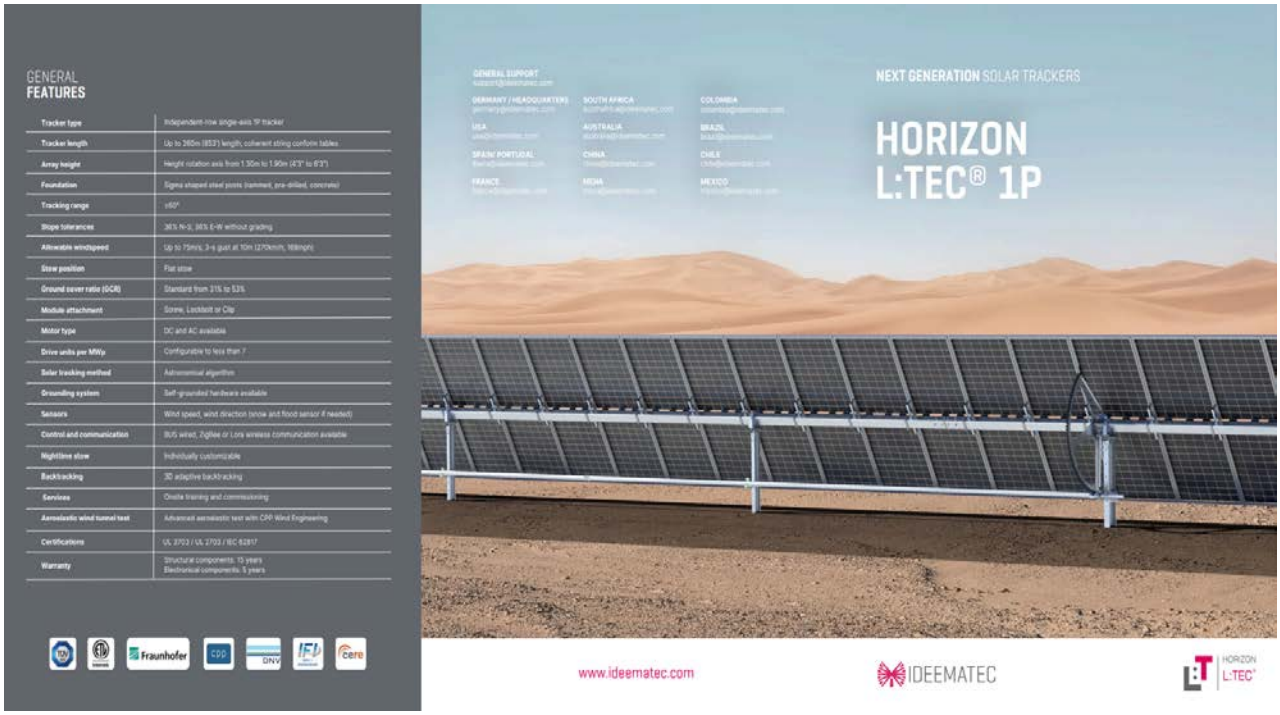

GENERAL
FEATURES

Tracker type	Independent-row single-axis 1P tracker
Tracker length	Up to 260m (853') length, coherent string conform tables
Array height	Height rotation axis from 1.30m to 1.90m (4'3" to 6'3")
Foundation	Sigma shaped steel posts (rammed, pre-drilled, concrete)
Tracking range	±60°
Slope tolerances	36% N-S, 36% E-W without grading
Allowable windspeed	Up to 75m/s, 3-s gust at 10m (270km/h, 168mph)
Stow position	Flat stow
Ground cover ratio (GCR)	Standard from 31% to 53%
Module attachment	Screw, Locktelt or Clip
Motor type	DC and AC available
Drive units per MWp	Configurable to less than 7
Solar tracking method	Astronomical algorithm
Grounding system	Self-grounded hardware available
Sensors	Wind speed, wind direction (snow and flood sensor if needed)
Control and communication	BUS wired, ZigBee or Lora wireless communication available
Nightime stow	Individually customizable
Backtracking	3D adaptive backtracking
Services	Onsite training and commissioning
Aeroelastic wind tunnel test	Advanced aeroelastic test with CPP Wind Engineering
Certifications	UL 3703 / UL 2703 / IEC 62817
Warranty	Structural components: 15 years Electronical components: 5 years

Fraunhofer cpp GNV IFI cere

GENERAL SUPPORT
GERMANY / HEADQUARTERS
SOUTH AFRICA
COLOMBIA
USA
AUSTRALIA
BRAZIL
SPAIN/ PORTUGAL
CHINA
CHILE
FRANCE
INDIA
MEXICO

NEXT GENERATION SOLAR TRACKERS

HORIZON L:TEC® 1P

www.ideematec.com

IDEEMATEC

HORIZON L:TEC®

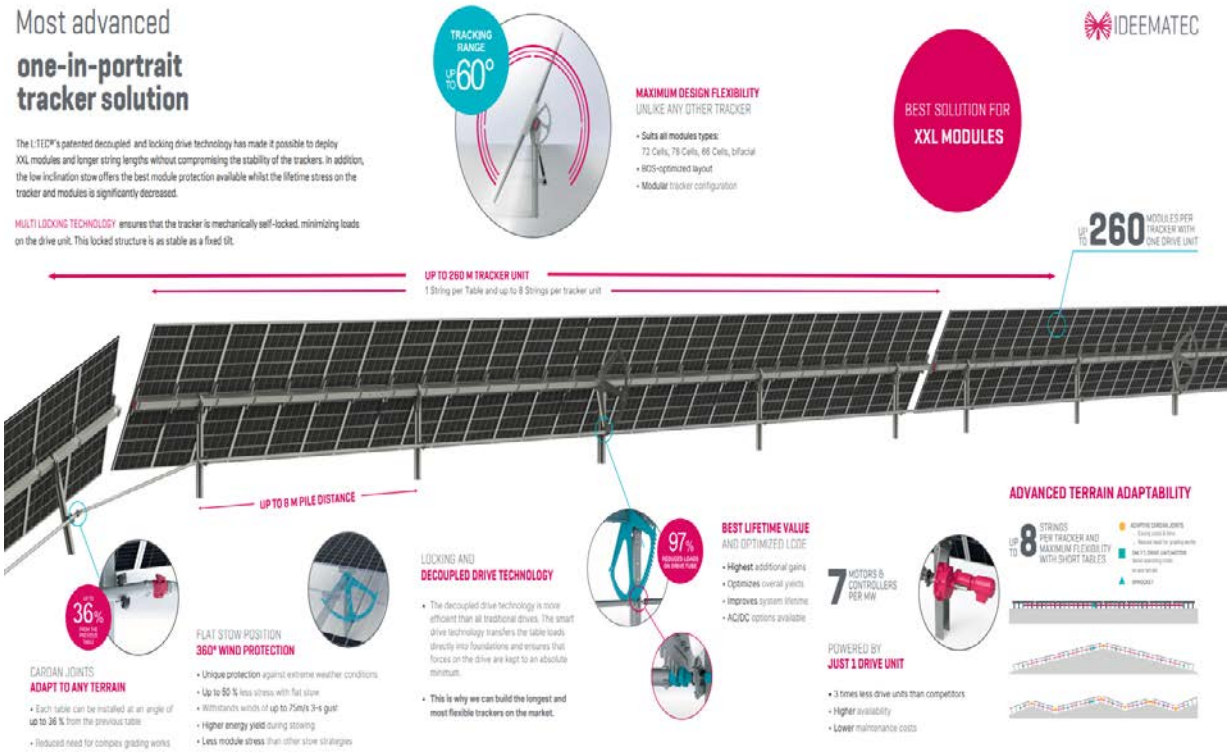

Most advanced
one-in-portrait tracker solution

The L:TEC®'s patented decoupled and locking drive technology has made it possible to deploy XXL modules and longer string lengths without compromising the stability of the trackers. In addition, the low inclination stow offers the best module protection available whilst the lifetime stress on the tracker and modules is significantly decreased.

MULTI LOCKING TECHNOLOGY ensures that the tracker is mechanically self-locked, minimizing loads on the drive unit. This locked structure is as stable as a fixed tilt.

TRACKING RANGE UP TO 60°

MAXIMUM DESIGN FLEXIBILITY
UNLIKE ANY OTHER TRACKER
- Suits all modules types: 72 Cells, 78 Cells, 66 Cells, bifacial
- BOS-optimized layout
- Modular tracker configuration

BEST SOLUTION FOR **XXL MODULES**

IDEEMATEC

UP TO 260 MODULES PER TRACKER WITH ONE DRIVE UNIT

UP TO 260 M TRACKER UNIT
1 String per Table and up to 8 Strings per tracker unit

UP TO 8 M PILE DISTANCE

UP TO 36%
CARDAN JOINTS
ADAPT TO ANY TERRAIN
- Each table can be installed at an angle of up to 36 % from the previous table
- Reduced need for complex grading works

FLAT STOW POSITION
360° WIND PROTECTION
- Unique protection against extreme weather conditions
- Up to 50 % less stress with flat stow
- Withstands winds of up to 75m/s 3-s gust
- Higher energy yield during stowing
- Less module stress than other stow strategies

97% MODULES LAND ON DRIVE TUBE

LOCKING AND
DECOUPLED DRIVE TECHNOLOGY
- The decoupled drive technology is more efficient than all traditional drives. The smart drive technology transfers the table loads directly into foundations and ensures that forces on the drive are kept to an absolute minimum.
- This is why we can build the longest and most flexible trackers on the market.

BEST LIFETIME VALUE
AND OPTIMIZED LCOE
- Highest additional gains
- Optimizes overall yields
- Improves system lifetime
- AC/DC options available

7 MOTORS & CONTROLLERS PER MW

POWERED BY
JUST 1 DRIVE UNIT
- 3 times less drive units than competitors
- Higher availability
- Lower maintenance costs

ADVANCED TERRAIN ADAPTABILITY

UP TO 8 STRINGS PER TRACKER AND MAXIMUM FLEXIBILITY WITH SHORT TABLES

Appendix G: Battery datasheet

BYD Battery Box

BATTERYBOX PREMIUM **LVL**

KEY FEATURES

Safety
LFP cells developed in-house
Proven in millions of EVs

Reliability
LFP expertise since 2002
1M+ systems in 100+ countries

High Performance
High power in on-grid / off-grid / backup scenarios

Space Saving
2 Premium batteries stack

Perfect Compatibility
Compatible with leading single & three phase inverters

BATTERYBOX PREMIUM LVL

Maximum capacity of
983 kWh

bydbatterybox.com

BYD BatteryBox

TECHNICAL PARAMETERS **PREMIUM LVL**

LVL15.4 (2021)

PERFORMANCE

Number of Modules	2
Usable Energy [1]	15.36 kWh
Max Cont. Output Current [2]	250 A
Peak Output Current [2]	375 A, 5 s
Dimensions(H/W/D)	660 x 650 x 575 mm
Weight	168 kg

GENERAL DATA

Nominal Voltage	51.2 V
Operating Voltage	40 - 57.6 V
Operating Temperature	-10°C to +50°C
Battery Type	Lithium Iron Phosphate (LiFePO4)
Communication	CAN
Protection Rating	IP20
Round-trip Efficiency	≥ 95%
Environment	Indoor
Mounting Method	Floor Stand
Certification	IEC62619 / CE / CEC / UN38.3
Applications	ON Grid / ON Grid + Backup / OFF Grid
Warranty [3]	10 Years
Compatible Inverters	victron energy SMA solis GOODWE Deye SUNGROW ...

[1] DC Usable Energy. Test conditions: 100% DOD, 0.2C charge & discharge at + 25°C. System Usable Energy may vary with different inverter brands.
[2] Charge derating will occur between -10°C and +6°C.
[3] Conditions apply. Refer to BYD Battery-Box Premium Limited Warranty Letter.

BYD Lithium Battery Co.,Ltd
Global Sales: batteryboxgrp@byd.com
Global Service: bboxservice@byd.com

BatteryBox EU Service Partner
EFT-Systems GmbH
www.eft-systems.de
info@eft-systems.de

BatteryBox AU Service Partner
Alps Power Pty Ltd
www.alpspower.com.au
service@alpspower.com.au

BatteryBox SA Service Partner
Afriplus Energy Group Pty Ltd
www.afriplusenergy.co.za
info@afriplusenergy.co.za

BatteryBox US Service
BYD America LLC
626-491-2333
us.homeenergy@byd.com

Appendix H: Simulation Loss diagram report Without Storage: fixed System

Loss diagram

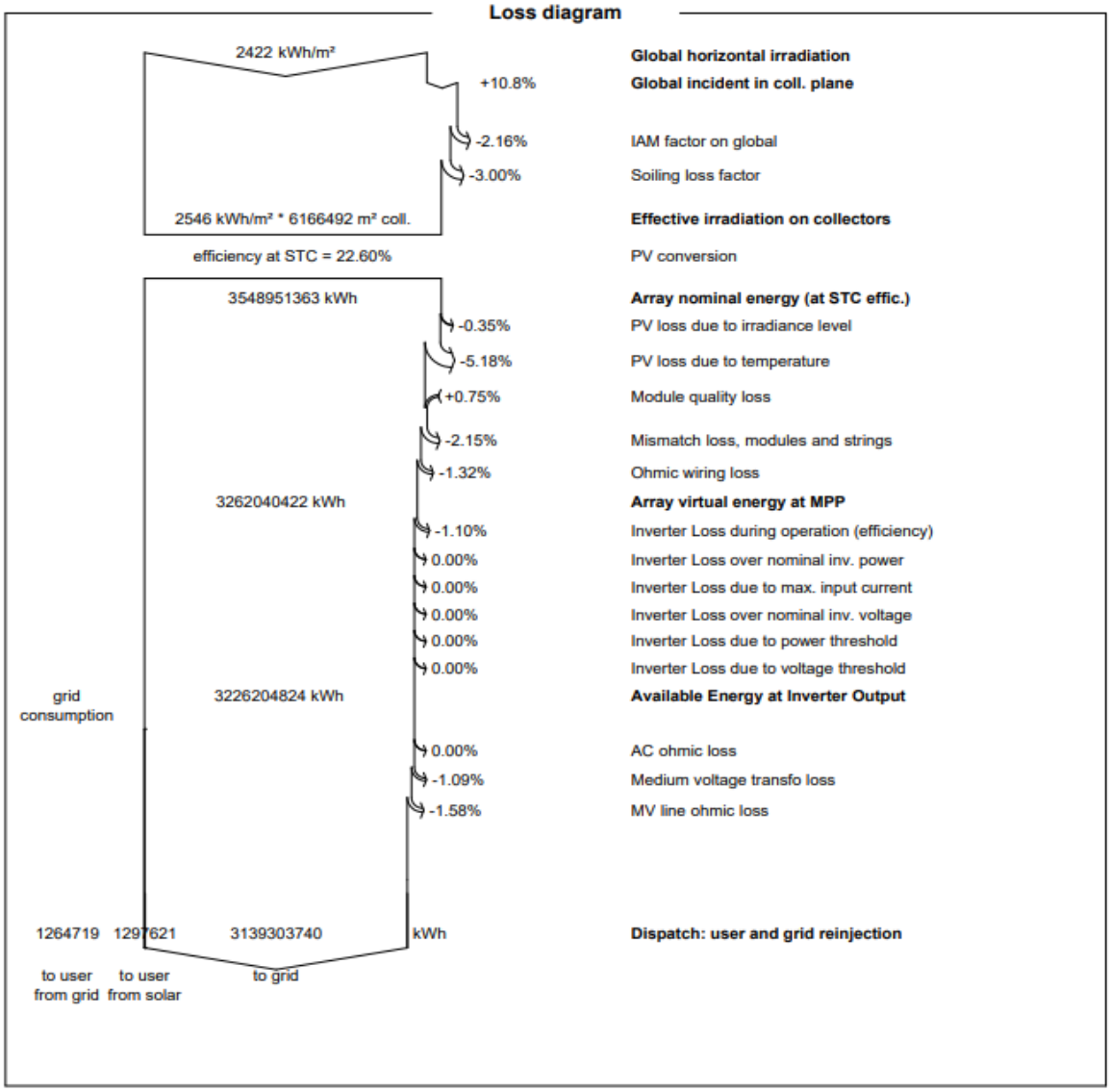

Loss diagram

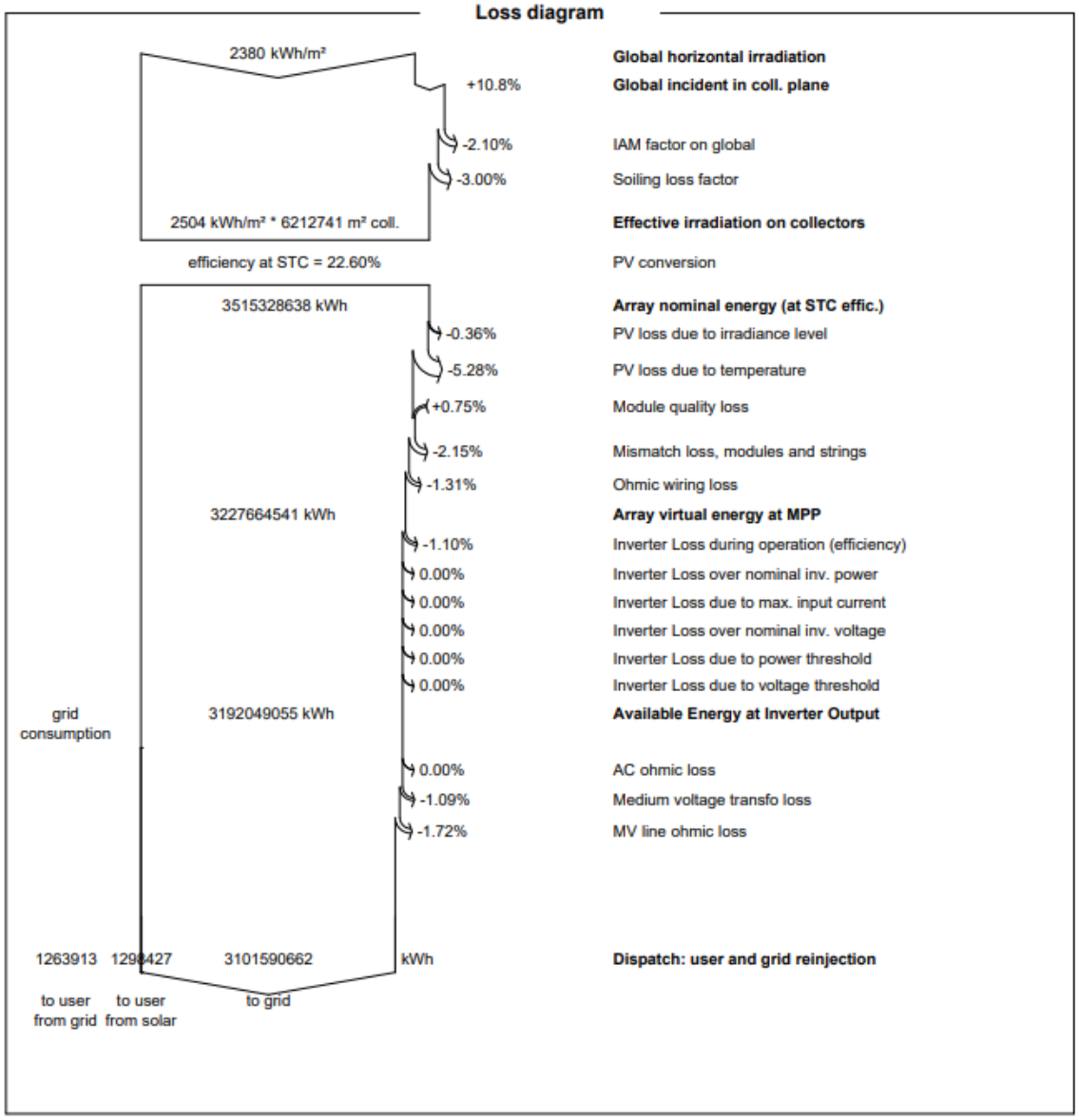

#---------- zenit 3.4.0 results ----------
calculated on 2024-09-11 at 08:59:10.389113
#Dolphin Site[Fixed System]
[Yearly values]

Calculation Step:	Unit	Sum	G/L	PR
Ghor:	[kWh/m2]	2415.536		
Gtlt:	[kWh/m2]	3120.094	29.20%	
Shading:				
Horizon:	[kWh/m2]	3116.625	-0.10%	100.00%
Row:	[kWh/m2]	2892.546	-7.20%	92.80%
External:	[kWh/m2]	2892.546	0.00%	92.80%
Dirt:	[kWh/m2]	2776.844	-4.00%	89.10%
Non-STC operation of PV modules:				
Reflection:	[kWh/m2]	2740.033	-1.30%	87.90%
Spectrum:	[kWh/kWp]	2712.633	-1.00%	87.00%
Irradiation:	[kWh/kWp]	2702.683	-0.40%	86.70%
Temperature:	[kWh/kWp]	2535.651	-6.20%	81.40%
Mismatch:	[kWh/kWp]	2515.365	-0.80%	80.70%
DC circuit:	[kWh/kWp]	2486.441	-1.10%	79.80%
Inverter:	[kWh/kWp]	2449.939	-1.50%	78.60%
Inverter power limitation:	[kWh/kWp]	2434.909	-0.60%	78.10%
Selfconsumption:	[kWh/kWp]	2432.923	-0.10%	78.10%
AC circuit 1:	[kWh/kWp]	2432.025	0.00%	78.00%
Transformer 1:	[kWh/kWp]	2408.101	-1.00%	77.30%
AC circuit 2:	[kWh/kWp]	2373.096	-1.50%	76.10%
Transformer 2:	[kWh/kWp]	2373.096	0.00%	76.10%

#---------- zenit 3.4.0 results ----------
calculated on 2024-09-11 at 08:43:26.725932
#Springbok Site[Fixed System]
[Yearly values]

Calculation Step:	Unit	Sum	G/L	PR
Ghor:	[kWh/m2]	2420.642		
Gtlt:	[kWh/m2]	3123.855	29.10%	
Shading:				
Horizon:	[kWh/m2]	3120.298	-0.10%	100.00%
Row:	[kWh/m2]	2897.538	-7.10%	92.90%
External:	[kWh/m2]	2897.538	0.00%	92.90%
Dirt:	[kWh/m2]	2781.636	-4.00%	89.10%
Non-STC operation of PV modules:				
Reflection:	[kWh/m2]	2745.005	-1.30%	88.00%
Spectrum:	[kWh/kWp]	2717.555	-1.00%	87.10%
Irradiation:	[kWh/kWp]	2707.629	-0.40%	86.80%
Temperature:	[kWh/kWp]	2535.499	-6.40%	81.30%
Mismatch:	[kWh/kWp]	2515.215	-0.80%	80.60%
DC circuit:	[kWh/kWp]	2486.316	-1.10%	79.70%
Inverter:	[kWh/kWp]	2449.827	-1.50%	78.50%
Inverter power limitation:	[kWh/kWp]	2436.236	-0.60%	78.10%
Selfconsumption:	[kWh/kWp]	2434.25	-0.10%	78.00%
AC circuit 1:	[kWh/kWp]	2416.278	-0.70%	77.40%
Transformer 1:	[kWh/kWp]	2392.632	-1.00%	76.70%
AC circuit 2:	[kWh/kWp]	2354.659	-1.60%	75.50%
Transformer 2:	[kWh/kWp]	2354.659	0.00%	75.50%

Appendix I: Simulation Loss diagram report Without Storage: Tracked System

Loss diagram

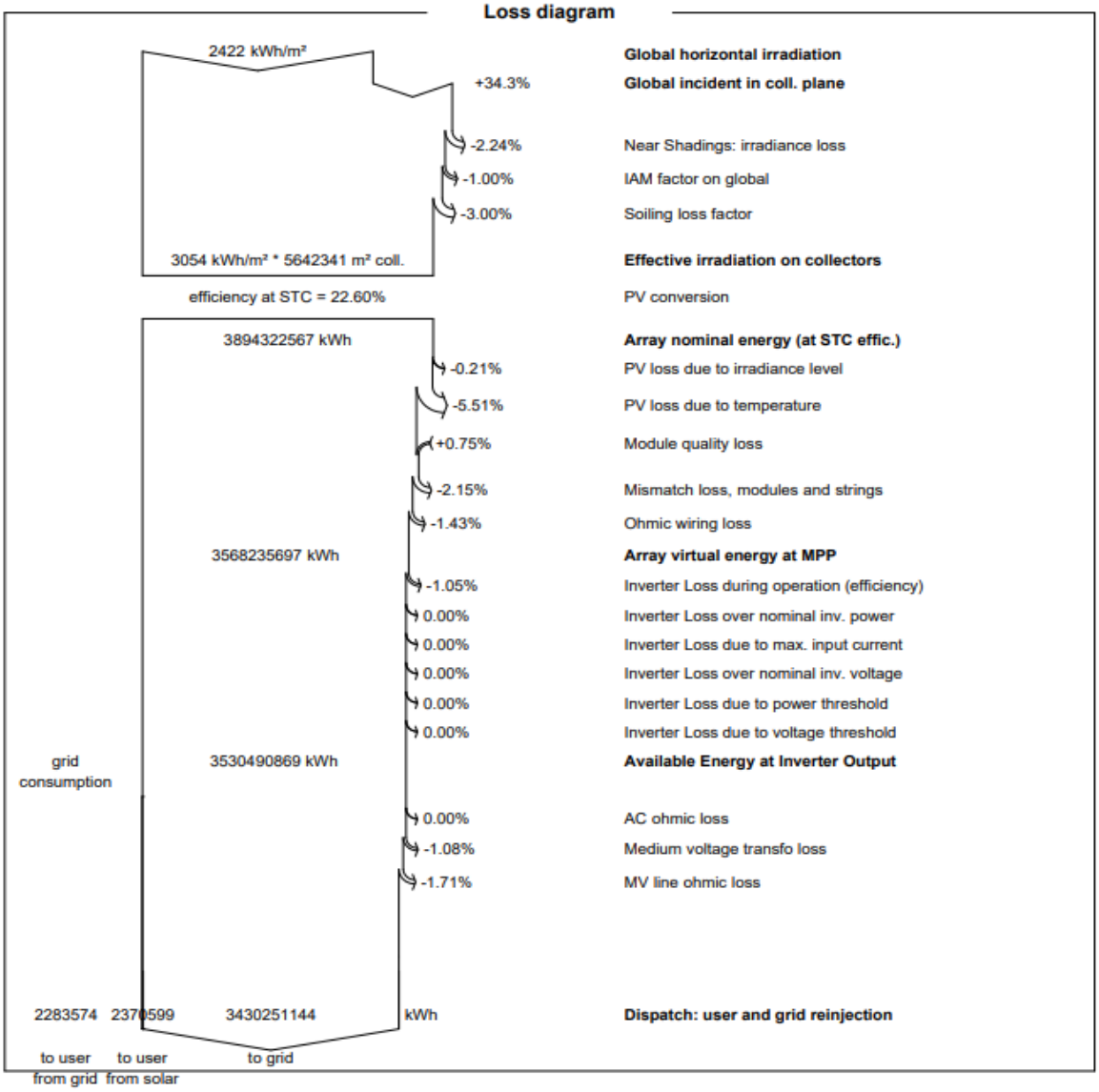

PVsyst V7.4.7
VC2, Simulation date:
10/09/24 13:26
with V7.4.7

Loss diagram

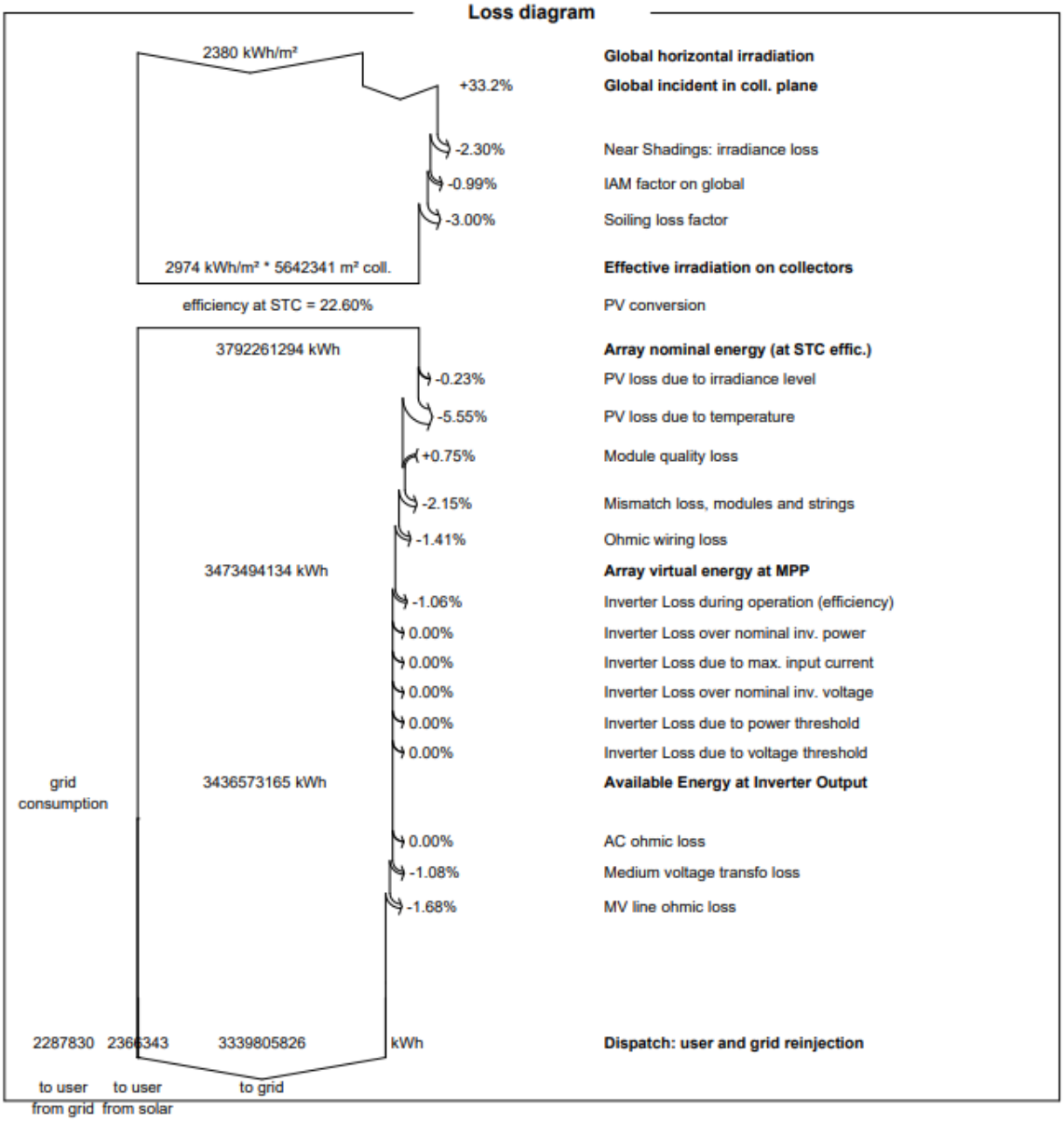

#---------- zenit 3.4.0 results ----------
calculated on 2024-09-11 at 08:03:24.323909
#Dolphin Site[Tracked System]
[Yearly values]

Calculation Step:	Unit	Sum	G/L	PR
Ghor:	[kWh/m2]	2415.536		
Gtlt:	[kWh/m2]	3178.38	31.60%	
Shading:				
Horizon:	[kWh/m2]	3177.596	0.00%	100.00%
Row:	[kWh/m2]	3165.398	-0.40%	99.60%
External:	[kWh/m2]	3165.398	0.00%	99.60%
Dirt:	[kWh/m2]	3038.782	-4.00%	95.60%
Non-STC operation of PV modules:				
Reflection:	[kWh/m2]	3000.456	-1.30%	94.40%
Spectrum:	[kWh/kWp]	2970.452	-1.00%	93.50%
Irradiation:	[kWh/kWp]	2962.348	-0.30%	93.20%
Temperature:	[kWh/kWp]	2782.712	-6.10%	87.60%
Mismatch:	[kWh/kWp]	2760.45	-0.80%	86.90%
DC circuit:	[kWh/kWp]	2728.637	-1.20%	85.90%
Inverter:	[kWh/kWp]	2688.917	-1.50%	84.60%
Inverter power limitation:	[kWh/kWp]	2662.986	-1.00%	83.80%
Selfconsumption:	[kWh/kWp]	2659.012	-0.10%	83.70%
AC circuit 1:	[kWh/kWp]	2658.033	0.00%	83.60%
Transformer 1:	[kWh/kWp]	2632.359	-1.00%	82.80%
AC circuit 2:	[kWh/kWp]	2594.22	-1.40%	81.60%
Transformer 2:	[kWh/kWp]	2594.22	0.00%	81.60%

#---------- zenit 3.4.0 results ----------
calculated on 2024-09-10 at 11:49:28.400727
#Springbok Site[Tracked System]
[Yearly values]

Calculation Step:	Unit	Sum	G/L	PR
Ghor:	[kWh/m2]	2420.642		
Gtlt:	[kWh/m2]	3183.488	31.50%	
Shading:				
Horizon:	[kWh/m2]	3182.306	0.00%	100.00%
Row:	[kWh/m2]	3170.196	-0.40%	99.60%
External:	[kWh/m2]	3170.196	0.00%	99.60%
Dirt:	[kWh/m2]	3043.388	-4.00%	95.60%
Non-STC operation of PV modules:				
Reflection:	[kWh/m2]	3005.58	-1.20%	94.40%
Spectrum:	[kWh/kWp]	2975.524	-1.00%	93.50%
Irradiation:	[kWh/kWp]	2967.459	-0.30%	93.20%
Temperature:	[kWh/kWp]	2781.761	-6.30%	87.40%
Mismatch:	[kWh/kWp]	2759.507	-0.80%	86.70%
DC circuit:	[kWh/kWp]	2727.744	-1.20%	85.70%
Inverter:	[kWh/kWp]	2688.055	-1.50%	84.50%
Inverter power limitation:	[kWh/kWp]	2663.529	-0.90%	83.70%
Selfconsumption:	[kWh/kWp]	2659.555	-0.10%	83.60%
AC circuit 1:	[kWh/kWp]	2658.577	0.00%	83.50%
Transformer 1:	[kWh/kWp]	2632.916	-1.00%	82.70%
AC circuit 2:	[kWh/kWp]	2590.953	-1.60%	81.40%
Transformer 2:	[kWh/kWp]	2590.953	0.00%	81.40%

Appendix J: Simulation Loss diagram report With Storage: fixed System

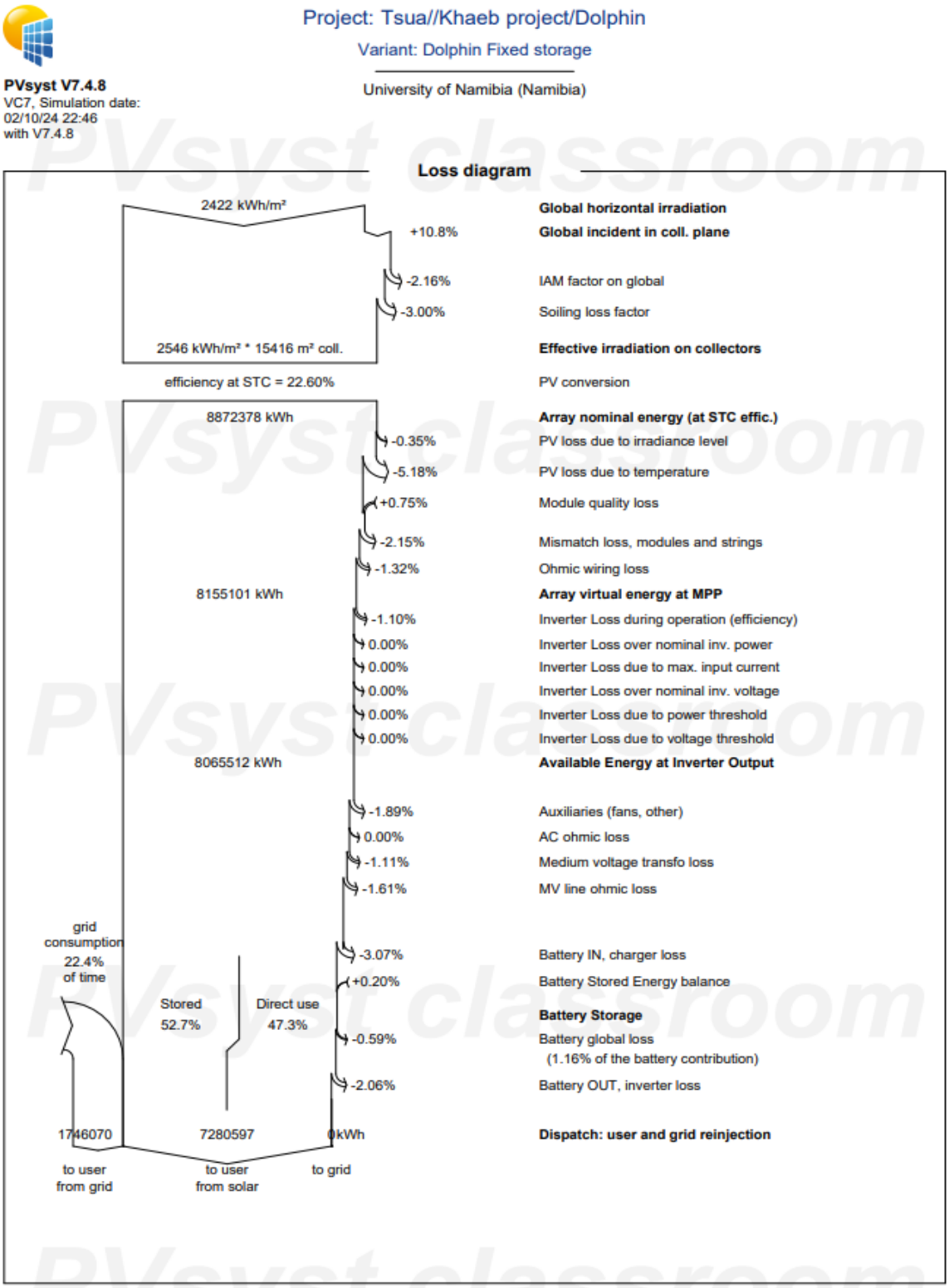

PVsyst V7.4.8
VC7, Simulation date:
02/10/24 22:49
with V7.4.8

Loss diagram

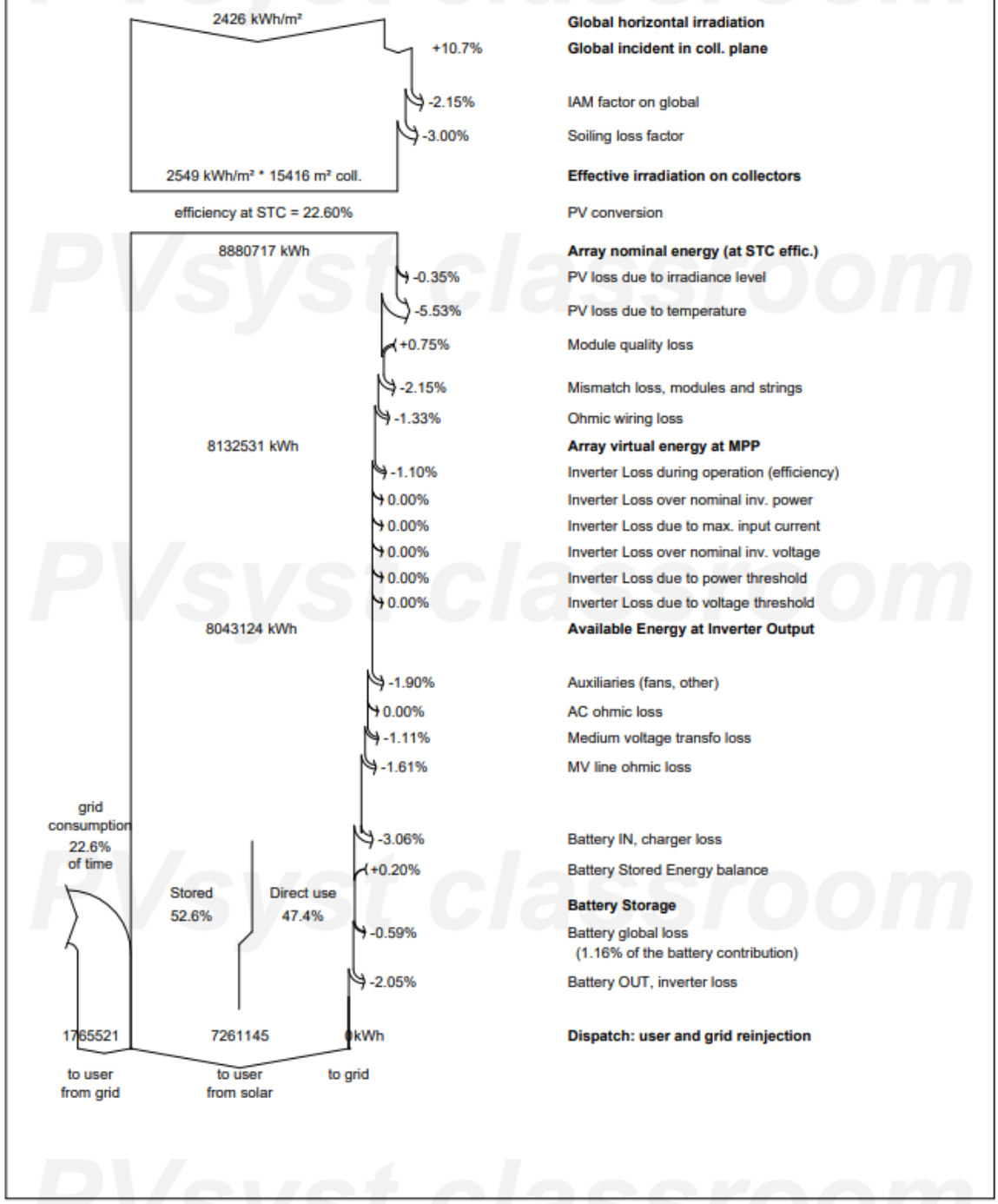

Appendix K: Simulation Loss diagram report With Storage: Tracked System

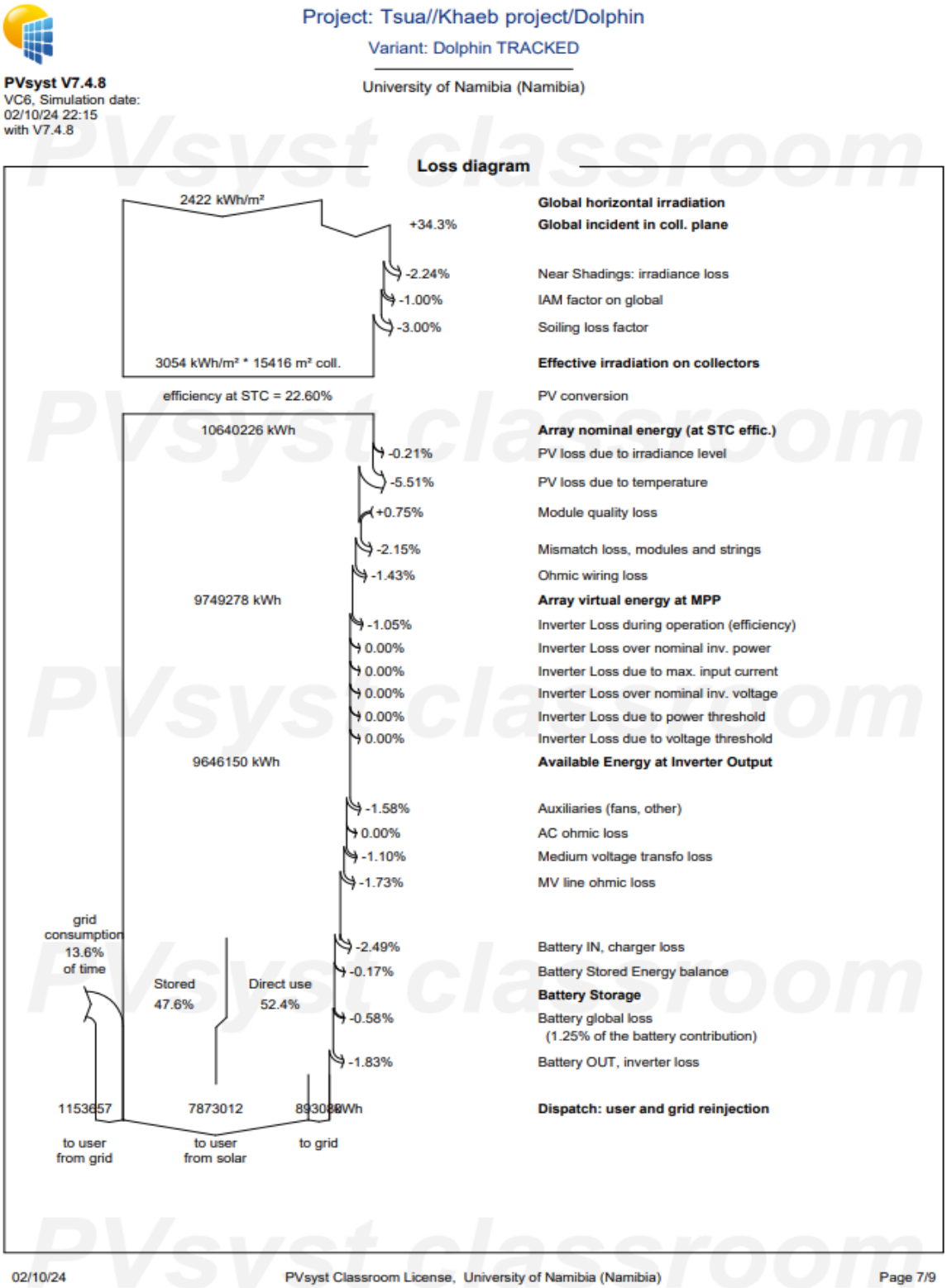

PVsyst V7.4.8
VC5, Simulation date:
02/10/24 22:33
with V7.4.8

Loss diagram

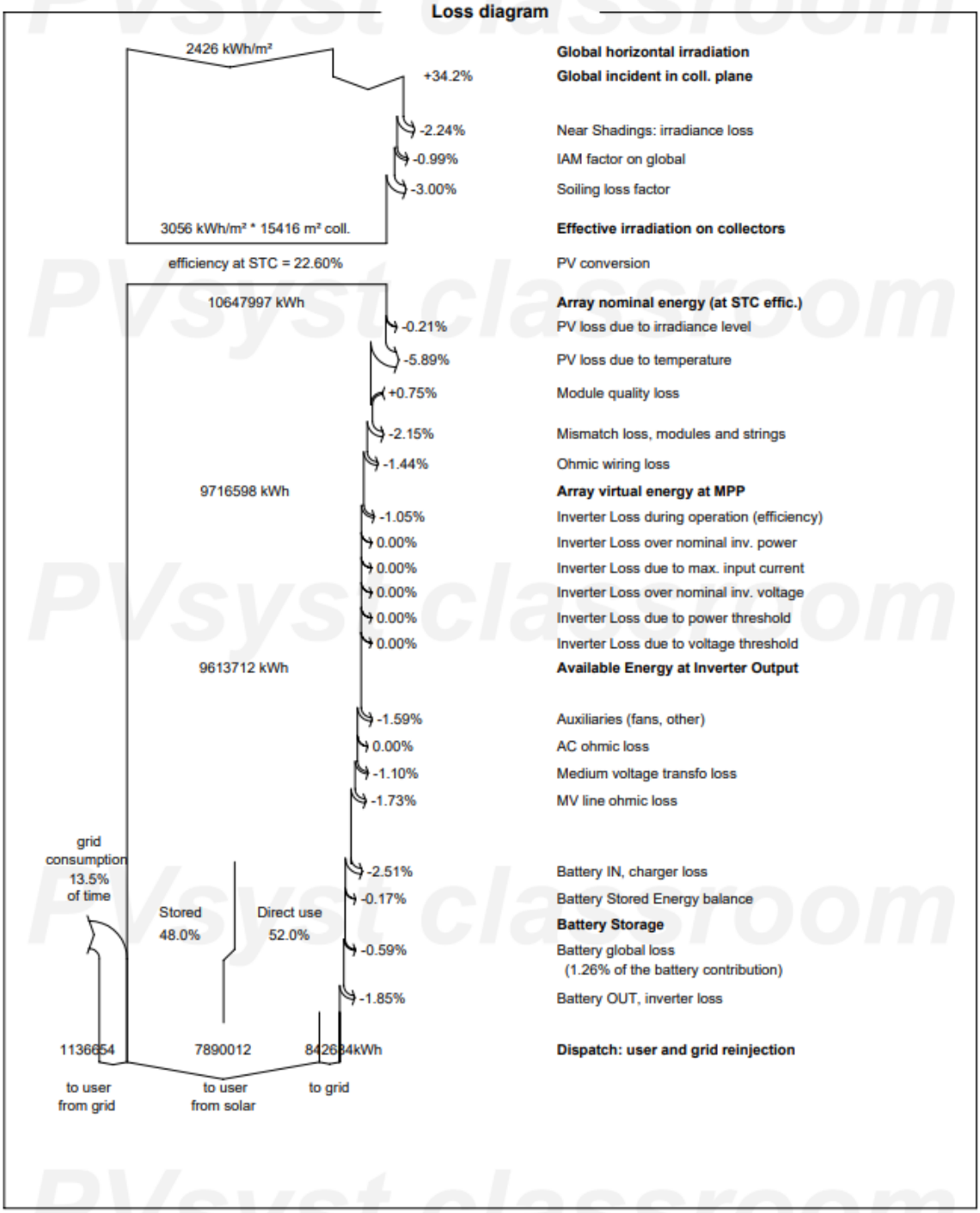

Appendix L: LCOE Scaling Sheets

Parameters	Units	Values	Subsystem	Full System
Capital Expenditure (CAPEX)	*USD$/kW*	1030	3484	1,393,600
Battery 10hr	*USD$/kWh*	139	44,053	17,621,160
Operational Expenditure (OPEX)		13	3484	1,393,600
Discount rate (WACC)	%	10%	10%	10%
Land Lease	*USD$*	28,555,800	28,555,800	28,555,800
Inflation Rate	%	4%	4%	4%
Degradation	*%/yr*	0.25	0.25	0.25
	years	30	30	30
First-year energy output	*kWh/yr*	PVsyst Simulation Result	PVsyst Simulation Result	PVsyst Simulation Result

Parameters	Units	INPUTS
	USD$	3,884,749,240
	USD$	46,672,600
	%	10%
	%	4%
	%/yr	0.25
	years	30
	kWh/yr	2,912,238,800

RESULT from PYTHON CODE
Fixed
0.167

Parameters	Units	Subsystem Outcome
Capital Expenditure (CAPEX)		3,588,520
Battery 10hr	*USD$/kWh*	6,123,353
Operational Expenditure (OPEX)		45,292
Land Lease	*USD$*	28,555,800
Discount rate (WACC)	%	10%
Inflation Rate	%	4
Degradation	%	0.25
System Lifetime	*years*	30
First-year energy output	*kWh/yr*	7280597

Units	Full System Outcome
USD$	1,435,408,000
USD$	2,449,341,240.00
USD$	18,116,800
%	10%
%	4
%	0.25
years	30
First-year energy output	2,912,238,800

Total CAPEX
3,884,749,240

Total OPEX
46,672,600

Dolphin Site Fixed

Parameters	Units	Values	Subsystem + Quanity	Full System
Capital Expenditure (CAPEX)	USD$/kW	1030	3484	1,275,144
Battery 10hr	USD$/kWh	139	44,053	16,123,361
Operational Expenditure (OPEX)	USD$/kW	13	3484	1,275,144
	USD$/kW	200	204	10,248
Discount rate (WACC)	%	10%	10%	10%
Land Lease	USD$	28,555,800	28,555,800	28,555,800
Inflation Rate	%	4%	4%	4%
Degradation	%/yr	0.25	0.25	0.25
	years	30	30	30
First-year energy output	kWh/yr	PVsyst Simulation Result	PVsyst Simulation Result	PVsyst Simulation Result

Parameters	Units	Subsystem Outcome
Capital Expenditure (CAPEX)	USD$	3,588,520
Battery 10hr	USD$/kWh	6,123,353
1d Trackers	USD$	696,800
Operational Expenditure (OPEX)	USD$/kW	16,576,872
Land Lease	USD$	28,555,800
Discount rate (WACC)	%	10%
Inflation Rate	%	4
Degradation	%	0.25
System Lifetime	years	30
First-year energy output	kWh/yr	8766092

	Units	Full System Outcome
	USD$	1,313,398,320
	USD$	2,241,147,234.60
	USD$	255,028,800.00
	USD$	16,576,872
	%	10%
	%	4
	%	0.25
	years	30
First-year energy output		3,208,389,672

Total CAPEX
3,809,574,355

Total OPEX
45,132,672

Parameters	Units	INPUTS
	USD$	3,809,574,355
	USD$	45,132,672
	%	10%
	%	4%
	%/yr	0.25
	years	30
	kWh/yr	3,208,389,672

RESULT from PYTHON CODE

Tracked
0.149

Dolphin Site Tracked

Parameters	Units	Values	Subsystem	Full System
Capital Expenditure (CAPEX)	USD$/kW	1030	3484	1,404,052
Battery 10hr	USD$/kWh	139	44,053	17,753,319
Operational Expenditure (OPEX)	USD$/kW	13	3484	1,404,052
Discount rate (WACC)	%	10%	10%	10%
Land Lease	USD$	28,555,800	28,555,800	28,555,800
		4%	4%	4%
		0.25	0.25	0.25
System Lifetime	years	30	30	30
First-year energy output	kWh/yr	PVsyst Simulation Result	PVsyst Simulation Result	PVsyst Simulation Result

		Subsystem
Parameters	Units	Outcome
Capital Expenditure (CAPEX)	USD$	3,588,520
Battery 10hr	USD$/kWh	6,123,353
Operational Expenditure (OPEX)	USD$/kW	45,292
Land Lease	USD$	28,555,800
Discount rate (WACC)	%	10%
Inflation Rate	%	4
Degradation	%	0.25
System Lifetime	years	30
First-year energy output	kWh/yr	7261145

		Full System
	Units	Outcome
	USD$	1,446,173,560
	USD$	2,467,711,299.30
	USD$	18,252,676
	%	10%
	%	4
	%	0.25
	years	30
First-year energy output	kWh/yr	2,926,241,435

Total CAPEX
3,913,884,859

Total OPEX
46,808,476

Parameters	Units	INPUTS
Total CAPEX	USD$	3,913,884,859
Total OPEX	USD$	46,808,476
	%	10%
Inflation Rate	%	4%
Degradation	%/yr	0.25
System Lifetime	years	30
	kWh/yr	2,926,241,435

RESULT from PYTHON CODE

Configuration	LCoE $/kWh
	0.168

SpringBok Site Fixed

Parameters	Units	Values	Subsystem + Quanity	Full System
Capital Expenditure (CAPEX)	USD$/kW	1030	3484	1,275,144
Battery 10hr	USD$/kWh	139	44,053	16,123,361
Operational Expenditure (OPEX)	USD$/kW	13	3484	1,275,144
1d Trackers	USD$/kW	200	204	10,248
Discount rate (WACC)	%	10%	10%	10%
Land Lease	USD$	28,555,800	28,555,800	28,555,800
Inflation Rate	%	4%	4%	4%
Degradation	%/yr	0.25	0.25	0.25
	years	30	30	30
First-year energy output	kWh/yr	PVsyst Simulation Result	PVsyst Simulation Result	PVsyst Simulation Result

Parameters	Units	INPUTS
	USD$	3,809,574,355
	USD$	45,132,672
	%	10%
	%	4%
	%/yr	0.25
	years	30
	kWh/yr	3,196,167,102

RESULT from PYTHON CODE
Tracked
0.149

SpringBok Site Tracked

		Subsystem
Parameters	Units	Outcome
Capital Expenditure (CAPEX)		3,588,520
Battery 10hr	USD$/kWh	6,123,353
1d Trackers	USD$	696,800
Operational Expenditure (OPEX)	USD$/kW	16,576,872
Land Lease	USD$	28,555,800
Discount rate (WACC)	%	10%
Inflation Rate	%	4
Degradation	%	0.25
System Lifetime	years	30
First-year energy output	kWh/yr	8732697

		Full System
	Units	Outcome
	USD$	1,313,398,320
	USD$	2,241,147,234.60
	USD$	255,028,800.00
	USD$	16,576,872
	%	10%
	%	4
	%	0.25
	years	30
First-year energy output		3,196,167,102

Total CAPEX
3,809,574,355

Total OPEX
45,132,672